

*Structure and conformation of photosynthetic
pigments and related compounds.
Conformation analysis of chlorophyll derivatives*



Submitted by

Dáire John Gibbons

*A report submitted to Trinity College Dublin, The University of Dublin for a
M.Sc. Chemistry degree by research*

September 2019

Under the supervision of Prof. Dr. Mathias O. Senge

Declaration

September 2018

Trinity College Dublin

I declare that this thesis has not been submitted as an exercise for a degree at this or any other university and it is entirely my own work. I agree to deposit this thesis in the University's open access institutional repository or allow the Library to do so on my behalf, subject to Irish Copyright Legislation and Trinity College Library conditions of use and acknowledgement.

.....
Dáire Gibbons B. Sc. Chemistry

Acknowledgements

First, I would like to thank my supervisor Prof. Dr. M. O. Senge for giving me the opportunity of being a research student in his group, and for his continued support, encouragement and guidance throughout this project. Special thanks are also due to Dr. Brendan Twamley who introduced me to X-ray crystallography and for his continued support in this field. I would also like to say thank you to all the members of the Senge group, particularly Keith J. Flanagan, for making this project such an enjoyable experience and making the lab a welcoming and enjoyable place to work.

Abbreviations

BChl	Bacteriochlorophyll
<i>Bre</i>	Breathing
CCDC	Cambridge Crystallographic Data Centre
Chl	Chlorophyll
CSD	Cambridge Structural Database
DCM	Dichloromethane
D_{ip}	Overall in-plane degree of distortion
D_{oop}	Overall out-of-plane degree of distortion
Et	Ethyl chain
GUI	Graphical User Interface
H ₂ cTEtTPP	Free base 2,3,7,8-tetraethyl-5,10,15,20-tetraphenylporphyrin
H ₂ DEtTPC	Free base 7,8-diethyl-5,10,15,20-tetraphenylchlorin (12) (also 12,13-diethyl-5,10,15,20-tetraphenylchlorin (13))
H ₂ DEtTPP	Free base 2,3-diethyltetraphenylporphyrin
H ₂ HEtTPP	Free base 2,3,7,8,12,13-hexaethyl-5,10,15,20-tetraphenylporphyrin
H ₂ OEP	Free base 2,3,7,8,12,13,17,18-octaethylporphyrin
H ₂ OEtTPP	Free base 2,3,7,8,12,13,17,18-octaethyl-5,10,15,20-tetraphenylporphyrin
H ₂ TPP	Free base 5,10,15,20-tetraphenylporphyrin
H ₂ tTEtTPC	Free base 2,3,7,8-tetraethyl-5,10,15,20-tetraphenylchlorin (14) (also 7,8,12,13-tetraethyl-5,10,15,20-tetraphenylchlorin (15))
H ₂ tTEtTPP	Free base 2,3,12,13-tetraethyl-5,10,15,20-tetraphenylporphyrin
H ₂ XETPC	Free base 5,10,15,20-tetraphenylchlorins (X = 2-4) with increasing number of β -ethyl substituents
H ₂ XEtTPP	Free base 5,10,15,20-tetraphenylporphyrins (X = 2-8) with increasing number of β -ethyl substituents
Ip	In-plane

<i>M-str</i>	Meso-stretching
NSD	Normal-coordinate Structural Decomposition
<i>N-str</i>	<i>N-stretching</i>
Oop	Out-of-plane
<i>Pro</i>	<i>Propeller</i>
<i>Rot</i>	Pyr-rotation
<i>Ruf</i>	<i>Ruffled</i>
<i>Sad</i>	<i>Saddle</i>
<i>Trn(x)</i>	Pyr-translation
<i>Trn(y)</i>	Pyr-translation
Zn(II)OEP	2,3,7,8,12,13,17,18-octaethylporphyrinato-zinc(II)
Zn(II)TPP	5,10,15,20-tetraphenylporphyrinato-zinc(II)
Zn(II)XEtTPC	5,10,15,20-tetraphenylchlorinato-zinc(II) (X = 2-4) with increasing number of β -ethyl substituents
Zn(II)XEtTPP	5,10,15,20-tetraphenylporphyrinato-zinc(II) (X = 2-8) with increasing number of β -ethyl substituents
<i>Wav(x)</i>	<i>Wave(x)</i>
<i>Wav(y)</i>	<i>Wave(y)</i>
3D	Three-Dimensional
δ_{ip}	Mean absolute in-plane deviation of the NSD minimum basis set from the observed structure
δ_{oop}	Mean absolute out-of-plane deviation of the NSD minimum basis set from the observed structure

Conference Abstracts

Dáire Gibbons, Keith J. Flanagan, Stefan S. R. Bernhard and Mathias O. Senge. "Cubane: Tecton for the future with potential as a self-assembly material", Centre for Synthesis and Chemical Biology (CSCB) "Recent Advances in Synthesis and Chemical Biology XVI", University College Dublin, Dublin, Ireland, 8th December 2017. P32

Dáire Gibbons, Keith J. Flanagan and Mathias. O. Senge. "Structure and Conformation of Photosynthetic Pigments and Related Compounds" RSC Organic Division — Ireland Regional Meeting, Queen's University Belfast, Northern Ireland, 2nd May 2018. P1

Dáire Gibbons, Keith J. Flanagan and Mathias. O. Senge. "Structure and Conformation of Photosynthetic Pigments and Related Compounds" Computer-Aided Drug Design Symposium and Workshop — Linking Design, Biology, Chemistry and Medicine, Trinity College Dublin, The University of Dublin, Ireland, 3rd and 4th of May 2018. P11

Dáire Gibbons, Keith J. Flanagan and Mathias. O. Senge. "Structure and Conformation of Photosynthetic Pigments and Related Compounds" 31st European Crystallographic Meeting, Oviedo, Spain 22nd–28th August 2018. MS32-P01

Contents Page

Declaration	ii
Acknowledgements	iii
Abbreviations	iv
Conference Abstracts	v
Chapter 1: Introduction	1
1.1 Chlorophyll and their derivatives – structure and function	1
1.2 Normal-coordinate Structural Decomposition (NSD) – conformational analysis of tetrapyrroles	2
Chapter 2: Aims and Objectives	4
2.1 Validation of NSD program	4
2.2 Conformational analysis of photosynthetic pigments	4
Chapter 3: Experimental	5
3.1 Analytical procedure	5
3.2 Normal-coordinate Structural Decomposition analysis	5
Chapter 4: Results and Discussion	8
4.1 Test Case	8
4.1.1 Free base 5,10,15,20-tetraphenylporphyrins (TPP)	8
4.1.2 Free base 2,3,7,8,12,13,17,18-octaethylporphyrin (OEP)	11
4.1.3 Free base <i>meso</i> tetraphenylporphyrins with graded degree of steric hindrance	12
4.1.4 Free base <i>meso</i> tetraphenylchlorins with graded degree of steric hindrance	15
4.1.5. Impact of Reduction on the distortion in the free base TETPCs vs TETPPs	17
4.2 Zinc(II) Compounds	18
4.2.1 Zn(II)TPP	19
4.2.2 Zn(II)OEP	20
4.2.3 Zn(II)XEtTPP	21
4.2.4 Zn(II)XEtTPC	23
4.3 NSD analysis of chlorophyll-related compounds	26
4.3.1 Bacteriochlorophyll a	26
4.3.2 Phytychlorins	27
4.3.2(a) Free base phytychlorins	27
4.3.2(b) Free base phytychlorins (continued)	29

4.3.2(c)	Metallated phytochlorins	30
4.3.2(d)	Metallated phytochlorins (continued)	35
4.3.3	β -substituted chlorins	35
4.3.3(a)	Freebase β -substituted chlorins	36
4.3.3(b)	Metallated β -substituted chlorins	38
4.3.3(c)	Fused β -substituted chlorins	43
Chapter 5: Conclusions and Future Work		49
Chapter 6: References		52
Chapter 7: Appendix		59

1. Introduction

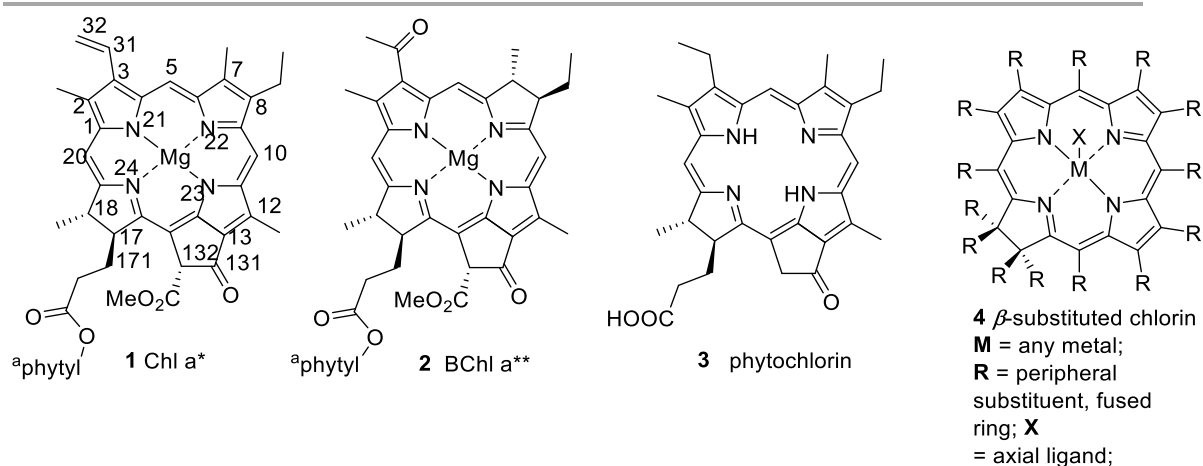
1.1 Chlorophyll derivatives – structure and function

Chlorophylls are essential molecules for life on the earth and the principal pigments of photosynthesis.¹ Thus far over a hundred chemically different natural chlorophylls (Chls) have been identified and classified as Chls a–f and bacteriochlorophylls (BChls) a–g.² Depending on the individual organism and photosystem they can function either as reaction centres or accessory pigments, while some, e.g., Chl a **1** (Figure 1) and Bchl b, can act both in charge separation and as a light harvesting dye. Both processes are intrinsically related to each other in the overall conversion of light energy into chemical energy (and thus both share biochemical reduction equivalents and oxygen).

Taking the most ‘visible’ pigments the Chls from Higher Plants as an example,³ one of the fundamental questions relates to the difference of reaction centre and antenna pigments at the molecular level. How can it be that the same pigment – albeit in different protein complexes – can have such drastically different photochemical properties, including transfer excitation energy in the antenna complexes and charge separation in the reaction centres? While the structural features of many (B)Chl-protein complexes have now been unravelled and established the importance of their spatial arrangement, axial coordination and neighbouring amino acids,^{1,4} a more detailed picture of variations of the chlorophyll chromophores at the molecular level is only slowly emerging.

Chlorophylls⁵ (Figure 1) and porphyrins, in general, are ubiquitous in nature. As well as their role in many biochemical processes, these tetrapyrroles have shown applications in photochemistry, electron transfer, catalysis (organocatalysis) and coordination chemistry.^{6,9} They have also been shown to exhibit a wide range of different macrocycle conformations. These can arise from the inherent flexibility of the porphyrin ring system, induced by metalation, *N*-substitution or protonation, steric effects of peripheral or axial substituents, π -aggregation or environmental effects, interaction with an apoprotein, or as the result of photochemical or redox

reactions. Like other macrocycles the aromatic rings can be stretched, twisted or bended.⁷ The various observations have been grouped together in the concept of the conformational flexibility of porphyrins which illustrates the interrelationship between macrocycle conformation and (altered) physiochemical properties and, *inter alia*, aims to explain the different biological functions of a given chromophore.^{5,8,9}



*1 Chl a = Chlorophyll a **2 BChl a = Bacteriochlorophyll a

^aPhytyl = C₂₀H₃₉

Figure 1 Natural and synthetic tetrapyrrolic macrocycles.

In contrast to hemes¹⁰ a clear correlation of conformational aspects with biological effects for chlorophylls (*e.g.*, with their roles in the photosynthetic electron transfer) has only recently been established through a comparative statistical analysis of the available protein structural data for bacterial photosynthetic reaction centres.¹¹ Similarly, the conformational fine-tuning of chlorophyll absorption has just been proven by Bednarczyk *et al.* for a light-harvesting complex.¹²

1.2 Normal-coordinate Structural Decomposition (NSD) – conformational analysis of tetrapyrroles

To date, a detailed comparative analysis of chlorophyll related molecules at a small molecule, high resolution level is still lacking. The measurement of the degree of nonplanarity of tetrapyrroles is and have been carried out

using UV-visible absorption spectroscopy, resonance Raman spectroscopy and X-ray crystallography graphical user interfaces. Calculations have been carried out using molecular mechanics on the compounds containing assumed D_{4h} symmetry.^{13a, 28} However, in recent times, some general trends in the structural chemistry of Chls have been elucidated by comparing the overall conformation by means of skeletal deviation plots.^{13b} The inspection of the overall degree of distortion, or a comparison of the impact of different substituent pattern has been performed.¹⁴ Classic examples are the BChl studies by Fajer *et al.*,¹⁵ investigations on synthetic non-natural metal complexes,¹⁶ Stolzenberg's fundamental comparisons of porphyrins and hydroporphyrins,¹⁷ and more.¹⁸

However, individual cases aside, no comprehensive and detailed analysis using the Normal-coordinate Structural Decomposition (NSD) method¹⁹ developed by Shelnutz and coworkers has been performed.⁹ This method allows a reliable description for comparative analyses and provides the most detailed information for a given porphyrin macrocycle. The NSD graphical user interface (NSDGUI) describes the macrocycle conformation in terms of displacements along the vibrational modes of the ring system and yields a total of 66 normal-modes or degrees of freedom. The resulting number of normal-modes is found by the program using the physical chemistry formula for calculating modes of vibrations in molecules ($3N-6$; N = number of atoms in the molecule). The program projects only the largest displacements along the lowest-energy vibrations that yield an accurate description of the structural characteristics. This "minimum basis set" consists of six out-of-plane and six in-plane modes of distortion¹⁹ (see Experimental section 3.2; Figure 2).

As a test case was performed to validate the NSD program, an NSD analysis was carried out for (B)Chl-related small molecule crystal structure analyses with coordinates deposited in the CCDC and in the following detail the conclusions that can be drawn therefrom.

2 Aims and Objectives

2.1 Validation of a NSD program

The primary objective is to use a NSD program to analyse the conformational analysis of photosynthetic pigments. Firstly however, the NSD program must be validated in order to determine that the results produced by this program are precise and reproducible. This validation forms the first part of the discussion where the conformations of well-studied porphyrins and chlorins are analysed and discussed in terms of how their conformations give rise to the 3D configurations observed in their crystal structures.

2.2 Conformational analysis of photosynthetic pigments

Once the NSD program is validated, the conformational analysis of chlorophyll-related compounds can then be conducted using this NSD. This program will describe the conformation of the macrocycle in terms of the out-of-plane (*oop*) and in-plane (*ip*) distortions (see, Experimental section 3.2). Since there is no small molecule crystal structure of chlorophyll a,¹⁴ the conformational analysis of the crystal structures of compounds that are the most structurally similar to chlorophyll, is conducted, in order to see how the crystal structure's environment affects their 3D structure. The crystal structures available *via* the Cambridge Crystal Structural Database (Version 5.39; May 2018)²⁰ are bacteriopheophorbides (bacteriochlorophyll a related structures; **2**), phytychlorins (**3**) and several β -substituted chlorins (**4**).

3 Experimental

3.1 Analytical procedure

Structural data was obtained from the Cambridge Crystal Structure Database (Version 5.39, May 2018).²⁰ The database was screened for all pertaining entries using the PC version of Conquest (Version 1.22).²¹ The selection of compounds was guided by their chemical relation to the naturally occurring (B)Chls, e.g., Chl a **1** or BChl a **2** (Figure 1). Thus, the primary focus was on compounds related to phytychlorin **3**, i.e. molecules similar to **2**. For comparative analyses related porphyrins and hydroporphyrins (chlorins) were included to investigate more fundamental structural aspects of hydroporphyrins. To keep the data set manageable, a plethora of compounds which central core consisted of *meso*-(tetra)substituted porphyrins (a pattern not found in nature; see Results and Discussions section 4.1.1), those with fused porphyrin macrocycles and/or heteroatom substitutions were omitted, although a large part form the validation test case. This procedure yielded a list of 30 chlorophylls (3 Bacteriochlorophyll a structures and 27 phytychlorins) and 49 β -substituted chlorins. Each compound was labelled using the six-character CCDC reference code (e.g., AECLPA01) and then given a scheme number (Eg. 1a). CIF files for the selected compounds were then downloaded and converted to protein database (pdb) format for NSD analysis using Mercury 3.8 (2015).²² Full referencing, nomenclature, CCDC codes and all chemical structures are given in the results and discussion (**Chapter 3**).

3.2 Normal-coordinate Structural Decomposition analysis

Shelnutt's NSD (Normal-coordinate Structural Decomposition) method was used to delineate, quantify and illustrate the various distortions modes present in tetrapyrrole macrocycles.¹⁹ The main distortions that 'adequately describe' the heterocycle's conformation are split into six out-of-plane (*oop*) and six in-plane (*ip*) modes. As shown in Figure 2, the out-of-plane modes are: *saddle* (*sad*), *ruffled* (*ruf*), *wave(x)* (*wav(x)*), *wave(y)* (*wav(y)*) and *propeller* (*pro*). The six in-plane modes of distortion are:

meso-stretching (*m-str*), N-stretching (*N-str*) pyr-translation (*trn(x)*), pyr-translation (*trn(y)*), breathing (*bre*) and pyr-rotation (*rot*).^{9, 19}

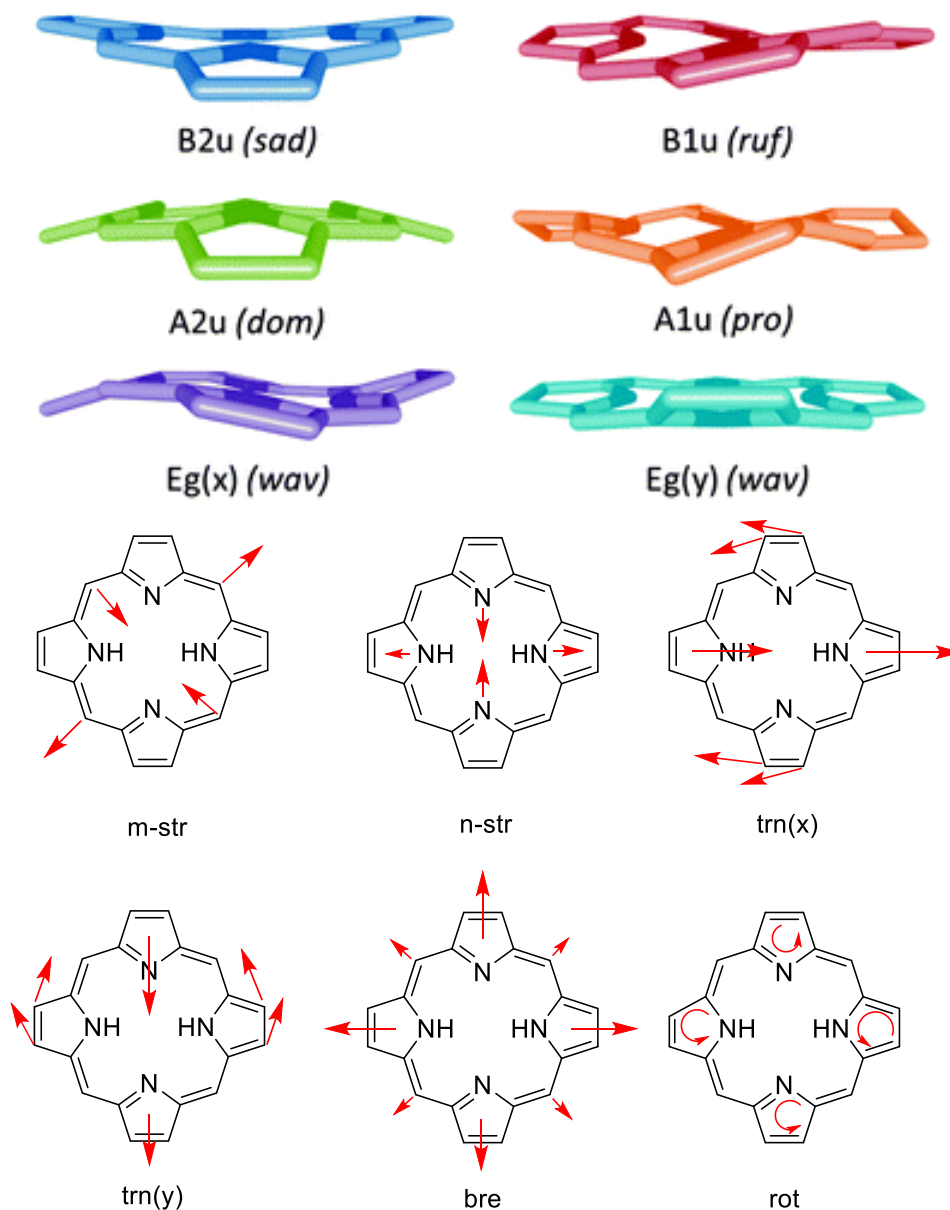


Figure 2 (Top) The six out-of-plane and six in-plane distortion modes as mentioned above.

As measures of the overall degree of distortion D_{oop} (out-of-plane) and D_{ip} (in-plane) are used, whereas δ_{oop} and δ_{ip} represent the mean absolute deviation of the NSD minimum basis set from the reference structure, a planar D_{4h} -symmetric metalloporphyrin skeleton. Full details of the mathematical procedure have been given before by Shelnutt *et al.*^{19, 20} NSD calculations were performed with the NSD GUI version of the program.²³

The output distortion modes were then transferred to Excel and was employed to create the graphical representation in this report. The full graphical representation is detailed in the appendix (Chapter 7).

4 Results and Discussion

4.1 Test case

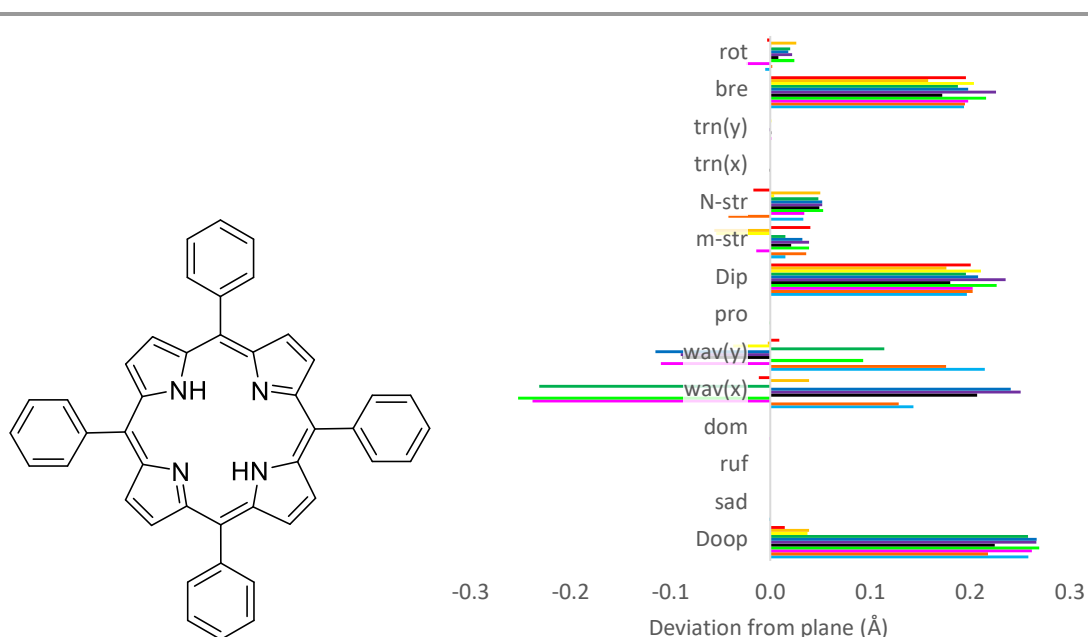
To be able to accurately determine the macrocycle conformation of chlorophyll and its derivatives and our attempts to present a simple visual depiction thereof, a test case study was carried out to assess the validity of the NSD method by analysing several common and well-studied porphyrin structures. The compounds were chosen based on the following categories: Free base 5,10,15,20-tetraphenylporphyrins (TPP); free base 2,3,7,8,12,13,17,18-octaethylporphyrins (OEP); free base porphyrins with β -ethyl and *meso* tetraphenyl groups (XEtTPP); the respective free base chlorins (XEtTPC); and the Zn(II) derivatives of the four ligands mentioned above. Within this text, the compound's out-of-plane and in-plane distortion modes will be compared and discussed to determine the factors that give rise to these distortions which contribute to the overall 3D structure, i.e. deviation from a previous 2D structure.

4.1.1 5,10,15,20-Tetraphenylporphyrins (TPP).

Free base TPPs²⁴ exhibit little to no out-of-plane (*oop*) distortion. The TPP compounds (Figure 3) with the highest D_{oop} , (0.225 – 0.269 Å; TPHPOR01-TPHPOR14; **5d-5i**), contain no solvates within the unit cell. The $wav(x)$ of these TPPs range from 0.207 – 0.253 Å and the $wav(y)$ range is from 0.088 – 0.115 Å, (absolute values given). For the structure of JIVRAH (**5a**), a benzaldehyde solvate yields a D_{oop} value of 0.015 Å and the $wav(x)$ and $wav(y)$ values are -0.012 and 0.009 Å, respectively. These distortions are due to a predominant intermolecular hydrogen bonding network between the aldehyde and the β -hydrogen atoms of the nearest porphyrin molecule. Additionally, there are several hydrogen $\cdots\pi$ -interactions between the aldehyde and the phenyl rings of the porphyrin at a distance of 2.883 (4) Å. This results in the benzaldehyde solvate being held above and below the porphyrin plane, staggering the porphyrin stacking and increasing its planarity.

The structures of SEMNIH and SEMNIH01 (**5b** and **5c**) show a marked decrease of almost 0.100 Å to the D_{oop} compared to the non-solvated structures of TPP.

This can be rationalized by the 1,3-dimethylbenzene solvent present in the unit cells. This solvent interacts with an α -carbon of one TPP and a phenyl ring of a different molecule of TPP.



	CCDC	Colour	Solvent
5a	JIVRAH	Red	Benzaldehyde
5b	SEMNIH	Orange	1,3-dimethylbenzene
5c	SEMNIH01	Yellow	1,3-dimethylbenzene
5d	TPHPOR01	Green	No solvent
5e	TPHPOR04	Blue	No solvent
5f	TPHPOR11	Purple	No solvent
5g	TPHPOR12	Black	No solvent
5h	TPHPOR13	Light Green	No solvent
5i	TPHPOR14	Magenta	No solvent
5j	XAGLOG	Orange	Anthracene
5k	XAGMAT	Blue	Pyrene

Figure 3 (Top) TPP (**5**) structures from the CCDC and NSD analysis of the X-ray crystallographic structures of the TPP compounds. (Bottom): Table containing CCDC reference code, colour corresponding to NSD analysis (above) and solvent in the unit cell.

Additionally, the phenyl rings interact via short hydrogen contacts in a head-to-head style packing system. This head-on interaction, as well as the solvent interactions, give rise to a slightly staggered head-on packing system. **5b** has distortions of 0.039 Å and -0.003 Å in the *wav(x)* and *wav(y)* modes, respectively, whereas distortions of -0.001 Å and -0.037 Å are seen in these modes in **5c**.

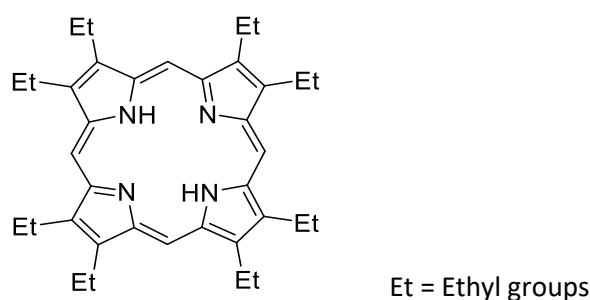
The introduction of a large aromatic solvate, as seen in XAGLOG (**5j**; anthracene) and XAGMAT (**5k**; pyrene), within the crystal structure yields similar D_{oop} values (0.218 Å and 0.258 Å, respectively) to the non-solvated TPPs. However, when looking at the specific distortion modes, a clear shift of preference from the $wav(x)$ to the $wav(y)$ mode is seen by the inclusion of a large aromatic solvent. These aromatic solvents give $wav(y)$ distortions of 0.176 Å in **5j** and 0.215 Å in **5k** and a $wav(x)$ distortion of 0.129 Å in and 0.143 Å, respectively.

The *oop* distortions give a good pictorial overview of how solvent effects influence the tetrapyrrole's conformation. However, a complete overview of the 3D configuration in TPPs is not obtained without discussing the in-plane (*ip*) distortion as well. The largest *ip* contribution to the TPP structure comes from the *bre* mode of *ip* distortion. This mode measures the total compression and stretching in the 24-atom tetrapyrrole ring. The TPP series contains a range of *bre* NSD values between 0.158 – 0.226 Å and from these values, there does not seem to be a correlation associated with the presence of a solvent in the unit cell. Other smaller contributions in this free base TPP series include *m-str* and *N-str* with a range of 0.04 – 0.056 Å in *m-str* and -0.042 to 0.053 Å in *N-str* (absolute values given). The smallest contribution seen is given by the *rot* mode. There is little to no *trn(x)* and *trn(y)* distortion in these TPP compounds. Therefore, this analysis proves that the small solvents can influence the macrocycle conformation due to intermolecular interactions resulting in a more planar *oop* conformation. The D_{oop} range is narrow in the TPPs with either no solvent or a large solvent incorporated into the 3D structure. In these types of TPPs, a clear preference of $wav(x)$ over $wav(y)$ distortion is clearly shown. However, in the *ip* distortion, no solvent effects are visible and the NSD values appear to be low, which is characteristic for TPP.

Overall, they are noticeably planar compounds and they have overall *oop* distortions (D_{oop}) ranging from 0.015 – 0.269 Å. The only significant *oop* distortion modes associated with these TPPs are the degenerate $wav(x)$ and $wav(y)$ distortion modes. Small solvents can influence the macrocycle conformation due to intermolecular interactions resulting in a more planar *oop* conformation. However, in the *ip* distortion, no solvent effects are visible and the NSD values appear to be generally characteristic for TPP.

4.1.2 2,3,7,8,12,13,17,18-Octaethylporphyrin (OEP).

Two crystal species of OEP were considered, OETPOR10 (**6a**) and OKOQUA (**6b**).²⁵ The structure of **6a** contains no solvent in its crystal structure and it has a slightly staggered end-on packing system via the β -ethyl groups (ethyl groups on Fischer's β -position of a porphyrin). The structure of **6b** contains a tetracyanoquinodimethane solvent within the unit cell.



	CCDC	Colour	Solvent
6a	OETPOR10	Blue	No solvent
6b	OKOQUA	Orange	Tetracyanoquinodimethane

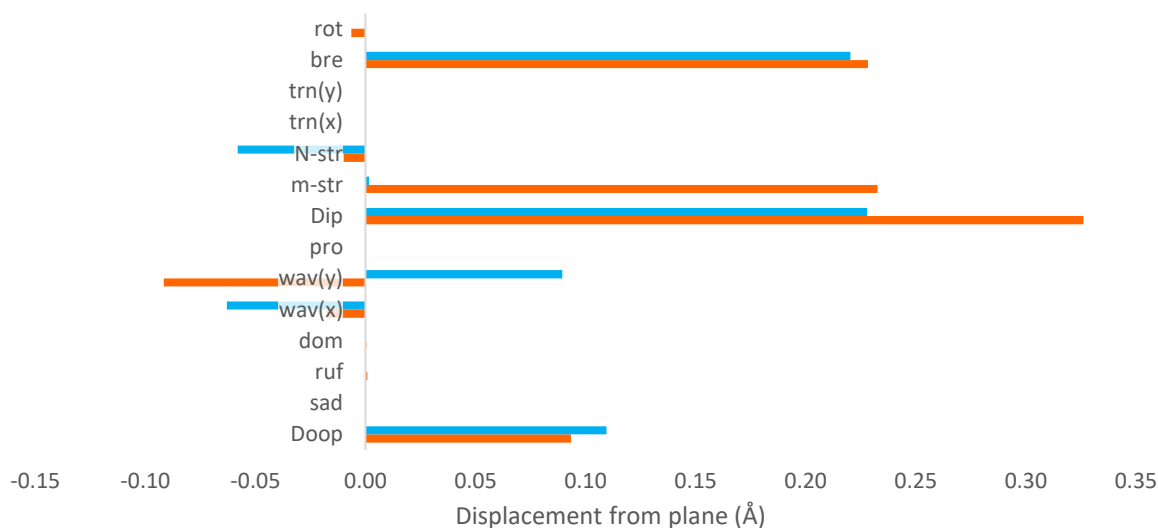


Figure 4 (Top): OEP (**6**) and table containing CCDC reference, colour in NSD analysis (below) and solvent in the unit cell. (Bottom): NSD analysis of the X-ray crystallographic structures of the OEP compounds listed in the table above.

The solvent in **6b** occupies a cavity in between two porphyrins. There is evidence of π -stacking between the porphyrin and the conjugated solvent (3.529 Å plane centroid to plane centroid distance). This plays a small role in changing the

packing system as it increases the mean plane distance of each porphyrin from each other by 3.616 Å. Therefore, this creates a cavity for the solvent to occupy itself. However, the solvent appears not to have any significant impact on the overall NSD.

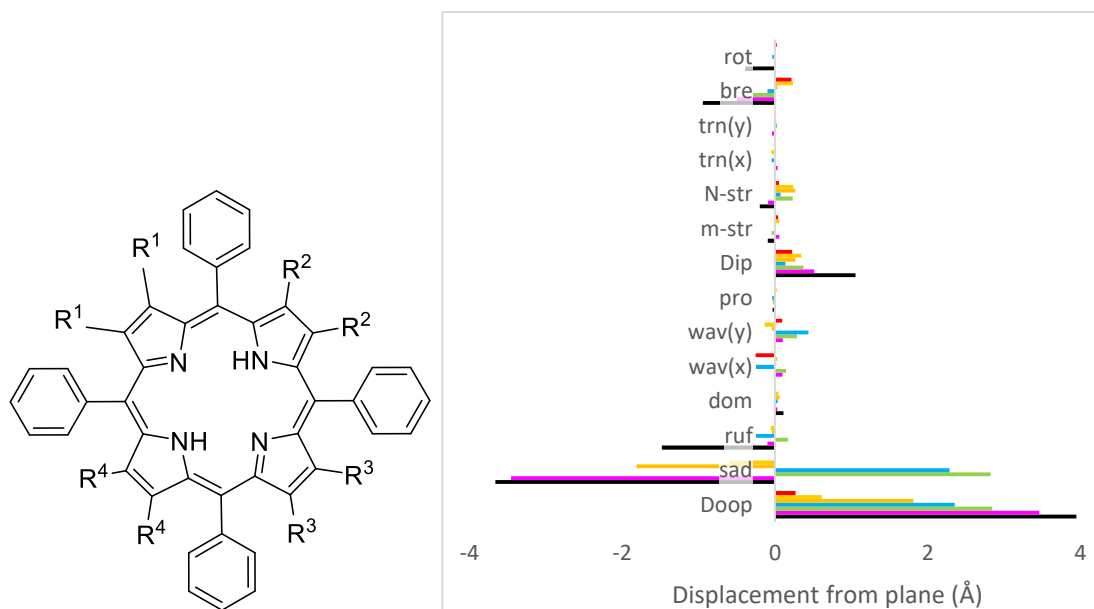
Both structures have very similar NSD profiles except the *wav(x)* mode of distortion, which is approximately three times larger in **6a** (-0.063 Å). Most of their *oop* distortions is given by *wav(x)* and *wav(y)* and they exhibit little contribution from *sad*, *ruf*, and *dom* distortion modes. For the *ip* distortion, NSDs indicate that there is very little contribution from *trn(x)*, *trn(y)* and *rot*. The main contribution derives from the *bre ip* distortion mode with values of approximately 0.220 Å. The most interesting distortion for these OEPs is *m-str*. For **6b**, the *m-str* deviation from the plane is greater than the non-solvated crystal structure by a factor of over 100 with values of 0.233 Å compared to 0.002 Å in **6a**.

4.1.3 *meso*-Tetraphenylporphyrins with graded degree of steric hindrance.

The next set of compounds, free base tetraphenylporphyrins with graded degree of β -ethyl substitution (**5**, **7-11**)^{26b,c}, shows the largest contrast within the series (XEtTPPs). For comparative reasons the TPP with the largest D_{oop} (**TPHPOR13**; **5h**) was chosen as a comparison for this discussion. By first looking at the D_{oop} of these compounds, there is a clear trend of increasing distortion (**11**>**10**>**9**>**8**>**7**>**5h**) (Figure 5).

Upon the addition of two ethyl groups to the β position (TATPOT01; **7**), there is almost a threefold increase in the D_{oop} . However, in the case where four ethyl groups are subject to a '*trans*' configuration (TATPUZ01; **8**) there is an increase of 1.198 Å. When four ethyl groups are substituted onto the β -position in a '*cis*' orientation (TATQAG01; **9**) there is an increase of 0.540 Å seen for the D_{oop} in this case. An almost identical increase occurs when six and eight ethyl groups are added to the periphery of the porphyrin macrocycle. These increases result in the highest D_{oop} being 3.949 Å. In the *sad* mode, the trend: **11**>**10**>**9**>**8**>**7**>**5h** is also evident. The distortion values are similar to that seen in the D_{oop} . This

indicates that the *sad* conformation has the largest contribution to the *oop* conformation and is most characteristic for this type of β -substitutions.



	CCDC	Colour	R ¹	R ²	R ³	R ⁴	Solvent
5h	TPHPOR13	Red	H	H	H	H	No solvent
7	TATPOT01	Yellow	Et	H	H	H	No solvent
8	TATPUZ01	Orange	Et	H	Et	H	DCM
9	TATQAG01	Blue	Et	Et	H	H	MeOH
10	TATQEK01	Green	Et	Et	Et	H	DCM
11	SATQOU	Magenta	Et	Et	Et	Et	EtOH
11a	QAWFIE	Black	Et	Et	Et	Et	DCM

Figure 5 (Top): XEtTPPs and the NSD analysis of the X-ray crystallographic structures of the XEtTPP compounds studied. (Bottom): Table that contains the CCDC reference code, colour corresponding to the NSD analysis (above), specific functional groups (**R¹-R⁴**) and solvent in the unit cell.

A similar trend to the above is observed for the *ruf* distortion mode with only a few exceptions: **7** possesses slightly more distortion than **8** and **9** is more distorted than TATQEK01 (**10**) and SATQOU (**11**). The similarities between this mode and the *sad* mode arises due to QAWFIE (**11a**) containing a significant *ruf* conformation. In the *dom* distortion mode, **11a** contains the highest *dom* distortion but there is no clear correlation between this distortion mode and the level of substitution in this series. The trend in this mode shows **8** possessing a higher *dom* conformation than **7**, which, in

turn, has more *dom* distortion than **9**, whose contribution to this mode is slightly higher than **10**. **9** and **5h** have almost no conformation in this mode. The structure of **5h** exhibits the largest *wav(x)* conformation which is almost identical to that of **9**. Porphyrin **9** contains the highest *wav(y)* distortion and **10** possesses the second highest *wav(y)* distortion in this series, while **11a** has no distortion in both these *wav* modes. This trend suggests an inverse relationship to the *wav* distortion modes and the overall non-planarity. The structure containing the lowest number of β -substitutions has the highest *wav(x)* contribution and the structure with the highest number of β -substitutions has the lowest *wav(x)* contribution. Interestingly, there appears to be a conformational relationship in the *wav(x)* and *wav(y)* distortion modes. The *trans* isomer **8**, shows a much larger contribution to both *wav(x)* and *wav(y)* distortion modes than its *cis* counterpart, **9**. For all the listed compounds, the contributions to the *pro* distortion mode appear to be quite negligible and no specific trend with regards to increasing β -substitutions is observed.

Clearly, as the number of β -ethyl chains increases, the more non-planar the compound becomes. This is due to an increase in the number of β -*meso* interactions, commonly known as *peri*-interactions.^{26d} The NSD also shows a shift in preference from *wav* to *sad* distortion. Moving onto the *ip* modes of distortion, the D_{ip} follows the reoccurring trend seen in the D_{oop} with a few exceptions. Porphyrin **9** has a lower D_{ip} than the TPP, **5h**, whose *ip* distortion is slightly lower than **8**. Less substituted porphyrin, **7**, being more distorted in the D_{ip} than **8**, is not as distorted as **10**. The next most distorted structure in this series is **11**. Moving onto **11a** involves a twofold increase in D_{ip} distortion. As, discussed in the TPP section, the D_{ip} distortion area is as significant as the D_{oop} .

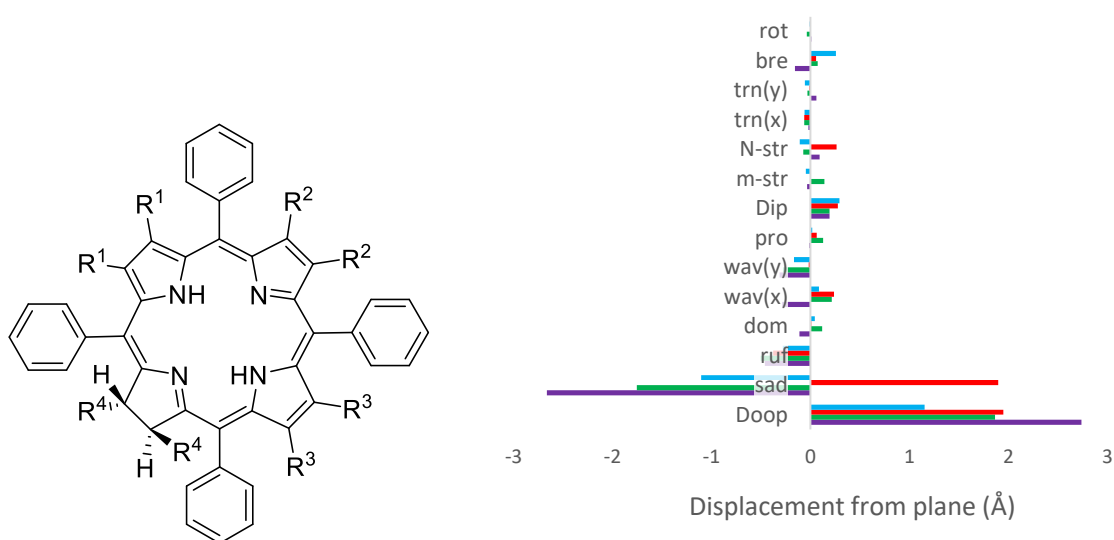
However, in comparison to the highly substituted porphyrin like **11a**, the D_{ip} modes, while still significant, appear to have less impact on the overall conformation. While **11a** contains the largest *m-str* distortion, the trend seen in the D_{oop} and *sad* mode is absent in this mode. The crystal species of porphyrins **8** and **9**, contain almost no *m-str* distortion. **5h**, **7**, **10** and **11** contain a similar and significant *m-str* conformation that are roughly half the distortion observed in **11a**. There is no trend observed in the *N-str* mode as the structure with the largest

distortion is **8**. This is closely followed by **7** and **10**. **11a** contains the next highest distortion and **5h**, **10** and **11** contain little to no distortion in this mode. The trend discussed in the *m-str* distortion is very similar to the *bre* distortion. **8** and **9** have the lowest degree of *bre* conformations. Structures **5h** and **7** have a slightly higher distortion than **8** and **9** in this mode and the structure with the next highest *bre* conformation is **11**. The structure of **12** has almost double the *bre* distortion seen in **10**. The contribution to this mode is then approximately doubled to get to the *bre* conformation in **11a**. For all the listed compounds, the contributions of *trn(x)* and *trn(y)* modes have very little input in the *ip* distortion. Similarly, the *rot* appears negligible with only compound **11a** showing any significant contribution. The *ip* distortions become less important as the number of β -substitutions increases as it appears to have less impact on the overall conformation.

This series presents an excellent example whereby increasing the steric bulk on the periphery of the porphyrin macrocycle, increases the distortion and the non-planarity of the structure and where this is reflected in significant differences in the NSD characteristics.

4.1.4 *meso*-Tetraphenylchlorins with graded degree of steric hindrance.

Chlorins related to the XEtTPPs are reflected in the XEtTPC series (Figure 6).²⁷ As seen in the porphyrin section, the higher number of ethyl groups on the β -carbons of the chlorin, the greater the planarity deviation from the macrocycle.







	CCDC	Colour	R ¹	R ²	R ³	R ⁴	Solvent
12	GELGUZ		Et	H	H	H	No solvent
13	GELJEM		H	Et	H	H	MeOH
14	GELQAP		H	H	Et	Et	DCM/MeOH
15	GELHAG		H	Et	Et	H	DCM

Figure 6 (Top): XEtTPC and NSD analysis of the X-ray crystallographic structures of the XETPC compounds listed in the table below. (Bottom): table containing CCDC reference, colour corresponding to the NSD analysis (above), specific functional groups (**R¹-R⁴**) and solvent in their unit cell.

GELGUZ (**12**) contains the smallest D_{oop} , GELJEM (**13**) has the second largest D_{oop} and the most interesting observation in the D_{oop} is that **13** (DEtTPC) has a larger D_{oop} than GELQAP (**14**; cis-TEtTPC). GELHAG (**15**; cis TEtTPC) contains the largest D_{oop} in the free base chlorins. The D_{oop} and *sad* distortion increase when the number of β -ethyl groups increase with the exception of **13** and **14**.

For the *ruf* distortion, a new trend is seen where **14** has a larger *ruf* than **15**. **15**, containing the second largest *ruf* conformation is then larger than **13**. **12** is the structure with the smallest *sad* and *ruf* distortion. In the *dom* distortion mode, the structures with the most *dom* distortions are the structures with four ethyl groups on the periphery of the chlorin heterocycle (**14**). **12** and **13** have a smaller *dom* distortion than **14** and **15**. The *wav*(*x*) distortion mode follows the same trend as the D_{oop} and *sad* as **15** has the largest distortion. **13** has the second largest distortion followed by **14** with the second smallest distortion and **12** has the smallest *wav*(*x*) distortion. The *wav*(*y*) mode follows a similar trend to the *dom* mode in these chlorins. **12** and **13** have the two smallest *wav*(*y*) conformations (**13** is the smallest). **14** and **15** contain the highest distortions in this mode (**15** is the highest). In the *pro* distortion mode, all contributions are negligible bar that of **14**. As seen in the porphyrin section, the higher number of ethyl groups on the β -carbons of the chlorin, the greater the distortion of the macrocycle.

Contrary to the *oop* modes of distortion in this series, the structures with the lowest number of ethyl groups on the β -positions have the highest D_{ip} . **12** and **13** have the highest D_{ip} whereas **14** and **15** have the lowest D_{ip} . Chlorin **13** contains the lowest *m-str* distortion. The structure with the second lowest conformation in this mode is **15**. The lesser substituted chlorin **12**, is slightly higher in terms of *m-str* distortion and **14** contains the highest *m-str* distortion as it is approximately

three times more distorted than **12**. The free base chlorin with the lowest *N-str* distortion is **14**. An addition of 0.020 Å to the *N-str* distortion yields the *N-str* distortion of **15**. **12** is slightly more distorted in this mode than **15**. Through the almost threefold increase of **12**'s *N-str* distortion, **13**'s *N-str* distortion is reached. In the *bre* mode, **13** and **14** is approximately three times lower than the *bre* distortion in **15**. DEtTPC **12** is almost 0.100 Å higher in its *bre* contribution than **15**. The *trn(x)*, *trn(y)*, and *rot* distortion modes appear to have no significant contribution to the 3D structures of these chlorins. Overall, the decrease in steric bulk, increases the *ip* distortion and there is no reduced bond placement effect on the *ip* modes.

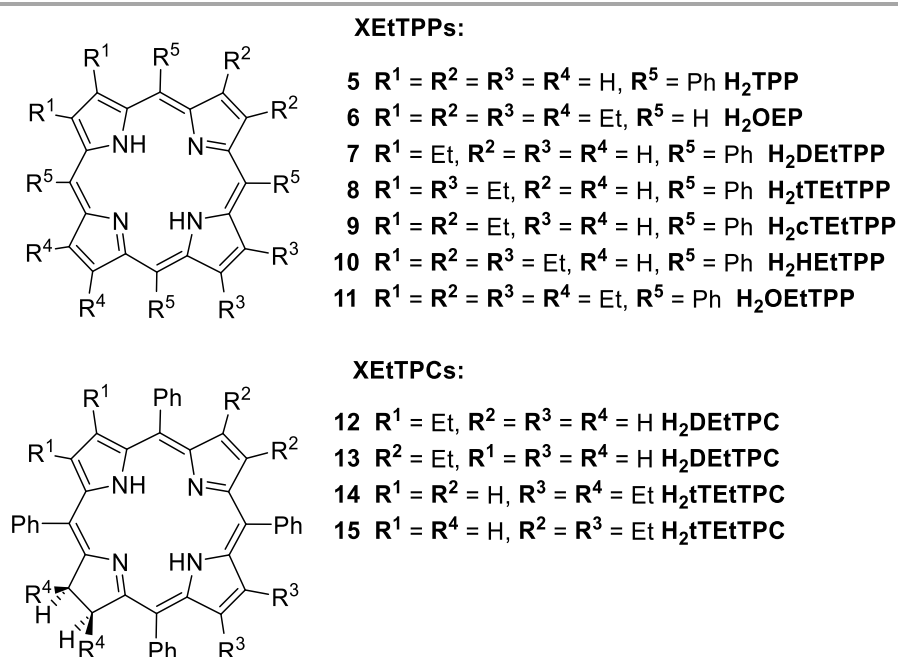
However, there is also a reduced bond placement trend observed in this section. This trend suggests that the further away the ethyl groups are from the saturated pyrrole, the more D_{oop} is present in the structure. For the *ip* modes the decrease in steric bulk increases the *ip* distortion and there is no reduced bond placement effect on the *ip* modes.

4.1.5 Impact of reduction on the distortion in the free base TETPCs vs TETPPs

The impact saturation of one ring has on the porphyrin macrocycle is of particular interest in the context of our discussion as this is one of the most convenient ways to induce ring distortions. In this case, a comparison between the XEtTPP and the XEtTPC series is illustrative. First we note, that in the diethyl-tetraphenylchlorin (DEtTPC) there are two known regioisomer crystal structures, the '*cis*' (**12**) and '*trans*' (**13**) to the reduced pyrrole ring (Scheme 1). These structures can be compared directly to the DEtTPP **7** to investigate the effect of reduction on the macrocycle. There is quite a significant trend in the D_{oop} where porphyrin **7** shows the smallest contributions, followed by **12** with an almost twofold increase and **13** has the largest D_{oop} . This trend is followed for both the *sad*, *ruf*, *wav(x)*, and *pro* distortion modes. However, in the *dom* and *wav(y)* distortion modes there is little to no contribution seen from the structure of **13**. In the *dom* distortion mode both compounds **7** and **12** are equal, but in the *wav(y)* compound **12**

shows a larger contribution. Overall, the reduced bond placement has a significant effect on the *oop* distortion.

Interestingly in the D_{ip} modes an inverse of the D_{oop} is evident; however, the difference between the values are much smaller. Compound **7** shows the largest D_{ip} followed by **12** and then **13**. The *m-str* distortion in **7** is greater than in **13** and **14**. The *N-str* mode is 0.136 Å larger in **8** than the absolute value of **13** while the deviation in this mode is 0.022 Å less in **8** compared to **14**. The *ip* distortions in the *trn(x)* and *trn(y)* mode are less in **8** than the chlorin derivatives. However, in the *bre* mode, **8** (0.235 Å) is more distorted than **14** (0.056 Å) but it is less distorted than **13** (0.257 Å). The final mode, *rot*, does not contribute very significantly to the overall distortion in these three compounds. Thus, the reduced bond placement seems to have an inverse effect on the *ip* distortions.



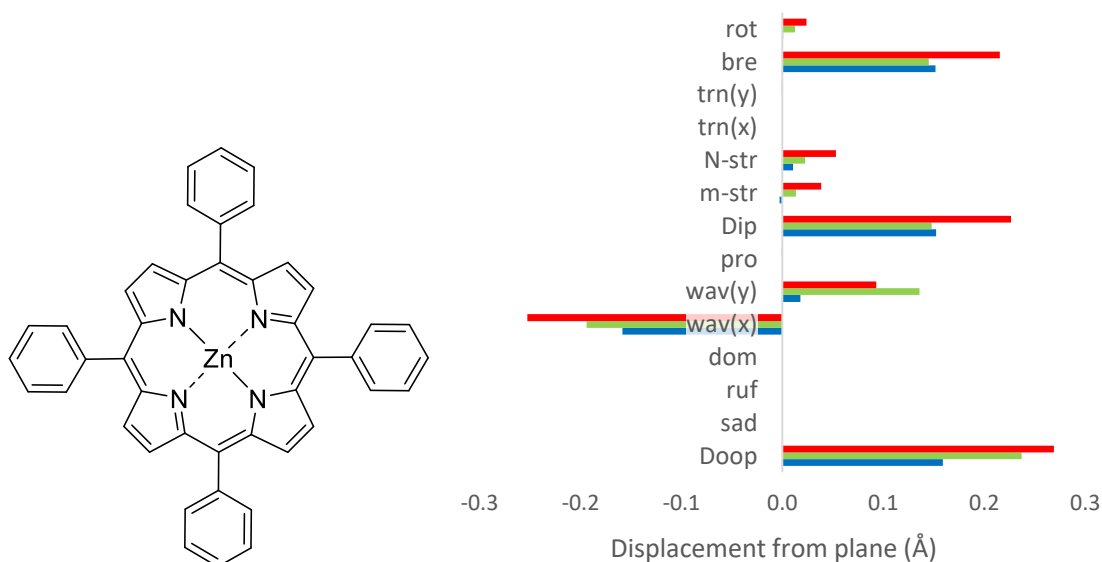
Scheme 1 Numbers of compounds and specific functional groups for the free base XEtTPPs and XEtTPCs.

4.2 Zinc(II) compounds

As many chlorophyll model studies utilize zinc(II) complexes, the available respective metalloporphyrins and –chlorins of the systems described above were analysed as well. The results of the analysis is described below.

4.2.1 Zn(II)TPP

The Zn(II)TPPs^{29, 31} have a slightly smaller deviation from the mean plane than the free base TPPs as shown by their D_{oop} values. ZZZTAY02 (**Zn5a**) and ZZZTAY03 (**Zn5b**), as with the free base TPP's there is little to no contributions to the D_{oop} with the only significant contributions found in the $wav(x)$ and $wav(y)$. Both Zn(II)TPPs were run at the solved at the same temperature. The crystal quality of Zn5a is better than that of Zn5b and accounts for the only noticeable difference between the two structures. There is a small decrease in the $wav(x)$ distortion mode in comparison to the TPP samples above and similar contributions found in the $wav(y)$. However, in the ip modes of distortion, there is a clear decrease in the distortion found in D_{ip} , $m-str$, $N-str$, bre , and rot distortion modes compared to the TPP's. No differences are observed for the $trn(x)$ and $trn(y)$. While the Zn(II) oop distortion is slightly less than that of the free base, there is a more notable difference in the ip distortion. While the crystal packing plays a role in the difference observed in distortion between the two sets of TPPs, the contraction of the Zn(II) metal in the core seems to be the main difference.



	CCDC	Colour
5h	TPHPOR13	Red
Zn5a	ZZZTAY02	Green
Zn5b	ZZZTAY03	Blue

Figure 7 (Top): Zn(II) TPP and NSD analysis of the X-ray crystallographic structures of the Zn(II) TPPs compounds and the freebase TPP (**5h**) listed in the table below. (Bottom): Table containing CCDC reference, colour corresponding to graph.

4.2.2 Zn(II)OEP

This next section comprises of the discussion of the NSD results of the Zn(II)OEPs ^{27b,32a} as well as comparing these results with the free base OEPs. The first observation is the inclusion of solvent appears to drastically increase the D_{oop} values as seen with OKOREL (**Zn6b**) with significant contributions seen in the *sad* mode. However, looking at the solvent-free structure of **6a** and ALOKOB (**Zn6a**), a slightly different trend is observed.

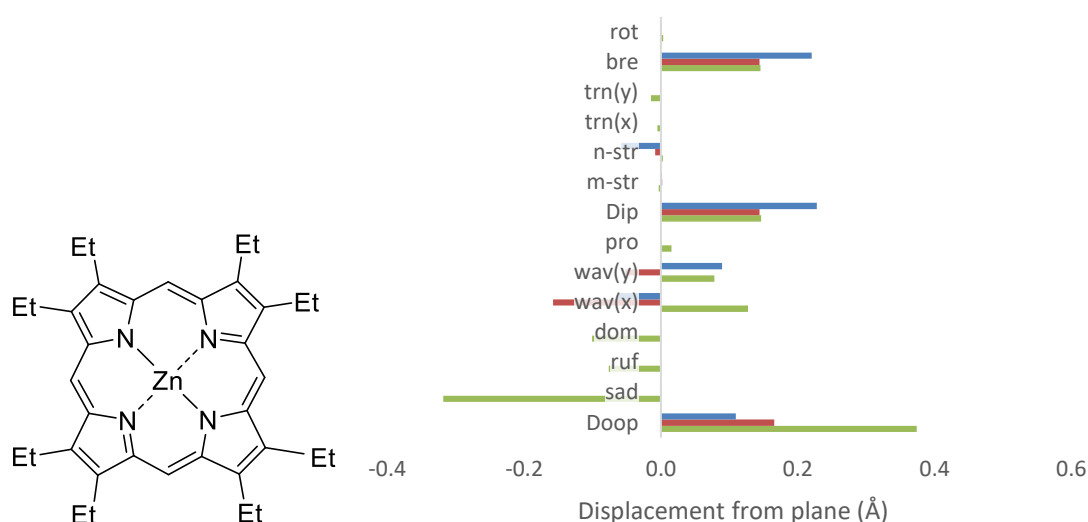


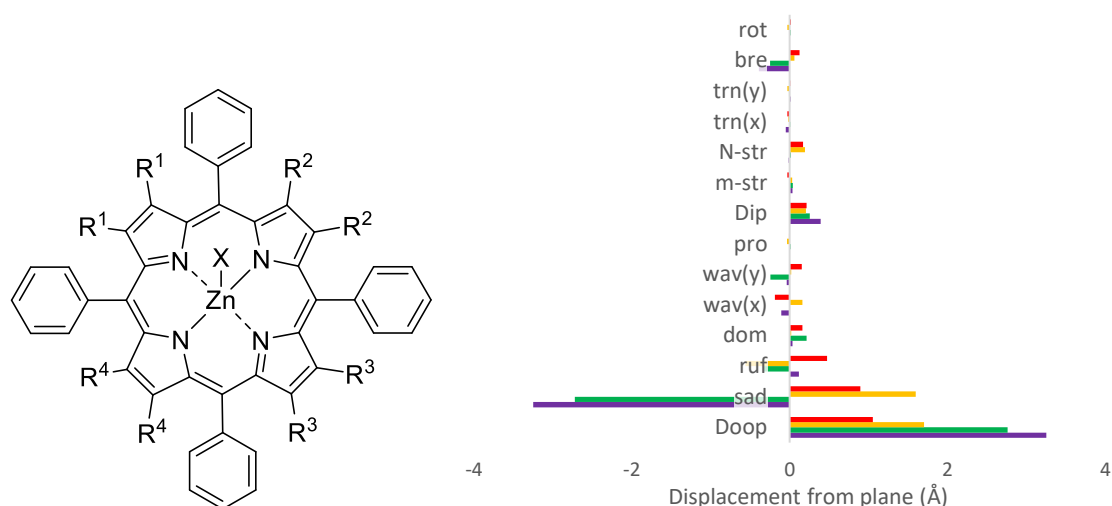
Figure 8 (Top): NSD analysis of the X-ray crystallographic structures of the Zn(II) OEPs compounds listed in the table below. (Bottom): Table containing CCDC reference for an OEP(**7a**) and Zn(II)OEP crystal structures, colours corresponding to NSD graph above and the solvent combined within the cell.

In general, there is a moderate increase in D_{oop} values which is a result of a significant increase in the *wav(x)* distortion mode values. This appears to be

coupled with a reduction in values of the *wav(y)* due to the inclusion of a Zn(II) metal centre into the core of the porphyrin. Secondly in the *ip* distortion modes, a decrease in values is observed as a result of Zn(II) inclusion to the core of the macrocycle. This appears to be independent of solvent effects as **Zn6a** and **Zn6b** have very similar overall values. Finally, it is noticed that the main distortion mode that affects this decrease is seen in the *bre* distortion mode. It represents the exact trend seen in the D_{ip} and the remaining *ip* distortion modes appear to have little to no effect. The only exception to this is seen in the *m-str* contribution of **Zn6a**. Overall, there generally seems to be an inverse relationship between the D_{oop} and the D_{ip} in the free base and Zn(II)OEPs. The free base OEPs have a smaller D_{oop} than the Zn(II) OEPs but they have a larger D_{ip} than the Zn(II) compounds. Therefore, the inclusion of a Zn(II) metal into the OEP core causes the macrocycle in this molecule to become more non-planar while reducing the *ip* distortion. This could be due to the fact that Zn(I) prefers to be in a tetrahedral geometry as opposed to square planar.

4.2.3 Zn(II)XEtTPP

When looking at the effect Zn(II) metal insertion has on more highly substituted systems, Zn(II)XEtTPPs (**Zn7–Zn11**)^{26b, 30b} shown in **Figure 7**. The Zn(II) complexes were compared to their free base counterparts (**7**, **8**, **10** and **11**). Taking the DEtTPP (**7** and **Zn7**), it is quite evident that a larger increase in D_{oop} is observed as a result of Zn(II) inclusion to the porphyrin core. This increase is the result of a general increase to all the *oop* distortion modes bar *pro*. The largest increases are seen in the *sad* and *ruf* distortion modes with the *dom* and *wav(x)* showing a more temperate increase in distortion. The increase in *dom* distortion is due to the presence of an axial ligand. The *wav(y)* only shows a minor increase in distortion. When looking at the *ip* distortion modes, it appears that the inverse happens here in comparison to the *oop*. There is a reduction in values in the D_{ip} , *m-str*, *N-str*, *trn(x)*, and *bre* distortion modes with the most significant deviations observed in the *N-str* and *bre* distortion modes. The increases of observed *trn(y)* and *rot* distortion modes are rather quite negligible.



	CCDC	Colour	R ¹	R ²	R ³	R ⁴	-X
Zn7	RUTNEZ		Et	H	H	H	3-methylpyridine
Zn8^a	RUTQAY		Et	H	Et	H	1-pyridine
Zn10	RUTRAZ		Et	Et	Et	H	None
Zn11^b	JICNIS		Et	Et	Et	Et	OCH ₃

Figure 9 (Top): Zn(II)XEtTPP series and NSD analysis of the X-ray crystallographic structures of the Zn(II)XEtTPPs compounds listed in the table below. (Bottom): Table containing CCDC reference, colour corresponding to NSD graph above, specific functional groups (**R¹-R⁴**), and axial ligand (X) attached to Zn(II) metal. ^aContains H₂O solvent. ^bContains MeOH solvent.

Moving to the tTEtTPP (**8** and RUTQAY; **Zn8**), the difference between the D_{oop} is rather less pronounced than in the DEtTPP above. A minor decrease is observed in the D_{oop} as a result of Zn(II) metal insertion to the porphyrin core. This is a result of a decrease in the *sad* character coupled with an increase in *ruf* and *wav(x)* character of the porphyrin macrocycle. The axial ligand does not seem to play a huge role here compared to the DEtTPPs as the *dom* distortion has decreased due to the Zn(II) metal and the axial ligand being inserted. In the *ip* distortion modes, there is only a moderate decrease in the D_{ip} as a result of Zn(II) metal insertion into the core of the porphyrin. This insertion results in a decrease in the *N-str* character of the porphyrin.

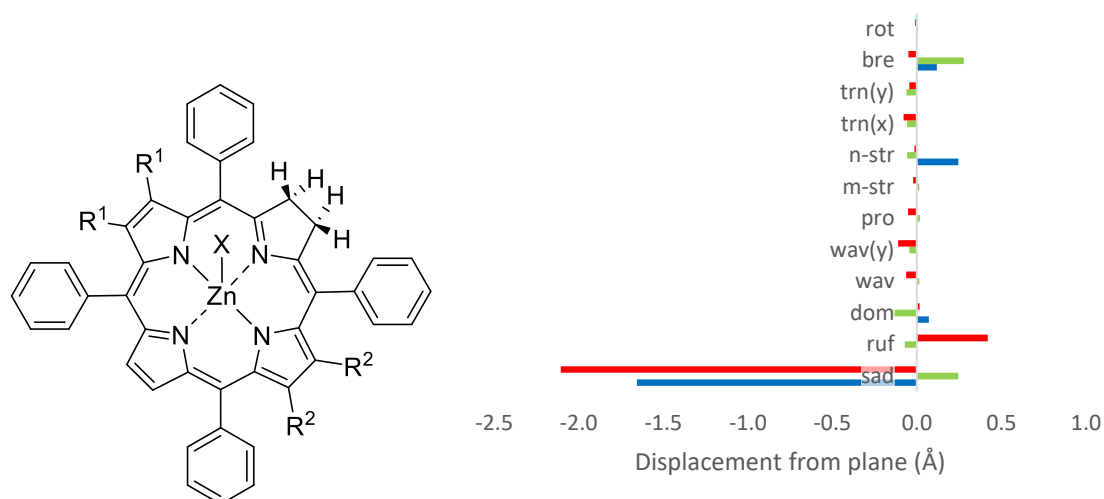
Looking at the HEtTPP porphyrin (**10** and RUTRAZ; **Zn10**), as with tTEtTPP above, there is only a small decrease in the D_{oop}. This stems from a moderate decrease in the *sad* and *wav(x)* distortion modes coupled with an increase of *ruf*

and *dom* character of these porphyrins. Similarly, there is a moderate decrease in the D_{ip} distortions due to a significant decrease in the *N-str* distortion mode. For the OEtTPP (**11** and JICNIS; **Zn11**) there is a moderate decrease in the D_{oop} due to a decrease in the *sad* and *wav(y)* distortion modes as a Zn(II) metal centre is inserted into the porphyrin. The rest of the *oop* distortion modes have little to no difference. The same result is seen here that was seen in the comparison between **8** and **Zn8** as the *dom* mode has decreased. In the D_{ip} , a moderate decrease is seen in its value as a result of the Zn(II) metal insertion. This is highlighted in the decrease seen in the *bre* distortion mode.

Overall, at small substitutions (DEtTPP) there is an increase in *oop* distortion when a Zn(II) metal centre is incorporated into the core. However, the opposite occurs in the *ip* distortion at this low substitution. As more ethyl groups are substituted onto the β -carbons of the Zn(II) porphyrins, there are decreases observed in both *oop* and *ip* distortions. The presence of an axial ligand only increases the *dom* distortion mode in the tTEtTPP (**8** & **Zn8**) and has no effect on the higher substitutions indicating no clear trend associated with the presence of axial ligands in these porphyrins.

4.2.4 Zn(II)XEtTPC

Similarly to the porphyrins, the Zn(II) metal in the core of the chlorins²⁷ increases the *oop* and decreases the *ip* conformations. GELJAI (**Zn12**) possesses the largest D_{oop} due to its large *sad* and *ruf* contributions as well as its significant *wav(y)* character. **13** has a slightly smaller D_{oop} which arises from its lesser *sad* and *ruf* distortions. **12** has the second smallest D_{oop} yet it has a large *sad* and a meaningful *ruf* and *wav(y)* conformations. GELQET (**Zn12a**) has the smallest D_{oop} which is almost 1.000 Å smaller than **13**. This large decrease is due to the axial ligand 'preventing' a large *sad* and shifting some *on* distortion to the *dom* mode by presumably electronic effects.



	CCDC	Colour	R ¹	R ²	X	Solvent
Zn12	GELJAI	Red	Et	H	-	No solvent
Zn12a	GELQET	Green	Et	H	Methoxy	DCM
Zn15	GELPIW	Blue	Et	Et	Methoxy	DCM

Figure 10 (Top): Zn(II)XEtTPC series and NSD analysis of the X-ray crystallographic structures of the Zn(II)XEtTPCs compounds listed in the table below. (Bottom): table containing CCDC reference code, colour corresponding to NSD graph (above), specific functional groups (**R¹-R²**), axial ligands (**X**) and solvent in their unit cell.

The *oop* distortion is almost inversely proportional to the *ip* distortion. GELJAI (**Zn12**) has a much lower D_{ip} than GELQET (**Zn12a**), **12** and **14**. **Zn12**'s *trn(x)*, *trn(y)* and *bre* distortions contribute to the structure's D_{ip} . **Zn12a** has the highest D_{ip} distortion due to its large *bre* and considerable *N-str* conformation whereas **14** has the second largest D_{ip} due to its the large *N-str* and *bre* character. The axial ligand in this case appears to greatly increase the *ip* distortion as well as decrease the D_{oop} . It is interesting to see the axial ligand cause an inverse relationship between the *oop* and *ip* conformations. The degree to which the axial ligand influences the 3D structure is already much clearer in the chlorins than seen in the porphyrin structures.

Upon increasing the number of ethyl groups on the periphery of these chlorins with a pentacoordinated metal centre (GELPIW; **Zn15**), the *oop* distortion increases. This is solely due to the *sad* distortion increasing. The *ip* distortion however slightly decreases and this is most likely due to the *ip* distortion shifting

from the *bre* mode to the *N-str* mode. It is clear once more, that upon the increase of ethyl groups on the periphery of the heterocycle, an increase is seen in the D_{oop} while a decrease is seen in the D_{ip} .

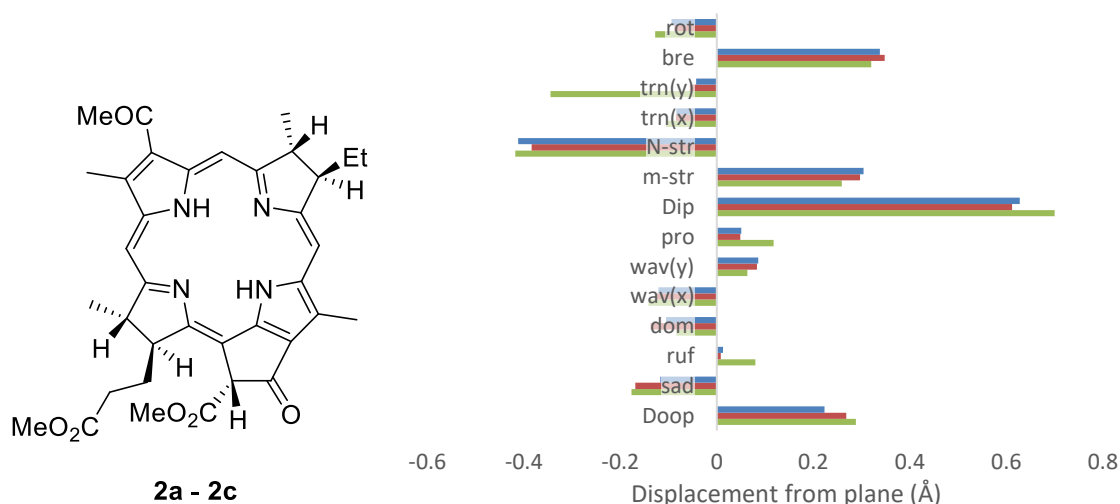
The most commonly observed conformations in metallated porphyrins and chlorins are *sad*, *ruf* and *dom*.²⁸ The Zn(II) complexes in particular, have shown to prefer pentacoordination, resulting in the coordination of axial ligands.²⁶ In some cases, there was not any degree of a *dom* configuration. Instead, there was a prominent *sad* or *ruf* distortion mode. The Zinc(II) metal insertion into the core also resulted in a decrease in the *ip* distortion due to the contraction of the Zinc(II)-N bond on the core.

4.3 NSD analysis of chlorophyll-related compounds.

Using the knowledge acquired in test cases, a conformational analysis of X-ray crystallographic structures that closely resemble chlorophyll was carried out next. A search of the Cambridge Structural Database^{20, 21} gave hits for 3 bacteriopheophorbides (related to bacteriochlorophyll a), 28 phytychlorins and 49 β -substituted chlorins. These three groups of compounds will be discussed in terms of their characteristic NSD profile and how the metal, peripheral substituents and other effects impact the observations of different conformations. The dimeric crystallographic structures that contained molecules of interest were omitted due to the lack of biological function of dimers in nature.

4.3.1 Bacteriochlorophyll a related structures

The structures of these freebase bacteriopheophorbide structures, WIKSEO, BAVSUM01 and BAVSUM (**2a-2c**)^{30a-30c} have small D_{oop} values in the range of 0.223–0.288 Å.



	Colour	CCDC	Solvent
2a	Blue	WIKSEO	-
2b	Red	BAVSUM01	C ₆ H ₆
2c	Grey	BAVSUM	C ₆ H ₆

Figure 11: (Top): Freebase Bacteriochlorophyll a and NSD analysis of the bacteriopheophorbide crystal structures listed in the table below. (Bottom): Table indicating the colour in the NSD graph (above), CCDC reference code and any solvent contained within the unit cell.

The D_{oop} distortions are representative of the *sad*, *dom* and *wav(x)* conformations. These contributions have a larger displacement than the main *oop* distortion mode (*sad*) in these bacteriopheophorbide compounds. These compounds possess larger D_{ip} than D_{oop} displacements (between 0.612–0.700 Å). This is the first example seen so far that the *ip* modes contribute a larger amount of distortion to the 3D structure than the *oop* conformations. The *m-str*, *N-str* and *bre* configurations are the most common in these three structures. The *ip* distortions are larger in structures **2a-2c**. The structures in Figure 11 are listed in order of increasing D_{oop} (**2a-2c**). The slight increase observed in the D_{oop} is due to the introduction of the benzene solvent to the unit cell.

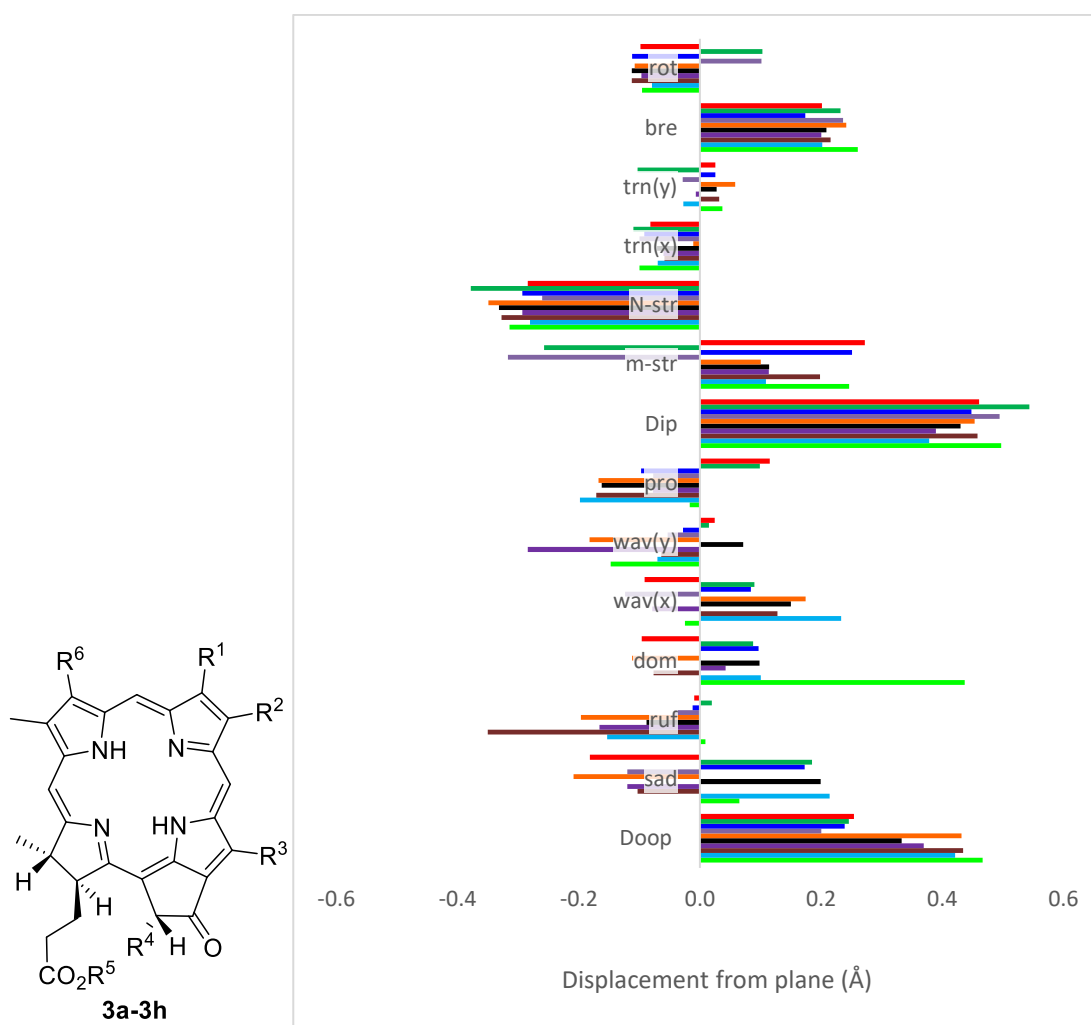
4.3.2 Phytochlorins

In this first section, the phytochlorins are separated into the free base, metal complexes and phytochlorin exceptions. The free base phytochlorins were separated into the following three sections — their structures are illustrated in Figures 12–16.

4.3.2(a) Free base phytochlorins

The phytochlorins, MPOPHA-BIXREF01 (**3a-3h**)³¹ possess D_{oop} values in the range of 0.201–0.467 Å. These are represented by large *sad* and *ruf* conformations as well as a *dom* conformation that is seen in one particular case (**3h**). The D_{ip} of the phytochlorins is in the range of 0.379–0.544 Å and possesses prominent *N-str* and *bre* character. The non-planarity in MPOPHA-MPOPHA03 (**3a-3c**) is contributed to the *sad* mode. In ROFVUE (**3d**), the inclusion of a CHO group at the β -position, R^1 (Figure 12), decreases the D_{oop} distortion by 0.053 Å compared to **3a** and also raises the D_{ip} . As the focus is shifted from the structures of **3a-3c** to the two independent molecules of BIPBOR (**3eⁱ** and **3eⁱⁱ**), a large increase in the D_{oop} is observed. A small decrease in the D_{ip} also occurs upon these functional group changes.

In **3f** (SOSZOP), the introduction of an acetyl group at the **R³** carbon of the phytychlorin decreases the D_{oop} and D_{ip} compared to the average of **3eⁱ** and **3eⁱⁱ**. This reduced distortion is visible *via* smaller contributions of all distortion modes bar *ruf*. The next pair of heterocycles to be discussed are the two independent molecules of BIPBIL (**3gⁱ** and **3gⁱⁱ**). The steric bulk of the alkyl chain at **R²** is increased from an ethyl to an *iso*-butyl group. The increase in electron density at this position increases the D_{oop} by a significant spike in *ruf* conformation. The D_{ip} is also increased by this change and stems from the large *m-str* character. The largest D_{oop} is observed in BIXREF01 (**3h**) and is surprisingly credited to the large *dom* contribution.



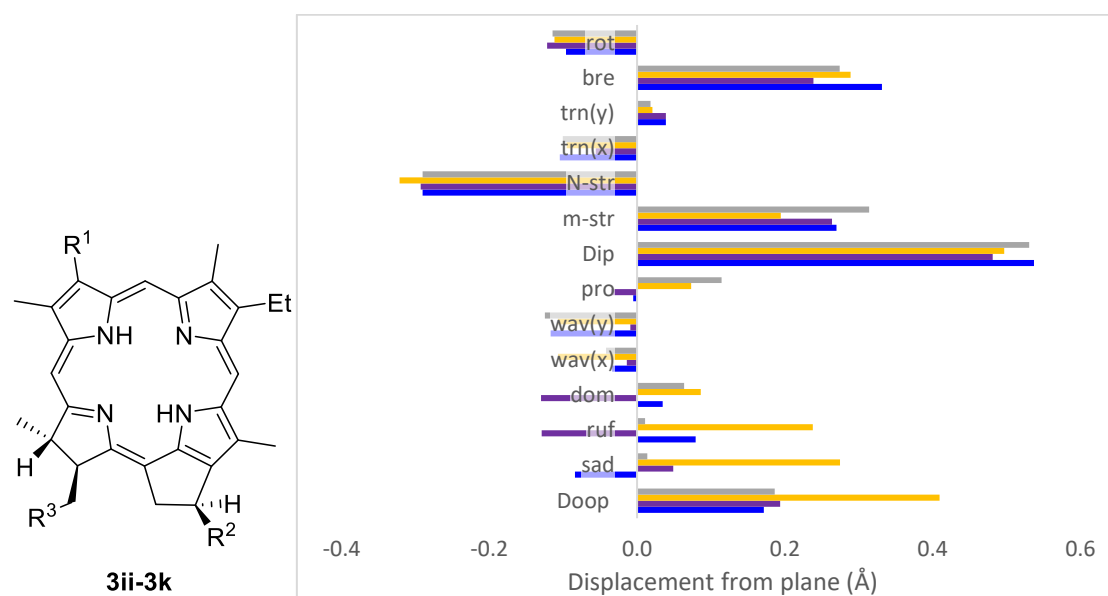
	CCDC	Colour	R ¹	R ²	R ³	R ⁴	R ⁵	R ⁶
3a	MPOPFA	Red	Me	Et	Me	CO ₂ Me	Me	Vinyl
3b	MPOPFA02	Green	"	"	"	"	"	"
3c	MPOPFA03	Blue	"	"	"	"	"	"
3d	ROFVUE	Yellow	CHO	"	"	"	Et	"
3e^{i*}	BIPBOR	Orange	Me	"	Et	H	Me	Et-2-ol

3e^{ii**}	" (N5-N8 ring)		"	"	"	"	"	"
3f	SOSZOP		"	"	OAc	"	"	"
3g^{i*}	BIPBIL		Me	ⁱ Bu	Et	H	Me	"
3g^{ii**}	" (N5-N8 ring)		"	"	"	"	"	"
3h	BIXREF01		"	CH ₂ ⁱ Bu	"	"	"	"

Figure 12: (Top): Free base phytychlorins (**3a-3h**) and NSD analysis of the X-ray crystallographic structures of the free base phytychlorins listed in the table below. (Bottom): Table indicating their CCDC reference codes, colour in the NSD graph (above) and specific functional groups (**R¹-R⁶**). *Superscript i: N1-N4 ring in crystal structure of the unit cell. **Superscript ii: N5-N8 ring in crystal structure of the unit cell.

4.3.2(b) Free base phytychlorins (continued)

The phytychlorins **3i-3k**³² in Figure 13 have a D_{oop} range of 0.172–0.410 Å and much larger D_{ip} values between 0.482–0.537 Å. These particular phytychlorins are characterised by a mixture of all possible distortion modes with the exception of **3iⁱ** being larger in distortion and characterised by large contributions from *sad* and *ruf* modes.







	CCDC	Colour	R ¹	R ²	R ³
3i^{i*}	RIWNIU		Et	H	Et
3ii^{**}	" (N5-N8 ring)		"	"	"
3j	KOVXUO		"	(C=O)	CH ₂ CO ₂ Me
3k	PEPJUR		3-OH-CF ₃ -ketone	"	"

Figure 13 Free base phytychlorins (**3i-3k**) and NSD analysis of the X-ray crystallographic structures of the free base phytychlorins listed in the table below. (Bottom): Table indicating their CCDC reference codes, colour in NSD graph (above) and specific functional groups (**R¹-R³**) in their unit cell. *Superscript i: N1-N4 ring in crystal structure of the unit cell. **Superscript ii: N5-N8 ring in crystal structure of the unit cell.

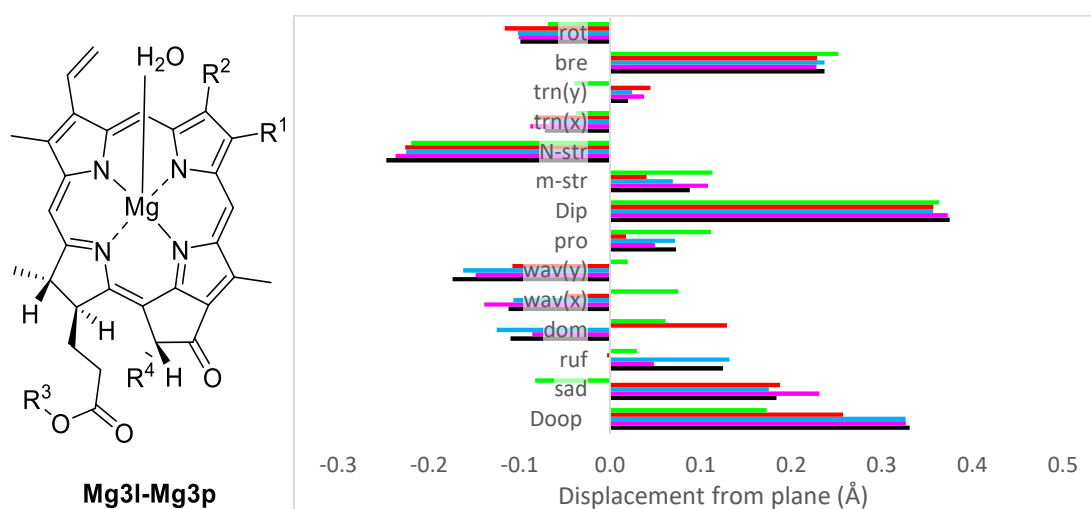
The *ip* distortion in these four compounds are represented by the *m-str*, *N-str* and *bre* contributions. The introduction of a carbonyl group at the **R²** position and an ester at the **R³** position as shown in Figure 13, decreases the *sad* and *ruf* conformations as shown in **3j**. A slight decrease in *ip* distortion is also seen as the *bre* character has decreased. The *sad*, *ruf* and *bre* decreases can all be due to the stretching induced by the alkyl and carbonyl planar intermolecular hydrogen bonds (C–H...O distance ranging from 2.483–2.514 Å). **3i** has a larger D_{oop} than **3ii** due to its larger *sad* and *ruf* character (Figure 13). This larger distortion arises from the β -substituents on the reduced pyrrole on the 24-atom mean-plane of **3i** participating in intermolecular hydrogen bonding. The large D_{ip} of **3i** and **3ii** is due to the intramolecular hydrogen bonding between the amine (NH₂) and imine (NH), resulting in the compression of the phytychlorin core. This results is unexpected as it would be hypothesised that these nitrogen atoms in **3k**, would create more intermolecular hydrogen bonds within the crystal packing system and therefore increase the molecule's non-planarity. In **3k**, the introduction of two oxygens and a CF₃ group decreases the D_{oop} . This is surprising as there are short non-classical intermolecular hydrogen bonding contacts between the methyl C-H of the methyl ester and the fluorines. However, this intermolecular bonding does not induce bending of the macrocycle. Overall, the structure of **3k** is the most planar structure of the phytychlorins **3i-3k**. It contains the highest *ip* distortion as the *m-str*, *N-str* and *bre* have become more distorted.

4.3.2(c) Metallated phytychlorins

The Mg(II) phytychlorins, (**Mg3l-Mg3p**)³³ (Figure 14) have D_{oop} values of 0.173–0.331 Å and a narrow D_{ip} range from 0.364–0.375 Å. They have prominent *sad*

distortions in the *oop* distortions and significant *N-str* and *bre* contributions to the D_{ip} . The order of increasing D_{oop} values is as follows: **Mg3l**, **Mg3m**, **Mg3n**, **Mg3o** and **Mg3p** (Figure 14). Mg(II) phytychlorin **Mg3l** obtains its non-planar character from the *pro* mode and the D_{ip} stems from contributions from the *m-str*, *N-str* and *bre* modes. The introduction of an acetyl group at the R^4 position instead of a hydrogen and changing the solvent from diethyl ether to water increases the D_{oop} of **Mg3m** by 0.085 Å and decreases its D_{ip} by 0.007 Å. The D_{oop} becomes larger because of the increase in *sad* and *dom* contributions. This decline in the D_{ip} is due to the smaller *m-str* and *bre* contributions.

Moving from **Mg3m** to **Mg3n**, the length of the ester chain on the reduced pyrrole substituted with an ethyl ester and the acetyl group at the R^4 position is replaced by an ester functional group. Thus, the structure of **Mg3n** experiences a significant *ruf* contribution. The D_{ip} remains the same and the *ruf* configuration arises due to the elongated ester's intermolecular hydrogen bonding on the reduced pyrrole. An aldehyde at the R^2 β -position instead of the methyl group creates the chemical structure of **Mg3o**. This structure only contains significant *sad*, *wav(x)* and *wav(y)* character. In terms of *ip* distortion, these changes in the structure increase the *m-str* and *N-str* character therefore generating meaningful *m-str*, *N-str* and *bre* conformations.



	CCDC	Colour	R ¹	R ²	R ³	R ⁴	Solvent
Mg3l	MPCHLM10	Red	Me	Me	Me	H	Et ₂ O
Mg3m	MCLPHD10	Green	Et	"	Me	COMe	H ₂ O
Mg3n	AECLPA01	Blue	"	"	Et	CO ₂ Me	"
Mg3o	ECPHBH	Magenta	"	CHO	Et	"	"

Figure 14: (Top): Mg(II)phytochlorins (**Mg3I–Mg5o**) and NSD analysis of the X-ray crystallographic structures of the Mg(II)phytochlorins (**Mg3I–Mg3p**) listed in the table below. (Bottom): Table indicating their CCDC reference codes, colour in the NSD graph above, specific functional groups (**R¹–R⁴**) and the solvents within their unit cells.

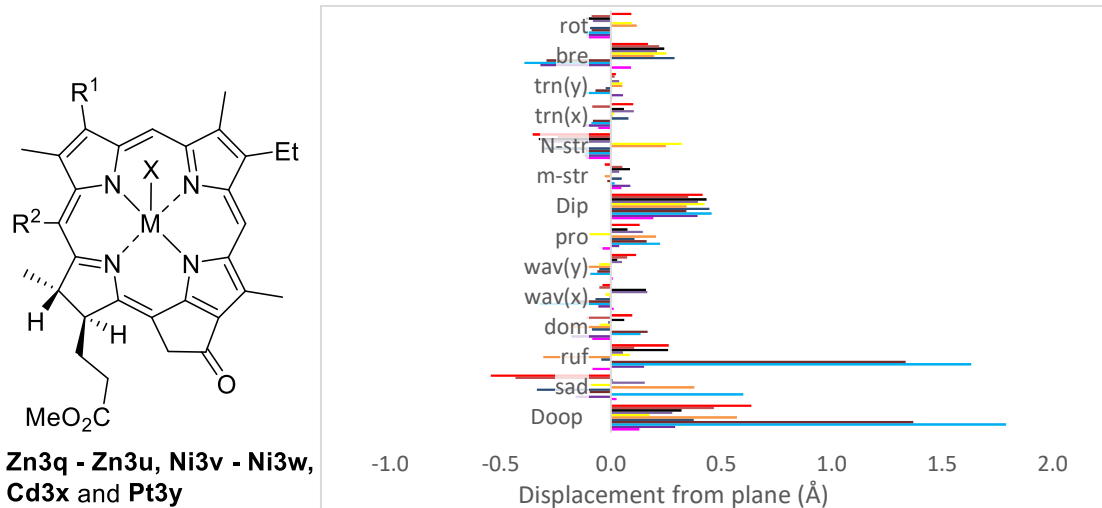
4.3.2(d) Metallated phytochlorins

The D_{oop} figures of the metallated phytochlorins in Figure 15.^{16, 34-36} exhibit a large range between 0.176–1.79 Å and contain significant *ruf* distortion. The D_{ip} of these compounds have a much narrower range (0.192–0.456 Å) and is represented by the significant *N-str* and *bre* character. CELRIU (**Zn3q**) has a D_{oop} of 0.636 Å and has large *sad* and *ruf* contributions as well as significant *wav(y)* character. The *N-str* contribution is the largest to the D_{ip} . The axial ligand stabilises lewis acidity of the Zn(II) metal and thus moving the Zinc and the nitrogen atoms out of the plane of the phytochlorin. The substitution of the hydroxylamine at the **R¹** position (Figure 15) for an acetyl group decreases the D_{oop} of MEHGUD (**Zn3r**) by 0.169 Å and the D_{ip} by 0.066 Å. The decrease in D_{oop} is highlighted by the decrease in the *sad*, *ruf* and *pro* modes. The decline in the D_{ip} is illustrative of the reduction in the *N-str* conformation. The removal of two hydrogen bond donors and the introduction of one hydrogen bond forces the macrocycle to be more planar while the contraction of the core by the Zn(II) metal is responsible for the D_{ip} difference between **Zn3q** and **Zn3r**.

A similar intramolecular metal-axial ligand bond exists in the first independent molecule of XOKGOV (**Zn3sⁱ**) as observed above. In this case, a nitrogen atom of the phenylpyridinyl ligand coordinates to the Zn(II) metal of another molecule of **Zn3sⁱ**. On one hand, the D_{oop} of **Zn3sⁱ** is lower than the Zn(II) phytochlorins seen above (**Zn3q** and **Zn3r**) as there is a much lower *sad* contribution. On the other hand, the D_{ip} is the highest of the phytochlorins encountered thus far due to the higher *N-str* and *bre* configurations. The nitrogen containing peripheral substituent that coordinates as an axial ligand to the Zn(II) metal is changed to a vinyl-pyridinyl group in the **Zn3tⁱ** and **Zn3tⁱⁱ** molecules of MIBJEO. The D_{oop} of

Zn3tⁱⁱ is 0.395 Å larger than that of **Zn3tⁱ**. The D_{ip} has decreased by 0.081 Å. The oxazole at **R¹** coordinates as an axial ligand to the Zn(II) metal through the nitrogen in the structure of ZOKMAP (**Zn3u**). This oxazole and toluene solvent slightly decrease the D_{oop} compared to **Zn3tⁱⁱ**. This decrease is shown by a slight decrease in *sad* and a large decrease in *ruf* and *dom* modes. The D_{ip} has increased however due to the bigger *N-str* and *bre* contributions.

The introduction of a methyl group to the *meso* position at **R²** in Figure 15 and changing the vinyl group at the β -position of **R¹** to an ethyl group increases the D_{oop} 0.421 Å in YOYAJ (**Ni3w**). The difference in D_{oop} values between HAHBAT (**Ni3v**) and **Ni3w** is because of the increase in *sad* and *ruf* mode. The D_{ip} of **Ni3w** has become higher compared to **Ni3v**. A Cd(II) metal in the core of the phytochlorin instead of a Ni(II) metal decreases the D_{oop} by an average of 1.58 Å (UMAZAJ; **Cd3x**). The structural changes result in a decrease in all of the *oop* modes bar the *dom* mode. The D_{ip} has also decreased which is highlighted by the smaller *bre* contribution. The D_{oop} and D_{ip} of KILQAZ (**Pt3y**) are smaller than those of **Cd3x**.



	CCDC	Colour	M	R ¹	R ²	X	Solvent
Zn3q	CELRIU	Red	Zn(II)	NOH	H	C=O	CHCl ₃
Zn3r	MEHGUD	Orange	"	CHO	"	(CH ₂) ₂ CO ₂ Me	CH ₂ Cl ₂
Zn3s^{i*}	XOKGOV	Black	"	4-ethynylphenylpyridine	"	pyr	Et ₂ O, THF
Zn3s^{ii*}	"	Yellow	"	"	"	"	"
Zn3t^{i*}	MIBJEO	Light Green	"	4-vinylpyridine	"	"	CH ₃ CN
Zn3t^{ii*}	"	Green	"	"	"	"	"






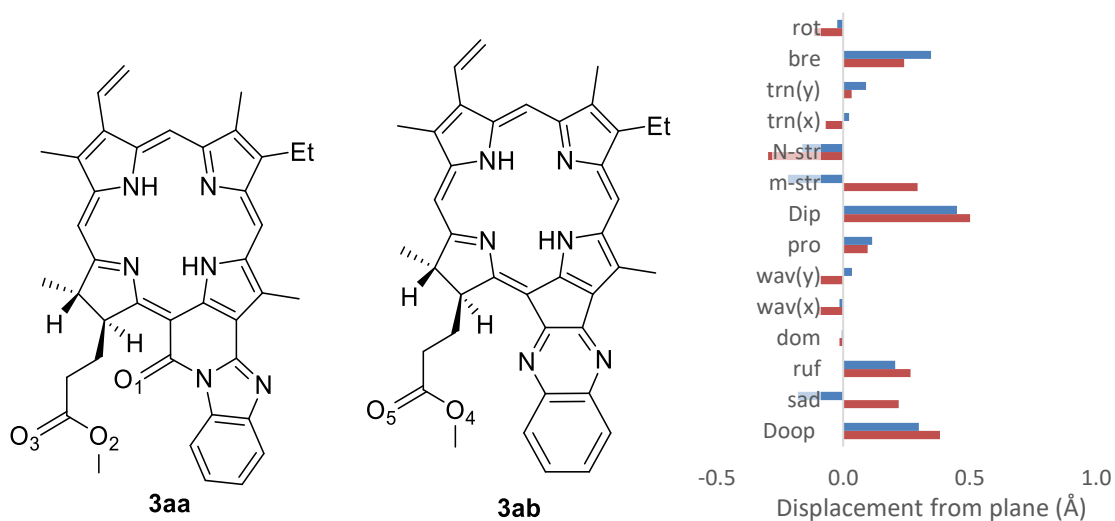
Zn3u	ZOKMAP		"	oxazole	"	oxazole	Toluene
Ni3v	HAHBAT		Ni(II)	vinyl	"	-	-
Ni3w	YOYAJ		"	Et	Me	-	-
Cd3x	UMAZAJ		Cd(II)	alcohol	H	-	-
Pt3y	KILQAZ		Pt(II)	Et	"	-	-

Figure 15 (Top): Metallated phytochlorins and NSD analysis X-ray crystallographic structures of the metallated phytochlorins listed in the table below. (Bottom): Table indicating CCDC reference code, colour corresponding to NSD graph above, metal (**M**) coordinated to the phytochlorin, specific functional groups (**R¹ -R³**), axial ligands (**X**) and solvent present in the unit cell. *Superscript i: N1-N4 ring in crystal structure of the unit cell. **Superscript ii: N5-N8 ring in crystal structure of the unit cell.

4.3.2(e) Free base phytychlorin exceptions



	Colour	CCDC
3z		FOXTUH
3aa		FOXWIY

Figure 16 (Top): Free base phytychlorin exceptions and NSD graph of the phytychlorin exceptions in the table (below). (Bottom): Table indicating the colours in the NSD graph (above) and the CCDC reference code.

The D_{oop} of FOXTUH (**3z**) is 0.084 Å less than FOXWIY (**3aa**).³⁷ The differing D_{oop} values can be attributed to O₁ on the fused ring in **3z**. The structures are less distorted in the *oop* modes and the *ip* modes have a more significant impact on the 3D structure as shown by the high *bre* values (Figure 16). Due to the structural diversity of these β-substituted chlorins (**4**) and the alternating reduced pyrrole's single bond location, these structures were divided into the following three sections: free base chlorins with no cyclic structure fused to the chlorin macrocycle (**free base chlorins**), metallated chlorins with no cyclic structure fused to the macrocycle (**metallated chlorins**) and chlorins with cyclic structures fused to the chlorin (**fused chlorins**). The latter two sections differ only by the presence of a metal. These sections are discussed below.

4.3.3 β-Substituted chlorins

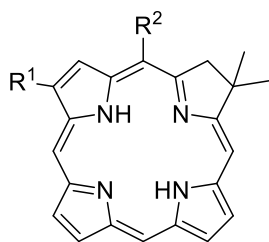
The following section discusses the β-substituted chlorins as photosynthetic agent derivatives. They are structurally similar to these agents due to their similar π-electrons in the chlorin core and the presence

of a ring fused to the macrocycle. This fused ring section of these chlorins explores the impact that changing this fused ring to the macrocyclic system has on the 3D structure. Whereas other sections explore the impact different metals, peripheral substituents and solvents have on structures with structurally similar parent compounds.

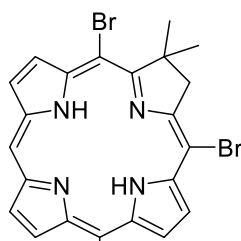
4.3.3(a) Free base β -substituted chlorins

The free base β -substituted chlorins PACRES-TIPBIF (**4a-4o**)³⁸⁻⁴⁸ in Figure 17 have a large range of D_{oop} values that range from 0.165–1.942 Å. The D_{ip} distortions in these chlorins have a smaller range between 0.199–0.509 Å. The main contribution to the D_{oop} is the *sad* mode while the main conformation in the D_{ip} is the *bre* mode.

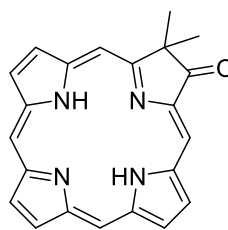
The structure of PACRES (**4a**) has small contributions to the D_{oop} and D_{ip} as there are only two ethyl groups on the periphery of the macrocycle. When a bromine atom is on the periphery as well as these ethyl groups (PACRIW; **4b**), the D_{oop} is increased by 0.125 Å. As seen in the test case, the more substituents on the periphery, the more *oop* distortion that is present. In the case of MUMGAD (**4c**) where there is an additional acetyl substituent on the periphery, there is no major change in the D_{oop} or D_{ip} as seen in the phytochlorins section. The structure of TACTID (**4d**) is similar to that of **4a-4c**. In **4d** though, there are 3 -substituents that greatly increase the D_{oop} and D_{ip} . The D_{oop} of **4d** is much larger than PACROC (**4e**) due to the higher number of peripheral substituents. The structure of **4e** is similar to that of **4a**, except **4e** has a carbonyl group on the reduced pyrrole next to the two ethyl groups. In comparison to **4a**, the presence of this carbonyl group appears to increase the D_{oop} by 0.109 Å in a much similar fashion to the oxygen containing phytochlorins and slightly decrease the D_{ip} by 0.029 Å. This increase in the D_{oop} is due to the rise in *ruf* character in the structure that is induced by intermolecular hydrogen bonding. The tetraphenyl chlorin derivatives (NOCGER, QAKLUJ and TIPBIF; **4m-4o**) have similar distortions, that have been previously seen in the test case.



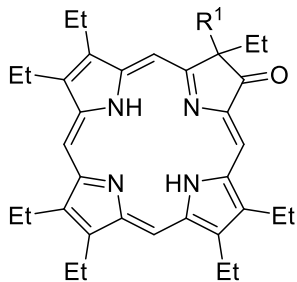
4a $R^1 = H, R^2 = H$
 4b $R^1 = Br, R^2 = H$
 4c $R^1 = COMe, R^2 = Br$



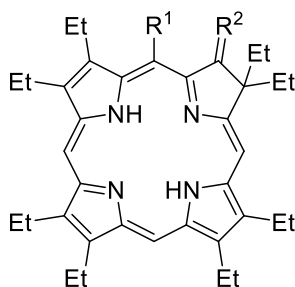
4d



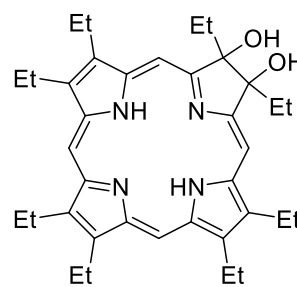
4e



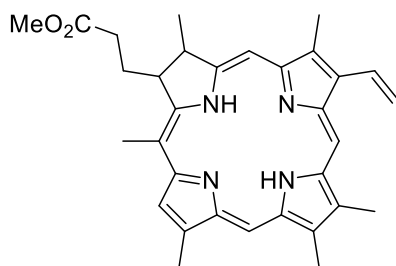
4f $R^1 = OH$
 4g $R^1 = Et$



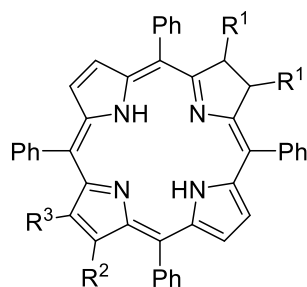
4hⁱ and 4hⁱⁱ $R^1 = H, R^2 = O$
 4i $R^1 = H, R^2 = N-OH$
 4j $R^1 = OCHO, R^2 = O$



4k



4l



4m $R^1 = CH(CN)_2, R^2 = R^3 = Br$
 4n $R^1 = nBu, R^2 = R^3 = H$
 4o $R^1 = CH(CN)_2, R^2 = NO_2, R^3 = H$

	CCDC	Colour	Solvent
4a	PACRES		-
4b	PACRIW		-
4c	MUMGAD		-
4d	TACTID		-
4e	PACROC		-
4f	WANDEX		-
4g	WANDAT		-
4h ^{i*}	WANBOF		-
4h ^{ii**}	" (N5-N8 ring)		-
4i	WANCAS		CHCl ₃
4j	WANCEW		"
4k	KOCZUX		MeCO ₂ Et
4l	PHLLCL10		-
4m	NOCGER		CHCl ₃ , MeOH
4n	QAKLUJ		DCM

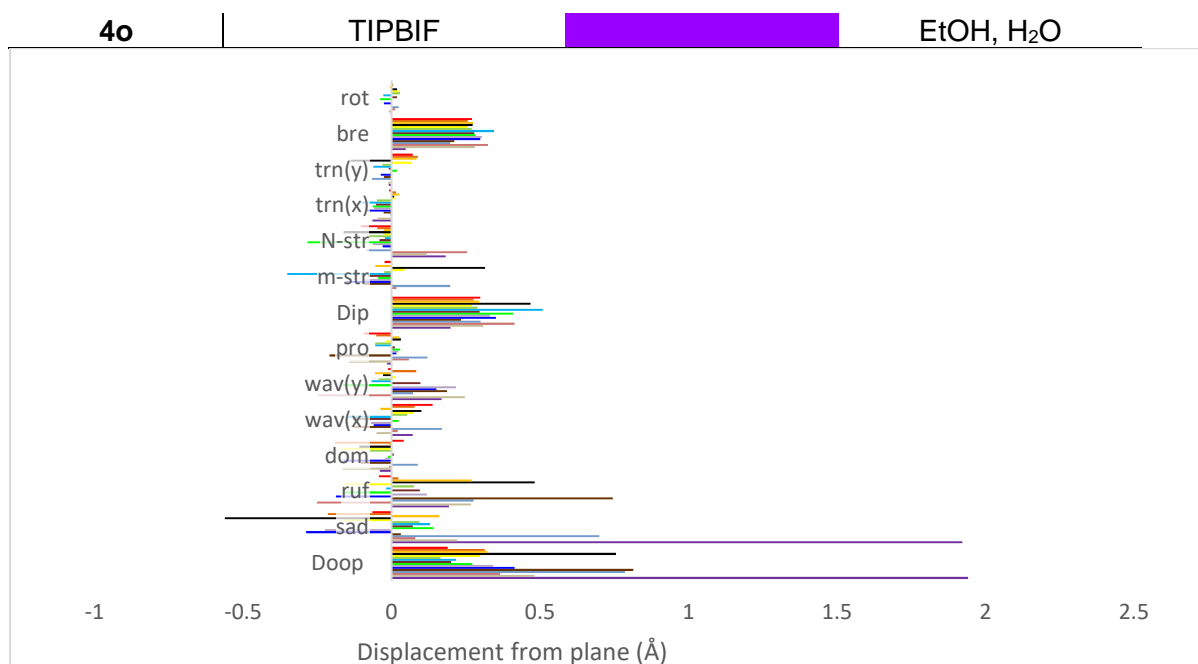


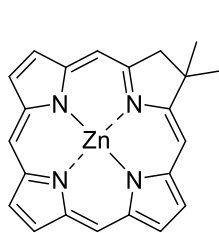
Figure 17 (Top): Free base β -substituted chlorins and table indicating CCDC reference code, colour in NSD graph (below) and solvent within unit cell. (Bottom): NSD analysis of the X-ray crystallographic structures of the free base β -substituted chlorins listed in the table above. *Superscript i: N1-N4 ring in crystal structure of the unit cell. **Superscript ii: N5-N8 ring in crystal structure of the unit cell.

4.3.3(b) M(II) β -substituted chlorins

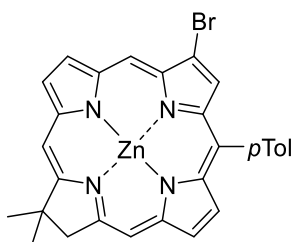
The D_{oop} of these metallated chlorins in Figure 18^{49–55} are in the range of 0.268–3.193 Å, which is the largest range observed so far. The main contributions are the *sad* and the *ruf* modes to the *oop* distortion. There is also a large D_{ip} range between 0.071–0.879 Å. The main contribution to the *ip* distortion is the *bre* mode. These are the largest ranges encountered thus far and already highlight the impact of metal insertion on the tetrapyrrole's conformation. The insertion of the Zn(II) metal into **4a** (yields, NIDFEM; **Zn4a**) slightly increases the D_{oop} due to the raise in *sad* contribution compared to the free base chlorin, but the largest difference is seen in the *dom* and *wav(y)* conformations. The D_{ip} however has slightly decreased upon metal insertion due to the contraction of the Zn(II)-N bond as shown in the test case.

The presence of a Fe(II) metal with a nitro group as the axial ligand (QUJZUQ; **Fe4h**) instead of a Zn(II) in the core, slightly decreases the D_{oop} but drastically reduces the ip distortion as the D_{ip} is 0.152 Å less in **Fe4h** compared to NIDFAI (**Zn6q**). In the first independent molecule of the structure with a CCDC reference code DOZVIX01 (**Ni4hⁱ**), a Ni(II) metal in the core increases the D_{oop} by 0.719 Å. This increase in non-planarity is solely due to the large *ruf* character as there is no *sad* nor *dom* contributions. In WANBIZ (**Ni4r**), the chemical differences between this structure and **Ni4hⁱ** are the presence of the hydroxylamine at the periphery instead of the oxygen as well as the switching of the ethyl groups and the sp^2 carbon location (Figure 18). The D_{oop} decreased by an average of 0.747 Å upon this transformation as the *sad* and *ruf* contributions decreased. Similar to **Fe4h**, the D_{ip} has dramatically decreased because of the small *bre* configuration.

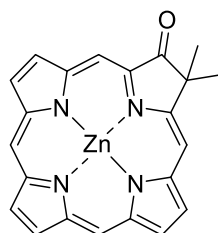
The structure of LAMDUZ (**Fe4g**) involves a Fe(III) metal in the centre of the chlorin with a chloride axial ligand. The Fe(III) metal, along with the axial ligand, increases the D_{oop} by 0.309 Å compared to **Ni4r**. The *sad* mode is the main configuration of the *oop* distortion and there are very similar contributions to the ip distortion that raise the D_{ip} by 0.050 Å. The structure of DOZVIX02, DOZVIX(N1-N4 ring) and DOZVIX(N5-N8 ring) (**Ni4g-Ni4gⁱⁱ**) are the Ni(II) β -substituted chlorins of the free base chlorin, **4g** (WANDAT). The D_{oop} is raised by 0.223–0.817 Å and the D_{ip} is lowered by 0.365–0.411 Å upon a Ni(II) insertion into the core of **4g**. The Ni(II) metal induces heightened *sad* and *ruf* contributions as well as a reduced *m-str* and *bre* contributions. Surprisingly, the structure of JUNZUN (**Ni4s**) has a lower D_{oop} than **Ni4g-Ni4gⁱⁱ** even though there are similar structures. The *sad* and *ruf* conformations have decreased and the D_{ip} is similar to **Ni4g-Ni4gⁱⁱ** as there are similar contributions.



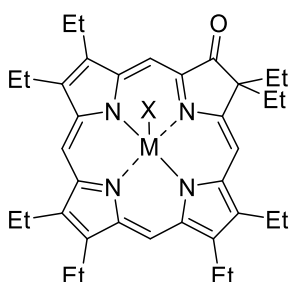
Zn4a



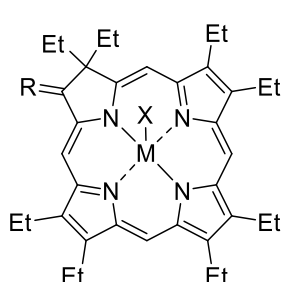
Zn4p



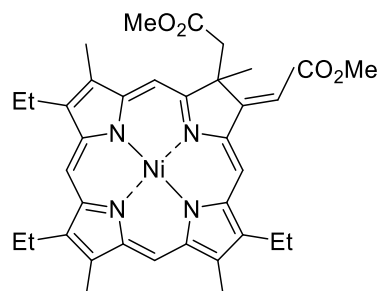
Zn4q



Fe4h, Ni4h^I and Ni4h^{II}



**Ni4r, Fe4g, Ni4g,
Ni4g^I and Ni4g^{II}**



Ni4s

	CCDC	Colour	Metal	R	Axial Ligand (X)	Solvent
Zn4a	NIDFEM		Zn(II)	-	-	C ₆ H ₁₂
Zn4p	XIPLEO		"	-	-	CHCl ₃
Zn4q	NIDFAI		"	-	-O=C	C ₆ H ₁₂
Fe4h	QUJZUQ		Fe(II)	-	-NO	CHCl ₃
Ni4h^I*	DOZVIX01		Ni(II)	-	-	-
Ni4h^{II}**	"		"	-	-	-
Ni4r	WANBIZ		"	NOH	-	C ₆ H ₁₄ , C ₅ H ₁₂
Fe4g	LAMDUZ		Fe(III)	-	-Cl	CHCl ₃
Ni4g	DOZVIX02		Ni(II)	-	-	-
Ni4g^I*	DOZVIX		"	O	-	-
Ni4g^{II}**	"		"	"	-	-
Ni4s	JUNZUN		"	-	-	MeOH

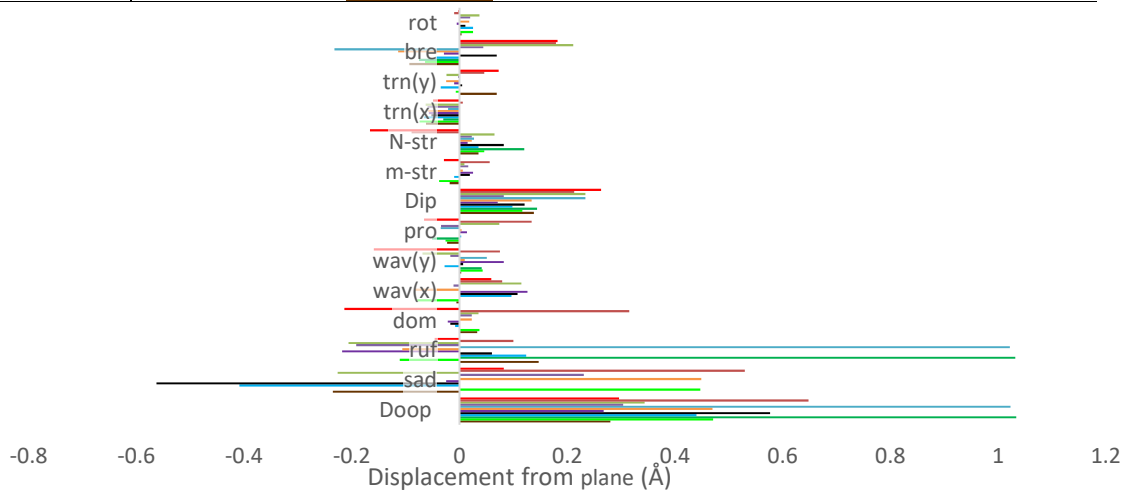
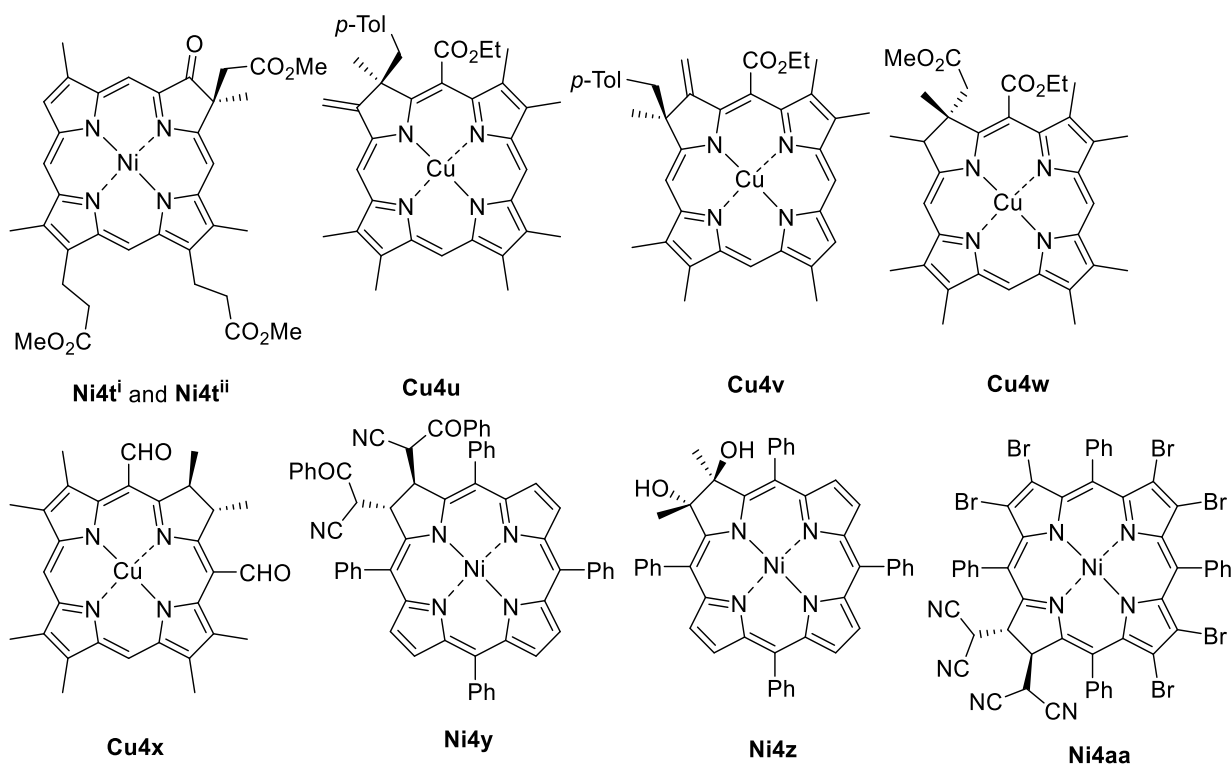


Figure 18 (Top): Metallated β -substituted chlorins and table indicating CCDC reference code, colour in NSD graph (below), metal in the chlorin core (**M**), functional group (**R**), axial ligand attached to the metal in the core and the solvent within the unit cell. (Bottom): NSD analysis of the X-ray crystallographic structures of the metallated β -substituted chlorins listed in the table above. *Superscript i: N1-N4 ring in crystal structure of the unit cell. **Superscript ii: N5-N8 ring in crystal structure of the unit cell.

The introduction of more polar peripheral substituents has increased the D_{oop} of the macrocycles of PASXEM(N1-N4 ring) and PASXEM(N5-N8 ring) (**Ni4tⁱ** and **Ni4tⁱⁱ**),⁵⁶ compared to **Ni4s** by 0.481 and 0.137 Å, respectively. These rises in the D_{oop} represent the increase in the *ruf* and *dom* conformations. These polar groups also increase the D_{ip} as there is a higher *bre* configuration in **Ni4tⁱ** and **Ni4tⁱⁱ**, according to the NSD profiles. The D_{oop} of NIJBUD (**Cu4v**) is 0.347 Å larger than that of NIJBOX (**Cu4u**).⁵⁷ The substituents around the ester group are the reason for this contrasting *oop* distortions. The D_{ip} of **Cu4v** is lower than the D_{ip} of **Cu4u** because of the lower *bre* distortion mode in **Cu4v**.

LICSEV (**Cu4w**)⁵⁸ has a slightly larger D_{oop} than **Cu4v** as the ester group on the reduced pyrrole induces a large *ruf* distortion that arises from intermolecular hydrogen binding. The D_{ip} has also been slightly enhanced due to the higher *m-str* and *N-str* configurations. The structures of LOGYAH (**Cu4x**)⁵⁹ and NOCGAN (**Ni4aa**)⁴² have large *sad* and *ruf* normal deformations. However, in the other two structures of XANDOI (**Ni4y**)⁶⁰ and ZAZNOF (**Ni4z**),⁶¹ this dramatic increase in distortion arises from solely from the large *ruf* conformation. To conclude however, a Ni(II) metal generally induces a large *ruf* conformation that is responsible for the large D_{oop} shown above. The D_{ip} of **Cu4x** contains little to no distortion compared to **Ni4y-Ni4aa** that all have large D_{ips} due to the extensive *bre* conformations present.



	CCDC	Colour	Metal	Axial Ligand (X)	Solvent
Ni4tⁱ*	PASXEM		Ni(II)	-	-
Ni4tⁱⁱ**	"		"	-	-
Cu4u	NIJBOX		Cu(II)	-	-
Cu4v	NIJBUD		"	-	-
Cu4w	LICSEV		Ni(II)	-	-
Cu4x	LOGYAH		Cu(II)	-	-
Ni4y	XANDOI		Ni(II)	-	-
Ni4z	ZAZNOF		"	-	-
Ni4aa	NOCGAN		"	-	CHCl ₃

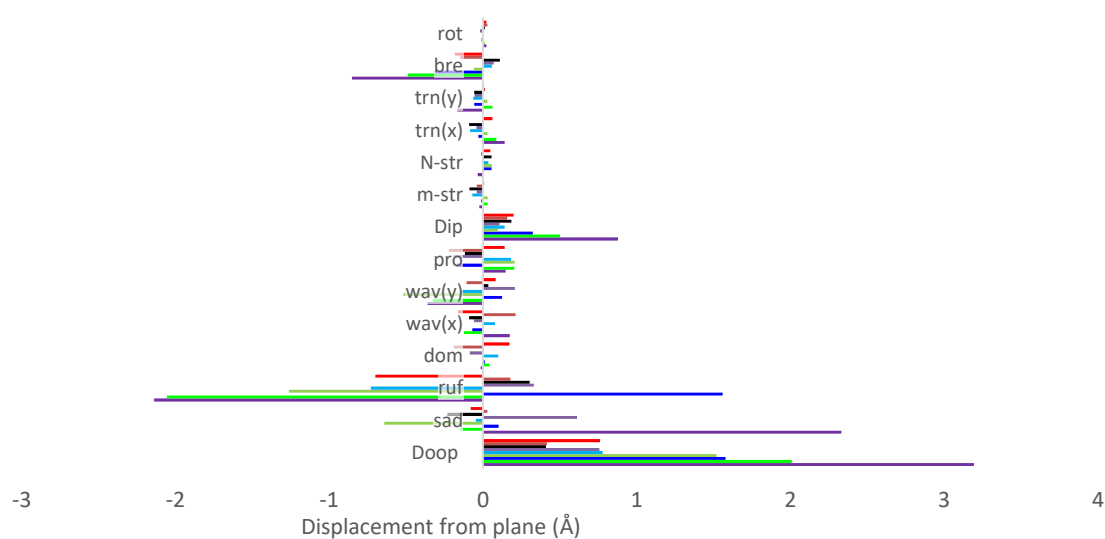


Figure 19 (Top): Metallated β -substituted chlorins and table indicating CCDC reference code, colour in NSD graph (below), metal in the chlorin core, axial

ligand attached to this metal and the solvent within the unit cell. (Bottom): NSD analysis of the X-ray crystallographic structures of the metallated β -substituted chlorins in this figure. *Superscript i: N1-N4 ring in crystal structure of the unit cell. **Superscript ii: N5-N8 ring in crystal structure of the unit cell.

Overall, the presence of a metal and an axial ligand in the core of the β -substituted chlorin increases the non-planarity. Depending on the metal and peripheral substituents, different *oop* and *ip* distortions can be also be observed and easily obtained.

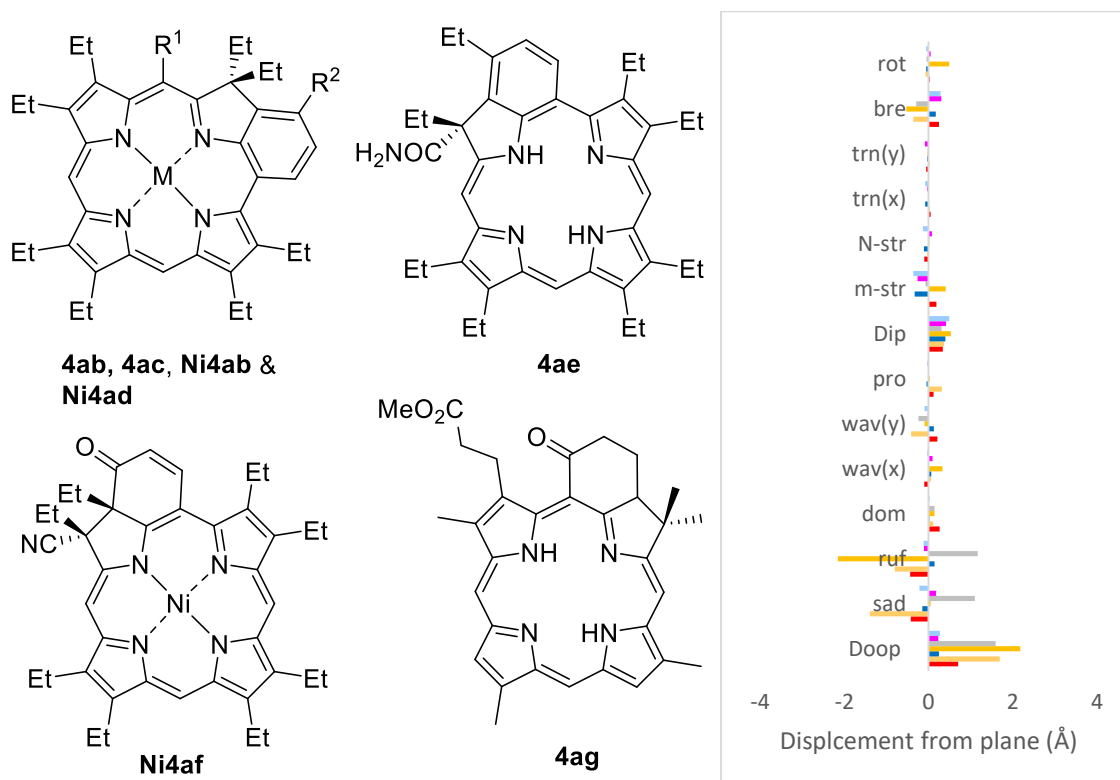
4.3.3(c) Fused β -substituted chlorins

The fused chlorins in this discussion are to be discussed due to the chemical structure's resemblance to chlorophyll related structures. They have the same number of π -electrons in the macrocycle. They also bear a ring that is fused to the periphery of the chlorin. It is a family of compounds that is worth discussing as the NSD profiles will demonstrate the conformational consequences of changing this fused ring on the periphery of this 16π tetrapyrrole, altering the nature of the peripheral substituent, the presence or absence of a metal in the core of the macrocycle, axial ligand effects and solvent effects have.

The D_{oop} values of these fused β -substituted chlorins (Figure 20 and 21) are in the range of 0.234–2.184 Å as well as D_{ip} values in a smaller range of 0.147–0.538 Å. The main contributions to the D_{oop} is *ruf* and the main conformation in the *ip* distortion modes is the *bre* mode. A fused benzene ring to the chlorin in JUNZIB (**4ab**)⁵⁵ yields a D_{oop} of 0.268 Å. The substitution of an ester onto the fused benzene in **4ab** yields the structure of QIRHEE (**4ac**).⁶² The resulting decreased D_{oop} and D_{ip} are caused by a lower *sad* conformation in the *oop* modes and a lower *m-str* conformation in the *ip* modes. In the structure of VUFTEV (**Ni4ad**),⁶⁴ the α,β -unsaturated aldehyde increases the D_{oop} of the structure even further than OEBPNI (**Ni4ab**)⁶³ due to peripheral interactions. These interactions thus cause a large *bre* conformation as there is significant expansion in the 24-atom mean-plane.

Using the structure of **4ab** as the parent compound, the substitution of an amide onto this structure instead of one of the ethyl groups adjacent to the benzene, as

well as placing an ethyl group on the benzene, results in an insignificant decline in the D_{oop} of XIXVAB (**4ae**).⁶⁵ There is a meaningful decrease in *sad* distortion and a rise in the *wav(y)* mode. The lesser D_{ip} represents a larger difference as the *bre* distortion decreases by 0.115 Å. The introduction of an amide slightly decreases the *oop* distortion and meaningfully decreases the *ip* distortion. Breaking the aromaticity of the fused ring to the chlorin is one reason for the large increase in the D_{oop} between **4ae** and XIXTUT (**Ni4af**).⁶⁵

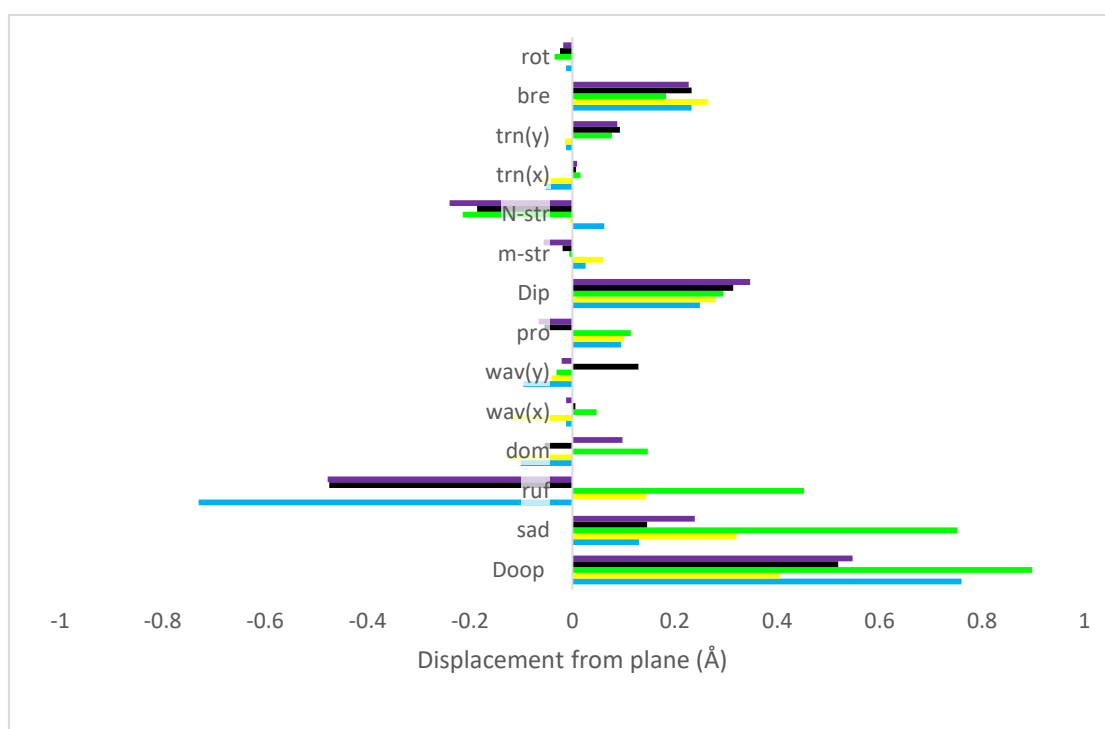
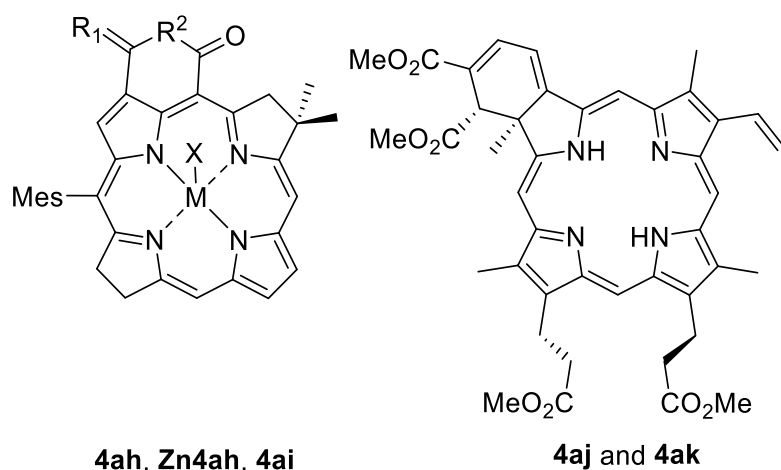


	Colour	CCDC	Metal (M)	Axial ligand (X)	Solvent	R ¹	R ²
4ab	Blue	JUNZIB	2H	-	-	H	H
4ac	Purple	QIRHEE	"	-	-	H	Ester
Ni4ab	Grey	OEBPNI	Ni(II)	-	-	H	H
Ni4ad	Yellow	VUFTEV	"	-	-	α , β -CHO	H
4ae	Dark Blue	XIXVAB	2H	-	-	-	-
Ni4af	Orange	XIXTUT	Ni(II)	-	-	-	-
4ag	Red	AHBONM	2H	-	-	-	-

Figure 20 (Top): Fused β -substituted chlorins and a table containing the colour corresponding NSD graph (below), CCDC reference number, metal in core (**M**), axial ligand attached to the metal (**X**), solvent in its unit cell and specific functional

groups (**R**¹ and **R**²). (Bottom) NSD analysis of the X-ray crystallographic structures of the metallated β -substituted chlorins listed in the table above.

Other reasons could be the changes in the peripheral substituents or the Ni(II) metal being introduced into the core. A cyclohexanone fused to a chlorin macrocycle with an ester and five methyl groups also substituted onto the periphery creates the structure of AHBONM (**4ag**).⁶⁶ In comparison to **4ae**, the D_{oop} has increased by 0.456 Å. The D_{ip} of **4ag** is 0.063 Å smaller than **4ae**. This is mainly due to the lesser *m-str* conformation observed in the packing system. In OJOXIV (**4ah**; Figure 21),⁶⁷ the polar iminopyranone fused to the free base chlorin generates a D_{oop} of 0.547 Å due to the moderate *sad* and large *ruf* conformations. This non-planarity is because of crystal packing interactions between the macrocycles and the cyclohexane solvent. The D_{ip} of **4ah** is slightly smaller than its D_{oop} (0.347 Å) and has meaningful *N-str* and *bre* configurations. The only structural difference between OJOXOB (**4ai**)⁶⁷ and **4ah** is that the **R**¹ substituent has a phenyl amine in **4ai** replaces the benzyl amine in **4ah**. These structural changes decrease the D_{oop} by 0.028 Å and the D_{ip} by 0.033 Å.

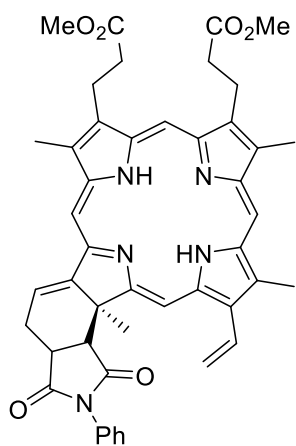


	Colour	CCDC	Metal (M)	Axial ligand (X)	Solvent	R ¹	R ²
4ah		OJOXIV	"	-	C ₆ H ₁₂	N-Bn	O
Zn4ah		OJOXUH	Zn(II)	THF	-	O	N-Ph
4ai		OJOXOB	2H	-	-	N-Ph	O
4aj		PIRCOI	"	-	-	-	-
4ak		PIRCIC	"	-	-	-	-

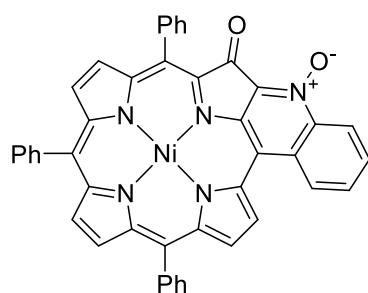
Figure 21 (Top): Fused β -substituted chlorins and a table containing the colour corresponding NSD graph (below), CCDC reference number, metal in core (M), axial ligand attached to the metal (X), solvent in its unit cell and specific functional groups (R¹ and R²). (Bottom) NSD analysis of the X-ray crystallographic structures of the metallated β -substituted chlorins listed in the table above.

The change in *sad* conformation in **4ai** makes the macrocycle more planar whereas the smaller *N-str* contribution from the core intramolecular hydrogen bonding, decreases the *ip* distortion. The main *oop* conformations observed in PIRCIC (**4aj**) and PIRCOI (**4ak**)⁶⁸ are *sad*, *ruf* and *dom*. Their sole contribution to the *ip* distortion is the *bre* mode. The fusing of a phthalimide species to a chlorin as well as the presence substitution of four methyl, two ester groups and a vinyl group (NEZLOV(N1-N4 ring) (**4alⁱ**) and NEZLOV(N5-N8 ring) (**4alⁱⁱ**)),⁶⁹ reduces the average *oop* distortion compared to **4aj** and **4ak**. The Ni(II) metal in the core of a quinolone oxide fused triphenylchlorin ((XUCBEE(N1-N4 ring) (**Ni4amⁱ**)) and (XUCBEE(N5-N8 ring) (**Ni4amⁱⁱ**)))⁷⁰ generates large *ruf* conformations as previously seen. Interestingly, the chlorin that has two rings fused to the macrocycle (YAQXET; **4an**)⁷¹ has slightly increased non-planarity compared to the free base chlorin that has only one ring fused to it (**4alⁱ** and **4alⁱⁱ**). The structures of YACGOB(N1-N4 ring) and YACGOB(N5-N8 ring) (**4aoⁱ** and **4aoⁱⁱ**)⁷² have *ruf* distortions due to the tetrafluoro-chromene annulated fused ring. They are more non-planar than a phthalimide fused ring to the chlorin macrocycle (**4alⁱ** and **4alⁱⁱ**) due to the ring as well as the sulfane's (**4aoⁱ** and **4aoⁱⁱ**) intermolecular interactions making increasing the *ruf* character in the structure. The structures also have meaningful *oop* distortion from the rest of the modes bar the *sad*. There is less *ip* distortion in these structures due to a small *bre* configuration.

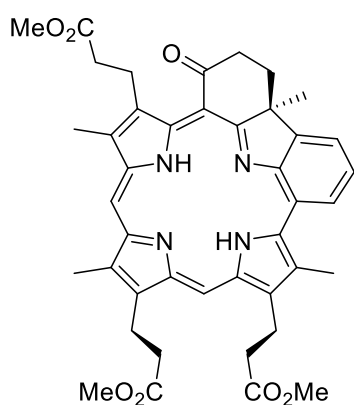
Overall, the non-planarity of these fused β -substituted chlorins depends on the metal in the core and the peripheral substituent. The fused rings make the chlorin macrocycle more planar as well as inducing specific conformations based on the ring's nature.



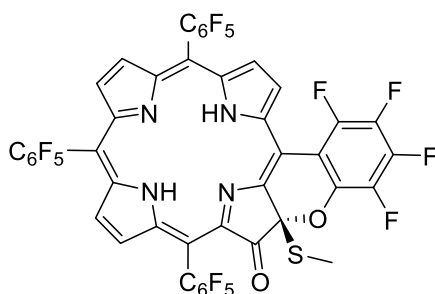
4alⁱ and 4alⁱⁱ



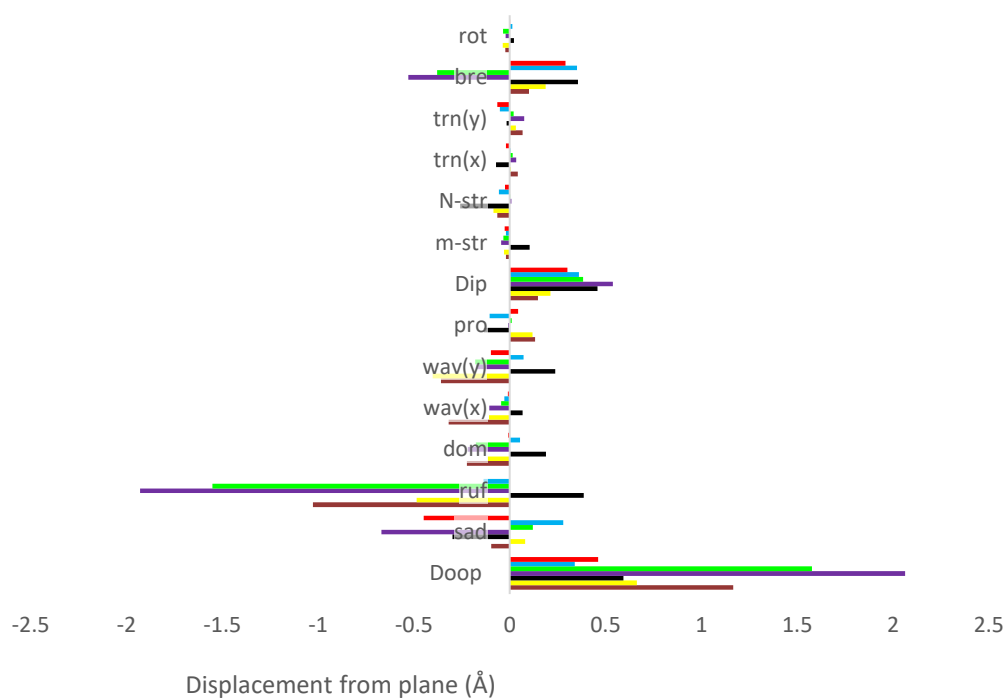
4amⁱ and 4amⁱⁱ



4an



4aoⁱ and 4aoⁱⁱ



Colour	CCDC	Metal (M)	Solvent
--------	------	-----------	---------

4al^{i*}		NEZLOV	2H	-
4al^{ii**}		"	"	-
Ni4am^{i*}		XUCBEE	Ni(II)	DCM, C ₅ H ₁₂
Ni4am^{ii**}			"	DCM, C ₅ H ₁₂
4an		YAQXET	2H	-
4o^{i*}		YACGOB	"	DCM, CH ₃ SH
4ao^{ii**}			"	DCM, CH ₃ SH

Figure 22: (Top): Fused β -substituted chlorins and NSD analysis of the X-ray crystallographic structures of the fused β -substituted chlorins listed in the table below. (Bottom): Table including colour of chlorin in NSD graph (above), CCDC reference code, metal in core of chlorin (**M**), the solvent and the specific functional groups (**R¹-R²**) in the unit cell. *Superscript i: N1-N4 ring in crystal structure of the unit cell. **Superscript ii: N5-N8 ring in crystal structure of the unit cell.

5. Conclusions and Future Work

In conclusion, the lack of peripheral interactions in TPPs and OEPs prevent any bending of the macrocycle and allows these structures to be quite planar. The increasing number of peripheral substitutions create nonplanar compounds as seen in the highly substituted porphyrins and chlorins. The presence of a Zn(II) metal centre influenced the *ip* modes of distortion more drastically than the *oop* distortion due to the Zn(II)-nitrogen bond contracting the macrocycle inwards.

In the chlorophyll derivatives, the *ip* distortions contribute more significantly to the 3D structure in the bacteriochlorophyll a related structures. Similarly, the free base phytychlorins have larger *ip* distortions than the *oop* distortions and in some cases, ester peripheral substituents on these structures are causing the structure to be planar *via* hydrogen bonding. In other cases, the intermolecular hydrogen bonding network created by the esters induces a large *ruf* conformation. Large *ip* distortions in the free base derivatives arise due to the hydrogen bonding within the macrocycle core. Inserting a Mg(II) metal into the phytychlorin core and attaching a water axial ligand to this metal slightly decreases the *ip* distortion compared to the free base. The *ip* distortion is still larger than *oop* distortion and

an interesting *dom* conformation is observed due to a solvent-axial ligand hydrogen bonding network. As esters are added to the periphery of the phytychlorin, the macrocycle becomes more non-planar as seen in the free base counterparts.

The presence of other metals in the core drastically increases the *oop* distortion of the phytychlorins. Overall, the presence of the metal in the core gives rise to different D_{oop} and D_{ip} distortions. Comparing the metallated phytychlorins with the free base phytychlorins, the presence of a metal in the core contracts the core and decreases the *ip* distortion. The *oop* distortion is in general increased due to the increased *ruf* normal deformation especially in the Ni(II) phytychlorin have the smallest *ip* distortion and the largest *oop* distortion of the whole phytychlorins. They phytychlorin exceptions have intramolecular hydrogen bonding and large π -extended fused rings that have lower *oop* distortion. The fused rings compress the structure to a significant extent that gives the macrocycle large *ip* distortion. The bacteriochlorophyll a related structures have a larger *ip* distortion than the phytychlorins. They are relatively planar compounds compared to the phytychlorins and the only difference between the three structures is the solvent-macrocycle interactions. The large *ip* distortion are the best representation of their 3D structure. To summarise the β -substituted chlorins, there was no trend in the *ip* distortion modes bar the fact that the majority of the structures have meaningful *bre* distortions. This would suggest that there is a moderate compression or expansion in the structure. With respect to the *oop* distortion, the metallated and more highly substituted (*meso*- and β -) chlorins are distorted. The metal derivatives were mainly represented by a large *ruf* distortion and sometimes a significant *sad* conformation. In the more highly substituted species, a large *sad* character was present in the structure.

Overall, this conformational analysis of well-studied porphyrins and chlorins, as well as chlorophyll related compounds, adequately describes the contributions that give rise to their 3D structure. The conformation varies depending on the metal in the core, axial ligands, peripheral substituents and solvent interactions. Without the small molecule crystal

structure of chlorophyll a (**1**, structure in introduction **1.1**), it is difficult to understand how chlorophyll's conformation contributes to its role in nature. However this analysis of structurally similar molecules (bacteriochlorophyll a-related structures, phytychlorins and β -substituted chlorins) provides the closest possible estimate of the macrocycle's biochemical role in nature. As mentioned by Fajer *et al.*, the protein environment 'helps control the macrocycle orientation and facilitates energetically favourable interactions by optimizing relative orientations of intermolecular short contacts to facilitate electron transfer'. In this context of this study, the packing system aids favourable macrocycle conformation that gives rise to the tetrapyrrole's function. Overall, the conformations arise to the protein's environment and indicate how the molecule is likely to carry out its specific biochemical function at an atomic level.

The overall goal for the future of this project is to create a NSD profile for a plethora of biologically relevant and chemically known macrocycles with known crystal structures. This will also further allow for further understanding of the chlorophyll's conformation towards its role by studying all of the possible conformations of tetrapyrrole's in nature. The next initial step would be to conduct a conformational analysis of chlorins, bacteriochlorins and isobacteriochlorins to observe the influence of further reduction, other peripheral substituents, metals and solvent on the macrocycle's configuration and how this contributes to the macrocycle's function. Specifically, how the conformational diversity alters the macrocycle's redox potential and light absorption properties by affecting the highest occupied and lowest unoccupied molecular orbitals of the protein chromophores. From this, further understanding will be available of the role in biochemical reaction mechanisms that these amazingly diverse molecules play in nature.

6 References:

- 1 M. O. Senge, A. A. Ryan, K. A. Letchford, S. A. MacGowan, T. Mielke, *Symmetry*, 2014, **6**, 781–843.
- 2 H. Scheer, *Chlorophylls*, CRC Press, Boca Raton, 1991.
- 3 A. A. Ryan, M. O. Senge, *Photochem. Photobiol. Sci.*, 2015, **14**, 638–660.
- 4 J. Deisenhofer, O. Epp, K. Miki, R. Huber, H. Michel, *Nature*, 1985, **318**, 618–624; G. McDermott, S. M. Prince, A. A. Freer, A. M. Hawthornewaite-Lawless, M. Z. Papiz, R. J. Cogdell, N. W. Isaacs, *Nature*, 1995, **374**, 517–521; P. Jordan, P. Fromme, H. T. Witt, O. Klukas, W. Saenger, N. Krauss, *Nature*, 2001, **411**, 909–917.
- 5 A. Forman, M. W. Renner, E. Fujita, K. M. Barkigia, M. C. W. Evans, K. M. Smith, J. Fajer, *Isr. J. Chem.*, 1989, **29**, 57–64; M. O. Senge, *J. Photochem. Photobiol. B: Biol.*, 1992, **16**, 3–36.
- 6 (a) E. B. Fleischer, *Acc. Chem. Res.*, 1970, **3**, 105–112; C. J. Medforth, M. O. Senge, K. M. Smith, L. D. Sparks, J. A. Shelnut, *J. Am. Chem. Soc.*, 1992, **114**, 9859–9869; M. O. Senge in *The Porphyrin Handbook*, ed. K. M. Kadish, K. M. Smith, R. Guilard, Academic Press, San Diego, 2000, Vol. 1, 239–347. (b) S. Fukuzumi, *Bull. Chem. Soc. Jpn.*, 2006, **79**, 177–195 (c) H. E. Toma, K. Araki, *Coord. Chem. Rev.*, 2000, **196**, 307–329. (d) W. R. Scheidt, Y. J. Lee, *Struct. Bonding*, 1987, **64**, 1–70.
- 7 M. O. Senge, *Chem. Commun.*, 2006, 243–256.
- 8 E. Gudowska-Nowak, M. D. Newton, J. Fajer, *J. Phys. Chem.*, 1990, **94**, 5795–5801.
- 9 M. O. Senge, S. A. MacGowan, J. M. O'Brien, *Chem. Commun.*, 2015, **51**, 17031–17063.
- 10 W. Jentzen, J. G. Ma, J. A. Shelnut, *Biophys. J.*, 1998, **74**, 753–763.
- 11 S. A. MacGowan, M. O. Senge, *Chem. Commun.*, 2011, **47**, 11621–11623.
- 12 D. Bednarczyk, O. Dym, V. Prabakar, Y. Peleg, D. H. Pike, D. Noy, *Angew. Chem. Int. Ed.*, 2016, **55**, 6901–6905.
- 13 (a) X. Z. Song, W. Jentzen, S. L. Jia, L. Jaquinod, D. J. Nurco, C. J. Medforth, K. M. Smith, J. A. Shelnut, *J. Am. Chem. Soc.*, 1996, **118**,

- 12975–12988; (b) C. Kratky, R. Waditschatka, J. E. Johansen, J. C. Plaquevent, J. Schreiber, A. Eschenmoser, *Helv. Chim. Acta*, 1985, **68**, 1312–1337.
- 14 M. O. Senge, S. A. MacGowan, in *Handbook of Porphyrin Science*, eds. K. M. Kadish, K. M. Smith, R. Guilard, World Scientific, Singapore, 2010, Vol. 13, 253–297.
- 15 K. M. Barkigia, L. Chantranupong, K. M. Smith, J. Fajer, *J. Am. Chem. Soc.*, 1988, **110**, 7566–7567.
- 16 M. O. Senge, K. M. Smith, *Photochem. Photobiol.*, 1991, **54**, 841–846.
- 17 A. M. Stolzenberg, M. T. Stershic, *J. Am. Chem. Soc.*, 1988, **110**, 6391–6402; A. M. Stolzenberg, L. J. Schussel, J. S. Summers, B. M. Foxman, J. L. Petersen, *Inorg. Chem.*, 1992, **31**, 1678–1686.
- 18 For a detailed description of all cases see references 5, 9 and 14.
- 19 W. Jentzen, X. Z. Song, J. A. Shelnut, *J. Phys. Chem. B*, 1997, **101**, 1684–1699.
- 20 C. R. Groom, I. J. Bruno, M. P. Lightfoot, S. C. Ward, *Acta Cryst*, 2016, **B72**, 171–179.
- 21 I. J. Bruno, J. C. Cole, P. R. Edgington, M. Kessler, C. F. Macrae, P. McCabe, J. Pearson, R. Taylor, *Acta Cryst*, 2002, **B58**, 389–397.
- 22 C. F. Macrae, I. J. Bruno, J. A. Chisholm, P. R. Edgington, P. McCabe, E. Pidcock, L. Rodriguez-Monge, R. Taylor, J. van de Streek, P. A. Wood, *J. Appl. Cryst.*, 2008, **41**, 466–470.
- 23 L. Sun, J. A. Shelnut, NSDGUI (Version 1.3 Alpha version), Sandia National Laboratory, Albuquerque, USA, 2000–2001.
- 24 (a) M. P. Byrn, C. J. Curtis, I. Goldberg, Y. Hsiou, S. I. Khan, P. A. Sawin, S. K. Tendick, C. E. Strouse, *J. Am. Chem. Soc.*, 1991, **113**, 6549–6557; (b) M. P. Byrn, C. J. Curtis, S. I. Khan, P. A. Sawin, C. E. Strouse, *J. Am. Chem. Soc.* 1990, **112**, 1865–1874; (c) G. L. Perlovich, W. Zielenkiewicz, Z. Kaszkur, J. Slowikowska, *J. Mol. Liq.* 2002, **95**, 243–259; (d) S. J. Silver, A. Tulinsky, *J. Am. Chem. Soc.*, 1967, **89**, 3331–3337; (e) G. Donnay, C. B. Storm, *Mol. Cryst.*, 1967, **2**, 287–292; (f) K. Kano, K. Fukuda, H. Wakami, R. Nishiyabu, R. F. Pasternack, *J. Am. Chem. Soc.*, 2000, **122**, 7494–7502; (g) B. L. Barker, G. G. Stanley, F. R. Fronczek, *CSD. Comm.*, 2002, CCDC

- 188202; (h) C. Brückner, J. Ogikubo, J. R. McCarthy, J. Akhigbe, M. A. Hyland, P. Daddario, J.L. Worlinsky, M. Zeller, J. T. Engle, C. J. Ziegler, M. J. Ranaghan, M. N. Sandberg, R. R. Birge, *J. Org. Chem.*, 2012, **77**, 6480–6494; (i) M. E. Light, T. Bandy, E. Stulz, CSD. Comm., 2016, CCDC 1476315; (j) Z. Li, Y. Hu, T. Li, *Mol. Cryst. Liq. Cryst.*, 2014, **605**, 135–145; (k) J. Blomker, W. Frey, *Z. Kristallogr. New Cryst. Struct.*, 2000, **215**, 267–268; (l) J. Blomker, W. Frey, *Z. Kristallogr. New Cryst. Struct.*, 2000, **215**, 263–264.
- 25 (a) J. W. Lauher, J. A. Ibers, *J. Am. Chem. Soc.*, 1973, **95**, 5148–5152; (b) M. M. Olmstead, A. de Bettencourt-Dias, H. M. Lee, D. Pham, A. L. Balch, *Dalton Trans.*, 2003, 3227–3232.
- 26 (a) W. W. Kalisch, M. O. Senge, *Tetrahedron Lett.*, 1996, **37**, 1183–1186; (b) M. O. Senge, W. W. Kalisch, *Inorg. Chem.*, 1997, **36**, 6103–6116; (c) Y. Yamamoto, A. Yamamoto, S. Furuta, M. Horie, M. Kodama, W. Sato, K. Akiba, S. Tsuzuki, T. Uchimara, D. Hasizume, F. Iwasaki, *J. Am. Chem. Soc.*, 2005, **127**, 14540–14541; (d) M. O. Senge, K. Dahms, H. -J. Holdt, A. Kelling, *Z. Naturforsch.*, 2015, **70**, 119–123.
- 27 M. O. Senge, W. W. Kalisch, S. Runge, *Tetrahedron*, 1998, **54**, 3781–3798.
- 28 W. Jentzen, M. C. Simpson, J. D. Hobbs, X.-Z. Song, T. Ema, N. Y. Nelson, C. J. Medforth, K. M. Smith, M. Veyrat, M. Mazzanti, R. Ramasseul, J.-C. Marchon, T. Takeuchi, W. A., III Goddard, J. A. Shelnut, *J. Am. Chem. Soc.*, 1995, **117**, 11085–11097.
- 29 W. R. Scheidt, J. U. Mondal, C. W. Eigenbrot, A. Adler, L. J. Radonovich, J. L. Hoard, *Inorg. Chem.*, 1986, **25**, 795–799.
- 30 (a) K. M. Barkigia, D. S. Gottfried, *Acta Crystallogr., Sect. C: Cryst. Struct. Commun.*, 1994, **50**, 2069–2072; (b) K. M. Barkigia, D. S. Gottfried, S. G. Boxer, J. Fajer, *J. Am. Chem. Soc.*, 1989, **111**, 6444–6446. (c) K. M. Barkigia, J. Fajer, K. M. Smith, G. J. B. Williams, *J. Am. Chem. Soc.*, 1981, **103**, 5890–5893.
- 30 (a) A. Ozarowski, H. M. Lee, A. L. Balch, *J. Am. Chem. Soc.*, 2003, **125**, 12606–12614; (b) K. M. Barkigia, M. D. Berber, J. Fajer, C. J. Medforth, M. W. Renner, K. M. Smith, *J. Am. Chem. Soc.*, 1990, **112**, 8851–8857.

- 31 (a) M. S. Fischer, D. H. Templeton, A. Zalkin, M. Calvin, *J. Am. Chem. Soc.*, 1972, **94**, 3613–3619; (b) K. Takahashi, M. Obayashi, Y. Nishikawa, *Kin. Daigaku Rik. Kenk. Hokoku.*, 1984, 85–92; (c) L. Kutschabsky, G. Reck, *CSD. Comm.*, 2003, CCDC 215718; (d) C. F. Chee, N. A. Rahman, S. M. Zain, S. W. Ng, *Acta Cryst.*, 2008, **E64**, o1986–o1987; (e) K. M. Smith, D. A. Goff, J. Fajer, K. M. Barkigia, *J. Am. Chem. Soc.*, 1982, **104**, 3747–3749; (f) M. O. Senge, F. W. Bobe, M. S. Huster, K. M. Smith, *Liebigs. Ann.*, 1991, 871–874; (g) K. M. Smith, D. A. Goff, J. Fajer, K. M. Barkigia, *J. Am. Chem. Soc.*, 1983, **105**, 1674–1676.
- 32 (a) M. O. Senge, K. M. Smith, *Acta Cryst.*, 1997, **C53**, 1314–1318; (b) M. O. Senge, K. M. Smith, *Z. Kristallogr.*, 1992, **199**, 239–248; (c) Y. Kinoshita, M. Kunieda, Y. Mikata, H. Tamiaki, *Tetrahedron Lett.* 2013, **54**, 1243–1246.
- 33 (a) C. Kratky, H. P. Isenring, J. D. Dunitz, *Acta Cryst.*, 1977, **B33**, 547–549; (b) C. Kratky, J. D. Dunitz, *Acta Cryst.*, 1977, **B33**, 545–547; (c) C. Kratky, J. D. Dunitz, *Acta Cryst.*, 1975, **B31**, 1586–1589; (d) R. Serlin, H.-C. Chow, C. E. Strouse, *J. Am. Chem. Soc.*, 1975, **97**, 7237–7242; (e) H.-C. Chow, R. Serlin, C. E. Strouse, *J. Am. Chem. Soc.*, 1975, **97**, 7230–7237.
- 34 (a) S. Knapp, B. Huang, T. J. Emge, S. Sheng, K. Krogh-Jespersen, J. A. Potenza, H. J. Schuga, *J. Am. Chem. Soc.*, 1999, **121**, 7977–7978; (b) A. Jesorka, A. R. Holzwarth, A. Eichhofer, C. M. Reddy, Y. Kinoshita, H. Tamiaki, M. Katterle, J.-V. Naubron, T. S. Balaban, *Photochem. Photobiol. Sci.*, 2012, **11**, 1069–1080; (c) Y. Shinozaki, I. Yoshikawa, K. Araki, K. Sugawa, J. Otsuki, *CrystEngComm.*, 2014, **16**, 9155–9157; (d) Y. Shinozaki, G. Richards, K. Ogawa, A. Yamano, K. Ohara, K. Yamaguchi, S. Kawano, K. Tanaka, Y. Araki, T. Wada, J. Otsuki, *J. Am. Chem. Soc.*, 2013, **135**, 5262–5265; (e) Y. Shinozaki, I. Yoshikawa, K. Araki, K. Ohara, K. Yamaguchi, S. Kawano, K. Tanaka, Y. Araki, T. Wada, J. Otsuki, *Chem. Lett.*, 2014, **43**, 862–864.
- 35 M. O. Senge, K. M. Smith, *Photochem. Photobiol.*, 1994, **60**, 139–142.
- 36 (a) I. de Boer, J. Matysik, M. Amakawa, S. Yagai, H. Tamiaki, A. R. Holzwarth, H. J. M. de Groot, *J. Am. Chem. Soc.*, 2003, **125**, 13374–13375; (b) I. A. Zamilatskov, E. V. Savinkina, A. N. Volov, M. S. Grigorev, I. S. Lonin, L. N. Obolenskaya, G. V. Ponomarev, O. I. Koifman, A. S. Kuzovlev,

- G. M. Kuzmicheva, A. Yu. Tsivadze, *Makroheterocikly (Russ.) (Macroheterocycles)*, 2012, **5**, 308–314.
- 37 (a) A. N. Kozyrev, V. Suresh, S. Das, M. O. Senge, M. Shibata, T. J. Dougherty, R. K. Pandey, *Tetrahedron*, 2000, **56**, 3353–3447.
- 38 M. Taniguchi, O. Mass, P. D. Boyle, Q. Tang, J. R. Diers, D. F. Bocian, D. Holten, J. S. Lindsey, *J. Mol. Struct.*, 2010, **979**, 27–45.
- 39 O. Mass, M. Ptaszek, M. Taniguchi, J. R. Diers, H. L. Kee, D. F. Bocian, D. Holten, J. S. Lindsey, *J. Org. Chem.*, 2009, **74**, 5276–5289.
- 40 R. Xiong, A. I. Arkhynchuk, D. Kovacs, A. Orthaber, K. Eszter Borbas, *Chem. Commun.*, 2016, **52**, 9056–9058.
- 41 R. Li, M. Zeller, T. Bruhn, C. Brückner, *Eur. J. Org. Chem.*, 2017, 1835–1842.
- 42 K. M. Shea, L. Jaquinod, R. G. Khoury, K. M. Smith, *Chem. Commun.*, 1998, **0**, 759–760.
- 43 R. Li, E. Meehan, M. Zeller, C. Brückner, *Eur. J. Org. Chem.*, 2017, **0**, 1820–1825.
- 44 M. O. Senge, W. W. Kalisch, I. Bischoff, *Chem. Eur. J.*, 2000, **6**, 2721–2738.
- 45 R. Li, E. Meehan, M. Zeller, C. Brückner, *Eur. J. Org. Chem.*, 2017, 1826–1834.
- 46 W. Hoppe, G. Will, J. Gassmann, H. Weichselgartner, *Z. Kristallogr., Kristallgeom., Kristallphys., Kristallchem.*, 1969, **128**, 18–31.
- 47 K. M. Barkigia, C. K. Chang, J. Fajer, *J. Am. Chem. Soc.*, 1991, **113**, 7445–7447.
- 48 J. L. Worlinsky, G. Zarate, M. Zeller, M. Ghandehari, G. Khalil, C. Bruckner, *J. Porphyrins. Phtalocyanines*, 2013, **17**, 836–849.
- 49 M. Taniguchi, M. Ptaszek, B. E. McDowell, P. D. Boyle, J. S. Lindsey, *Tetrahedron*, 2007, **63**, 3850–3863.
- 50 C. Muthiah, M. Ptaszek, T. M. Nguyen, K. M. Flack, J. S. Lindsey, *J. Org. Chem.*, 2007, **72**, 7736–7749.

- 51 W. Robert Scheidt, H. F. Duval, T. J. Neal, M. K. Ellison, *J. Am. Chem. Soc.*, 2000, **122**, 4651–4659.
- 52 P. A. Connick, K. J. Haller, K. A. Macor, *Inorg. Chem.*, 1993, **32**, 3256–3264.
- 53 S. Cai, E. Belikova, L. A. Yatsunyk, A. M. Stolzenberg, F. A. Walker, *Inorg. Chem.*, 2005, **44**, 1882–1889.
- 54 A. M. Stolzenberg, P. A. Glazer, B. M. Foxman, *Inorg. Chem.*, 1986, **25**, 983–991.
- 55 K. M. Barkigia, M. A. Thompson, J. Fajer, R. K. Pandey, K. M. Smith, M. G. H. Vicente, *New. J. Chem.*, 1992, **16**, 599–607.
- 56 F.-P. Montforts, A. Meier, G. Scheurich, G. Haake, J. W. Bats, *Angew. Chem., Int. Ed.*, 1992, **31**, 1592–1594.
- 57 J. J. Lin, K. R. Gerevske, P. A. Liddell, M. O. Senge, M. M. Olmstead, R. G. Khoury, B. E. Weeth, S. A. Tsao, K. M. Smith, *J. Org. Chem.*, 1997, **62**, 4266–4276.
- 58 P. A. Liddell, K. R. Gerzevske, J. J. Lin, M. M. Olmstead, K. M. Smith, *J. Org. Chem.*, 1993, **58**, 6681–6691.
- 59 W. W. Kalisch, M. O. Senge, K. Ruhlandt-Senge, *Photochem. Photobiol.*, 1998, **67**, 312–323.
- 60 N. Chaudhri, N. Grover and M. Sankar, *CSD Comm. (Private Communication)*, 2017.
- 61 S. Banerjee, M. Zeller, C. Brückner, *J. Porphyrins Phthalocyanines.*, 2012, **16**, 576–588.
- 62 E. Skrzypczak-Jankun, *CSD Comm. (Private Communication)*, 2000, CDC 144165.
- 63 D. P. Arnold, R. Gaete-Holmes, A. W. Johnson, A. R. P. Smith, G. A. Williams, *J. Chem. Soc., Perkin Trans. 1*, 1978, 1660–1670.
- 64 M. O. Senge, M. da G. H. Vicente, S. R. Parkin, H. Hope, K. M. Smith, *Z. Naturforsch., B: Chem. Sci.*, 1992, **47**, 1189–1202.

- 65 G. Li, R. Mehta, T. Srikrishnan, D. J. Nurco, W. A. Tabaczynski, J. L. Alderfer, K. M. Smith, T. J. Dougherty, R. K. Pandey, *Chem. Commun.*, 2000, 1172–1173.
- 66 A. Pelter, J. A. Ballantine, P. Murray-Rust, V. Ferrito, A. F. Psaila, *Tetrahedron Lett.*, 1978, **19**, 1881–1884.
- 67 M. Ptaszek, D. Lahaye, M. Krayner, C. Muthiah, J. S. Lindsey, *J. Org. Chem.*, 2010, **75**, 1659–1673.
- 68 I. Meunier, R. K. Pandey, M. O. Senge, T. J. Dougherty, K. M. Smith, *J. Chem. Soc., Perkin Trans. 1*, 1994, 961–969.
- 69 A. F. Uchoa, K. T. de Oliveira, M. S. Baptista, A. J. Bortoluzzi, Y. Iamamoto, O. A. Serra, *J. Org. Chem.*, 2011, **76**, 8824–8832.
- 70 J. Akhigbe, M. Luciano, M. Zeller, C. Brückner, *J. Org. Chem.*, 2015, **80**, 499–511.
- 71 A. S. Phadke, B. C. Robinson, K. M. Barkigia, J. Fajer, *Tetrahedron*, 2000, **56**, 7661–7666.
- 72 N. Hewage, M. Zeller, C. Brückner, *Org. Biomol. Chem.*, 2017, **15**, 396–407.

7. Appendix

Table 1. Full experimental details of NSD conformation analysis of the compounds studied [Å].

#	Compound	M	CSD #	Out-of-plane distortions						In-plane distortions									
				D_{oop}	δ_{oop}	B_{2u}	B_{1u}	A_{2u}	$E_{g(x)}$	$E_{g(y)}$	A_{1u}	D_{ip}	δ_p	B_{2g}	B_{1g}	$E_{u(x)}$	$E_{u(y)}$	A_{1g}	A_{2g}
<i>Test cases – free base compounds</i>																			
<i>5,10,15,20-Tetraphenylporphyrin</i>																			
5a	5,10,15,20-Tetraphenylporphyrin bis(benzaldehyde) clathrate	2H	JIVRAH	0.0146	0.0076	0	0	0	-0.0115	0.009	0	0.2006	0.0158	0.0396	-0.0167	0	0	0.1959	-0.0026
5b	5,10,15,20-Tetraphenylporphyrin bis(<i>m</i> -xylene) clathrate	2H	SEMNIH	0.0389	0.009	0	0	0	0.0389	-0.0026	0	0.1765	0.0118	-0.056	0.0496	0	0	0.1577	0.0261
5c	5,10,15,20-Tetraphenylporphyrin bis(<i>m</i> -xylene) clathrate	2H	SEMNIH01	0.0373	0.0033	0.0001	0.0003	-0.0001	-0.0009	-0.0372	0.0001	0.2109	0.013	-0.0542	0.004	-0.0001	0.0007	0.2038	0.0012
5d	5,10,15,20-Tetraphenylporphyrin	2H	TPHPOR01	0.258	0.0355	0	0	0	-0.2314	0.1142	0	0.196	0.0185	0.015	0.0482	0	0	0.1883	0.0201
5e	5,10,15,20-Tetraphenylporphyrin	2H	TPHPOR04	0.2668	0.0371	-0.0001	-0.0002	-0.0001	0.2406	-0.1151	0.0002	0.208	0.0215	0.0323	0.0519	-0.0002	0	0.198	0.0183
5f	5,10,15,20-Tetraphenylporphyrin	2H	TPHPOR11	0.2663	0.0399	-0.0004	-0.0004	0	0.2507	-0.0898	0.0002	0.2357	0.0251	0.0393	0.0521	-0.0003	-0.0006	0.2255	0.0215
5g	5,10,15,20-Tetraphenylporphyrine	2H	TPHPOR12	0.2248	0.0379	0.0003	-0.0002	-0.0001	0.2071	-0.0876	0.0003	0.1803	0.0186	0.021	0.0487	-0.0007	0.0006	0.1721	0.0083
5h	5,10,15,20-Tetraphenylporphyrin	2H	TPHPOR13	0.2691	0.0399	-0.0001	0.0003	-0.0003	-0.2525	0.093	-0.0006	0.2266	0.0238	0.0385	0.053	0.0001	-0.0004	0.2156	0.0238
5i	5,10,15,20-Tetraphenylporphyrin	2H	TPHPOR14	0.262	0.0361	0.0003	0.0004	-0.0005	-0.238	-0.1095	0.0002	0.2027	0.0223	-0.0143	0.0338	0.0002	0.0006	0.1979	-0.0239
5j	5,10,15,20-Tetraphenylporphyrin anthracene clathrate	2H	XAGLOG	0.218	0.0159	0.0005	-0.0004	-0.0002	0.1285	0.1761	0	0.2026	0.0201	0.0362	-0.0423	0.0003	0.0002	0.1948	0.0016
5k	5,10,15,20-Tetraphenylporphyrin phenanthrene clathrate	2H	XAGMAT	0.2582	0.0259	-0.0008	-0.0003	0.0003	0.1432	0.2149	0.0004	0.1969	0.0149	0.0146	0.0333	0.0003	-0.0001	0.1935	-0.0047
<i>2,3,7,8,12,13,17,18-Octaethylporphyrin</i>																			
6a	2,3,7,8,12,13,17,18-Octaethylporphyrin	2H	OETPOR10	0.1095	0.0113	0	0	0	-0.063	0.0895	0	0.2279	0.0183	0.0016	-0.058	0	0	0.2204	0.0001
6b	2,3,7,8,12,13,17,18-Octaethylporphyrin 7,7,8,8-tetracyanoquinodimethane clathrate	2H	OKOQUA	0.0933	0.0055	0.0001	0.0009	0.0004	-0.0176	-0.0917	-0.0001	0.3262	0.0109	0.2327	-0.0099	0.0002	0	0.2283	-0.0064
<i>XEtTPP series</i>																			
7	2,3-Diethyl-5,10,15,20-tetraphenylporphyrin	2H	TATPOT01	0.6164	0.0088	-0.5955	-0.0552	0.0443	0.0307	-0.1374	0.0223	0.3458	0.0283	0.056	0.2424	-0.0475	0.0018	0.2354	-0.0056
8	2,3,12,13-Tetraethyl-5,10,15,20-tetraphenylporphyrin dichloromethane solvate	2H	TATPUZ01	1.8137	0.0376	-1.8118	-0.0398	0.0614	-0.0075	-0.0396	0.0075	0.268	0.0377	-0.0015	0.2658	-0.0041	0.0138	0.0309	-0.0028
9	2,3,7,8-Tetraethyl-5,10,15,20-tetraphenylporphyrin methanol solvate	2H	TATQAG01	2.3542	0.054	2.2852	-0.2476	0.0358	-0.2502	0.4398	-0.0334	0.1369	0.0611	-0.0072	0.0752	-0.0424	0.0216	-0.0973	-0.0361
10	2,3,7,8,12,13-Hexaethyl-5,10,15,20-tetraphenylporphyrin dichloromethane solvate	2H	TATQEK01	2.8466	0.0498	2.8231	0.1686	0.0008	0.1449	0.289	-0.0259	0.3753	0.0727	-0.0422	0.2340	-0.0068	0.0167	-0.2898	-0.0041
11	2,3,7,8,12,13,17,18-Octaethyl-5,10,15,20-tetraphenylporphyrin ethanol solvate	2H	SATQOU	3.46	0.069	-3.4555	-0.099	0.0	0.0997	0.1026	0.0096	0.5151	0.1049	0.0565	-0.0896	0.0365	-0.0391	-0.5012	-0.0026
11a	2,3,7,8,12,13,17,18-Octaethyl-5,10,15,20-tetraphenylporphyrin bis(dichloromethane) clathrate	2H	QAWFIE	3.9489	0.177	-3.6587	-	0.1127	0	0	-0.0301	1.0546	0.1751	-0.0942	-0.1978	0	-0.0005	-0.954	0.3924

<i>XeTPC series</i>																			
12	7,8-Diethyl-5,10,15,20-tetraphenylchlorin	2H	GELGUZ	1.153 6	0.02 51	-1.103	-0.2781	0.0443	0.0856	-0.1647	0.0177	0.2932	0.0344	-0.0458	-0.1062	-0.0574	-0.0573	0.2568	-0.0086
13	12,13-Diethyl-5,10,15,20-tetraphenylchlorin	2H	GELJEM	1.950 1	0.02 45	1.8972	-0.3766	0.0091	0.2393	-0.0182	0.0636	0.277	0.0421	0.0019	0.2638	-0.0623	-0.0102	0.056	-0.0039
14	2,3,7,8-Tetraethyl-5,10,15,20-tetraphenylchlorin)•CH ₂ Cl•CH ₂ OH	2H	GELQAP	1.866 6	0.03 81	-1.7541	-0.503	0.1185	0.2167	-0.2773	0.1289	0.1931	0.0457	0.1427	-0.0732	-0.0624	-0.0289	0.0744	-0.0361
15	7,8,12,13-Tetraethyl-5,10,15,20-tetraphenylchlorin	2H	GELHAG	2.739 1	0.04	-2.6645	-0.4588	-0.11	-0.2868	-0.3127	-0.0103	0.1949	0.0663	-0.0335	0.0924	-0.0208	0.0611	-0.1551	0.0096
<i>Test cases – metal complexes</i>																			
<i>5,10,15,20-Tetraphenylporphyrins and 2,3,7,8,12,13,17,18-octaethylporphyrins</i>																			
Zn5a	(5,10,15,20-Tetraphenylporphyrinato)zinc(II)	Zn(II)	ZZZTAY02	0.23 68	0.03 10	0	0	0	-0.1939	0.1359	0	0.1480	0.0093	0.0136	0.0226	0	0	0.1451	0.0126
Zn5b	(5,10,15,20-Tetraphenylporphyrinato)zinc(II)	Zn(II)	ZZZTAY03	0.15 93	0.01 15	0	0	0	-0.1583	0.0179	0	0.1522	0.0081	-0.0028	0.0105	0	0	0.1518	0.0008
Zn6a	(2,3,7,8,12,13,17,18-Octaethylporphyrinato)zinc(II)	Zn(II)	ALOKOB	0.16 58	0.00 61	0.0001	0	0.0002	-0.1576	-0.0517	0.0001	0.1444	0.0095	0.0019	-0.0083	0	-0.0001	0.1441	-0.0003
Zn6b	(2,3,7,8,12,13,17,18-Octaethylporphyrinato)zinc(II) hemikis(7,7,8,8-tetracyanoquinodimethane)	Zn(II)	OKOREL	0.37 44	0.00 76	-0.3183	-0.0763	-0.1007	0.1273	0.0782	0.0156	0.1465	0.0085	-0.0034	0.0027	-0.0053	-0.0146	0.1456	0.0033
<i>XeTPPs and XeTPCs</i>																			
Zn7	3-Picoline(2,3-diethyl-5,10,15,20-tetraphenylporphyrinato)zinc(II)	Zn(II)	RUTNEZ	1.05 43	0.02 28	0.8957	0.4732	0.1616	-0.1868	0.1558	-0.0098	0.2151	0.0179	-0.0284	0.1698	-0.0274	0.0092	0.1244	0.0173
Zn8	Pyridine(2,3,12,13-tetraethyl-5,10,15,20-tetraphenylporphyrinato)zinc(II) hydrate	Zn(II)	RUTQAY	1.70 38	0.03 83	1.5998	-0.5617	0.0215	0.1616	0.0217	-0.0318	0.2086	0.0273	0.0303	0.1925	-0.0156	-0.0302	0.0601	-0.0276
Zn10	(2,3,7,8,12,13-Hexaethyl-5,10,15,20-tetraphenylporphyrinato)zinc(II)	Zn(II)	RUTRAZ	2.761	0.0422	-2.7218	-0.3307	0.2131	0.0014	-0.2446	0.0114	0.2534	0.0583	0.0405	0.0175	0.0067	-0.0084	-0.2490	0.0113
Zn11	Methanol(2,3,7,8,12,13,17,18-octaethyl-5,10,15,20-tetraphenylporphyrinato)zinc(II) methanol solvate	Zn(II)	JICNIS	3.252	0.0676	-3.2477	0.1176	0.0373	-0.1042	-0.0383	-0.0019	0.3933	0.0864	0.0373	-0.0122	-0.0474	0.0136	-0.3882	0.0019
Zn12	(7,8-Diethyl-5,10,15,20-tetraphenylchlorinato)zinc(II)•CH ₂ Cl ₂	Zn(II)	GELJAI	2.1513	0.0348	-2.1053	0.4205	0.0173	-0.0625	-0.1107	-0.0513	0.1056	0.0406	-0.021	-0.0141	-0.0776	-0.0444	-0.0495	-0.0094
Zn12a	(7,8-Diethyl-5,10,15,20-tetraphenylchlorinato)zinc(II)•MeOH	Zn(II)	GELQET	0.299	0.0153	0.2451	-0.0708	-0.1475	0.0149	-0.0447	0.018	0.2959	0.0217	0.0144	-0.0569	-0.0569	-0.0613	0.2776	0.0058
Zn15	Methanol(7,8,17,18-tetraethyl-5,10,15,20-tetraphenylchlorinato)zinc(II)•CH ₂ Cl ₂ •C ₂ H ₅ OH	Zn(II)	GELPIW	1.6573	0.0336	-1.6558	0	-0.0719	0	0	0	0.2731	0.0221	0	0.2454	-0.0001	0	0.1196	0
<i>Bacteriochlorophyll (a or b) derivatives</i>																			
2a	Methyl bacteriopephorbide a	2H	WIKSEO	0.22 26	0.02 51	-0.1174	0.0133	-0.1051	-0.121	0.0856	0.0509	0.6275	0.0557	0.3041	-0.4118	-0.0836	-0.0425	0.3376	-0.0944
2b	Methyl bacteriopephorbide a•0.5C ₆ H ₆	2H	BAVSUM01	0.26 82	0.02 96	-0.1692	0.0078	-0.137	-0.1235	0.0829	0.0487	0.6124	0.0538	0.2974	-0.3842	-0.0849	-0.0562	0.3476	-0.0882
2c	Methyl bacteriopephorbide•C ₆ H ₆	2H	BAVSUM	0.28 79	0.04 39	-0.1771	0.0797	-0.0842	-0.1419	0.0632	0.1179	0.7003	0.0796	0.2592	-0.4177	-0.1047	-0.3452	0.3197	-0.1281
<i>“Chlorophyll derivatives” = Phytochlorins</i>																			
<i>Free base phytochlorins</i>																			
3a	Methyl pheophorbide a	2H	MPOPHA	0.2 541	0.0263	-0.1818	-0.0094	-0.0962	-0.0914	0.0242	0.1151	0.4611	0.0521	0.2724	-0.2844	-0.0817	0.0257	0.2013	-0.0983
3b	“	2H	MPOPHA02	0.2 461	0.0274	0.1851	0.0199	0.0884	0.0899	0.0151	0.099	0.5441	0.0695	-0.2568	-0.3779	-0.1095	-0.1031	0.2324	0.1031
3c	“	2H	MPOPHA03	0.2 386	0.0291	0.1733	-0.0122	0.0969	0.0844	-0.0283	-0.0972	0.448	0.0533	0.2511	-0.2927	-0.0923	0.0256	0.1741	-0.112
3d	Ethyl pheophorbide b	2H	ROFVUE	0.2 00	0.0172	-0.1197	-0.0429	-0.0002	-0.1237	-0.0533	-0.0769	0.4949	0.0568	-0.3167	-0.2602	-0.0999	-0.0284	0.2364	0.1014
3e^d	Methyl [4,5-Diethyl]-bacteriopephorbide d (mol. 1 N1-N4)	2H	BIPBOR	0.4 31	0.0304	-0.2086	-0.1963	-0.1118	0.1746	-0.1823	-0.1674	0.4534	0.0676	0.1006	-0.3493	-0.0108	0.0584	0.2415	-0.1078
3e^h	“ (mol. 2 N5-N8)	2H	“	0.3332 0.3694	0.0567 0.0373	0.1991 -0.1197	-0.0883 -0.1657	0.0984 0.0422	0.15 -0.0788	0.0714 -0.2841	-0.1622 -0.0776	0.4304 0.3898	0.0493 0.0536	0.1144 0.1136	-0.3319 -0.2931	-0.0706 -0.0602	0.0275 -0.0067	0.2089 0.2003	-0.1123 -0.0966
3f	Methyl [12-acetyl-8-ethyl]-bacteriopephorbide d	2H	SOSZOP	0.4346	0.0409	-0.1027	-0.3503	-0.0765	0.1281	-0.0639	-0.1711	0.4584	0.0517	0.1981	-0.3276	-0.0583	0.032	0.2156	-0.1122
3g^d	Methyl [4-isobutyl-5-ethyl]-bacteriopephorbide d (mol. 1 N1-N4)	2H	BIPBIL	0.4215	0.05	0.2139	-0.1532	0.1003	0.233	-0.0703	-0.1979	0.3786	0.0533	0.1091	-0.2807	-0.0697	-0.0275	0.2019	-0.079
3g^h	“ (mol. 2 N5-N8)	2H	BIPBIL																

3h	Methyl [8-neopentyl-1,2-ethyl]-bacteriopheophorbide d	2H	BIXREF01	0.467	0.0099	0.0654	0.0092	0.4372	-0.0245	-0.1473	-0.0166	0.4976	0.0538	0.2462	-0.3142	-0.0997	0.0371	0.2604	-0.0956
3i	17-Decarboxyethyl-13'-deoxo-17-propylphytyochlorin (mol.1 N5-N8 ring)	2H	RIWNIU	0.4096	0.0215	0.2748	0.2378	0.0862	-0.1071	-0.1072	0.0732	0.4968	0.054	0.1944	-0.3217	-0.0955	0.0206	0.2889	-0.1117
3ii	" (mol. 2 N1-N4)	2H	"	0.1865	0.0235	0.014	0.0108	0.0635	-0.0419	-0.1246	0.1146	0.5308	0.0525	0.3141	-0.2903	-0.1007	0.0183	0.2743	-0.1145
3j	Methyl phytyochlorin	2H	KOVXUO	0.1937	0.02	0.0489	-0.1291	-0.1302	-0.014	-0.0089	-0.0353	0.4816	0.0541	0.2639	-0.2931	-0.0557	0.0388	0.2388	-0.1216
3k	Methyl 3'-deethyl-3-(4,4,4-trifluoro-1-hydroxy-3-oxo-but-1-en-1-yl)phytyochlorin enol	2H	PEPJUR	0.1716	0.0112	-0.0841	0.0795	0.0347	-0.0339	-0.1169	-0.005	0.5372	0.0591	0.2698	-0.2905	-0.1045	0.0391	0.3313	-0.096
<i>Metallophytyochlorins</i>																			
<i>Chlorophyllides</i>																			
Mg3l	(H ₂ O)(Methyl pyrochlorophyllide a)magnesium(II)Et ₂ O	Mg(II)	MPCHLM10	0.173	0.0277	-0.0827	0.0297	0.0613	0.0754	0.0195	0.1113	0.3636	0.0571	0.1132	-0.2195	-0.0371	-0.0391	0.2523	-0.0684
Mg3m	(H ₂ O)(Methyl chlorophyllide a)+H ₂ O	Mg(II)	MCLPHD10	0.2576	0.0107	0.1879	-0.0031	0.1292	-0.0487	-0.1079	0.0179	0.3571	0.0462	0.0405	-0.2261	-0.0829	0.0447	0.2289	-0.1163
Mg3n	(H ₂ O)(Ethyl chlorophyllide a)+H ₂ O	Mg(II)	AECLPA01	0.3265	0.0231	0.1755	0.1318	-0.1249	-0.1068	-0.1621	0.0719	0.3566	0.0473	0.0695	-0.2251	-0.067	0.0246	0.237	-0.1018
Mg3o	(H ₂ O)(Ethyl chlorophyllide b)+H ₂ O	Mg(II)	ECPHBH	0.3268	0.0217	0.2312	0.0485	-0.0859	-0.1387	-0.1483	0.0494	0.3729	0.052	0.1083	-0.2367	-0.0881	0.0376	0.2281	-0.1008
Mg3p	(H ₂ O)(Ethyl chlorophyllide a)+H ₂ O	Mg(II)	AECLPA10	0.331	0.0248	0.1838	0.1252	-0.11	-0.1115	-0.1739	0.0729	0.3745	0.0497	0.0878	-0.2467	-0.0717	0.0203	0.2372	-0.0992
<i>Other metallophytyochlorins</i>																			
Zn3q	[(Methyl 3'-deethyl-3-carboximino-phytyochlorinato)zinc(II)] _n ·nCHCl ₃ (catena-μ ² -13 ¹ -O...Zn polymer)	Zn(II)	CELRIU	0.6362	0.0395	-0.5434	0.2619	0.0974	-0.0383	0.1141	0.1297	0.4165	0.0458	-0.0277	-0.3536	0.1015	0.0227	0.1681	0.0929
Zn3r	[Methyl 3'-oxophytochlorinato)zinc(II)] _n ·nCH ₂ Cl ₂ (catena-μ ² -17 ² -oxo...Zn polymer)	Zn(II)	MEHGUD	0.4673	0.0096	-0.4322	0.1054	-0.1108	-0.0523	0.0742	-0.0028	0.351	0.0502	0.0514	-0.2407	-0.0846	0.0174	0.2184	-0.0868
Zn3s	[Methyl 3'-deethyl-3-((4-(pyridin-3-yl)phenyl)ethynyl)phytyochlorinato]zinc(II) [catena-(μ-zinc-pyridin polymer) (mol. 1 N1-N5)]	Zn(II)	XOKGOV	0.3207	0.0281	0.0070	0.2587	0.0611	0.1599	0.0282	0.0757	0.4334	0.0451	0.0866	-0.3260	0.0586	-0.0024	0.2412	-0.1115
Zn3se	" (mol. 2, N6-N10)	Zn(II)	"	0.2786	0.045	0.1542	0.0551	-0.0132	0.165	0.0509	0.1444	0.3941	0.0431	0.0374	-0.3028	0.1041	0.0369	0.2084	-0.0811
Zn3t	[(Methyl 3',3'-dihydro-3 ² -(4-pyridyl)phytyochlorinato)zinc(II)] _n ·0.5nC ₂ H ₄ N (catena-μ ² -pyridyl-N...Zn polymer)(mol. 1, N1-N4)	Zn(II)	MIBJEO	0.1755	0.0337	-0.0898	0.0868	-0.0508	-0.0246	-0.0538	-0.0956	0.4243	0.0511	0.005	0.3222	0.0154	0.0537	0.2527	0.096
Zn3u	" (mol. 2, N5-N8)	Zn(II)	"	0.5712	0.0404	0.3788	-0.306	-0.1816	-0.0056	-0.1208	0.2037	0.3427	0.0528	-0.0274	0.2488	0.0071	0.0514	0.1962	0.1168
Zn3v	(Methyl 3'-deethyl-3-(1,3-oxazol-5-yl)-phytyochlorinato)zinc(II) [catena-μ-Zn-oxazolyl-N polymer]	Zn(II)	ZOKMAP	0.3746	0.0215	-0.3348	-0.0432	-0.0853	-0.0703	-0.0519	0.1072	0.4459	0.0489	0.0496	-0.3119	0.0801	-0.0227	0.2885	-0.0946
Ni3w	(Methyl pyropheophorbidato a)nickel(II)	Ni(II)	HAHBAT	1.3693	0.0443	-0.0965	1.3349	0.1668	-0.1605	-0.0604	0.1624	0.3422	0.0455	-0.016	-0.1132	-0.0817	-0.0701	-0.2914	-0.0867
Ni3x	(Methyl 20-methyl-phytyochlorinato)nickel(II)	Ni(II)	YOYVAJ	1.7901	0.0481	0.6005	1.632	0.134	-0.3224	-0.0935	0.2228	0.4558	0.0547	0.0176	-0.1197	-0.0885	-0.1278	-0.3914	-0.1257
Cd3y	(Methyl 3'-deethyl-3-hydroxymethyl-phytyochlorinato)cadmium(II) [catena-(μ ² -Bacteriochlorophyll)-cadmium polymer]	Cd(II)	UMAZAJ	0.2908	0.0294	-0.1604	0.1501	-0.178	-0.0564	-0.0032	0.0378	0.3925	0.0777	0.0879	-0.1191	-0.1215	0.055	-0.3194	-0.1108
Pt3z	(Methyl phytyochlorinato)platinum(II)	Pt(II)	KILQAZ	0.1283	0.0174	0.0257	-0.0831	-0.0847	0.0129	0.0089	-0.0384	0.192	0.0458	0.048	-0.1124	-0.0566	0.0055	0.091	-0.1022
<i>Other phytyochlorins</i>																			
3a	Benzimidazol(2,1-n)purpurin-18 13 ¹ -imino-13 ² -imide methyl ester	2H	FOXTUH	0.2985	0.0222	-0.1789	0.2057	-0.0064	-0.0152	0.0352	0.1151	0.4504	0.0349	-0.2186	-0.1607	0.0235	0.0895	0.3466	-0.0229
3aa	Methyl 3',3'-dihydro-13'-deoxo-quinoxaline(2,3-n)phytyochlorin	2H	FOXWY	0.3826	0.0285	0.2192	0.2666	-0.0143	-0.0975	-0.0908	0.0966	0.5015	0.0515	0.2943	-0.2972	-0.0691	0.0327	0.2405	-0.1135
<i>β-Substituted Chlorins</i>																			
<i>Free base chlorins</i>																			
4a	7-Hydro-8,8-dimethylporphyrin	2H	PACRES	0.1888	0.0201	-0.0636	-0.0431	0.0405	0.1381	-0.0122	-0.0942	0.2989	0.0308	-0.0231	-0.1028	-0.0079	0.0707	0.2706	0.0015
4b	3-Bromo-7-hydro-8,8-dimethylporphyrin	2H	PACRIW	0.314	0.0148	-0.2142	0.0227	-0.1911	0.0783	0.0828	-0.0523	0.276	0.032	0.0019	-0.0475	0.0146	0.0888	0.2565	0.0057
4c	2-Acetyl-5-bromo-7-hydro-8,8-dimethylporphyrin	2H	MUMGAD	0.3225	0.0144	0.1609	0.27	-0.0103	-0.0374	-0.0557	0.0246	0.2952	0.0342	-0.0545	-0.027	0.0261	0.0844	0.2749	-0.0058
4d	5,10-Dibromo-7,7-dimethyl-15-phenyl-8-hydroporphyrin	2H	TACTID	0.7558	0.0199	-0.5614	0.482	-0.1093	0.0999	-0.0288	0.0321	0.4682	0.0342	0.3145	-0.1618	0.0094	-0.1384	0.273	0.0188
4e	7,7-Dimethyl-8-oxoporphyrin	2H	PACROC	0.298	0.0068	-0.1641	-0.1624	-0.1707	0.0762	0.0123	-0.0194	0.2704	0.0295	0.0434	-0.0283	0.0128	0.0659	0.2555	0.0245
4f	3,7,8,12,13,17,18-Heptaethyl-3-hydroxy-2-oxochlorin	2H	WANDEX	0.1654	0.0187	0.0944	0.0756	-0.0715	0.052	-0.0438	-0.0549	0.2894	0.0292	-0.0251	-0.0768	-0.0491	-0.0309	0.2704	0.0275
4g	20-chloro-3,3,7,8,12,13,17,18-octaethyl-2-oxochlorin	2H	WANDAT	0.2168	0.0119	0.1296	-0.0182	-0.0011	-0.1492	-0.0676	-0.0551	0.5087	0.0347	-0.3514	-0.022	-0.1066	-0.061	0.3449	-0.0279
4h	3,3,7,8,12,13,17,18-octaethyl-2-oxochlorin unknown solvate (mol. 1 N1-N4)	2H	WANBOF	0.2013	0.0072	0.0707	0.0954	0.0080	-0.1297	0.0971	0.0104	0.2973	0.0296	-0.0791	-0.0412	-0.0533	-0.0104	0.2777	0.0185
4h	" (mol. 2 N5-N8)	2H	"	0.2724	0.0123	0.1407	-0.1614	-0.0132	0.0237	-0.1636	0.0294	0.4093	0.0311	-0.0453	-0.2828	-0.0627	0.0166	0.2824	-0.0387
4i	3,3,7,8,12,13,17,18-octaethyl-2-(hydroxyimino)chlorin chloroform solvate	2H	WANCAS	0.3422	0.0091	-0.2236	0.1192	-0.0218	-0.0688	0.2172	0.0234	0.3311	0.0287	-0.0994	-0.0626	-0.0581	-0.0035	0.304	-0.0004

4j	3,3,7,8,12,13,17,18-octaethyl-2-oxo-20-formyloxchlorin chloroform solvate	2H	WANCEW	0.4135	0.0119	-0.2883	-0.1866	-0.1624	-0.0604	0.151	0.0164	0.3519	0.0321	-0.1553	-0.0298	-0.088	-0.036	0.2985	-0.0256
4k	cis-2,3-Dihydroxy-2',3',7,8,12,13,17,18-octaethylporphyrin ethyl acetate solvate	2H	KOCZUX	0.8136	0.0531	0.0324	0.7457	-0.1017	-0.1269	0.1866	-0.2087	0.234	0.0298	-0.0927	-0.0032	-0.0266	-0.0255	0.2117	-0.0023
4l	Phyllochlorine ester	2H	PHLLCL10	0.7863	0.0256	0.6967	0.2761	0.0894	0.1697	0.072	0.1209	0.2995	0.0372	0.1972	-0.0855	-0.0047	-0.0656	0.1965	0.0236
4m	2,3-bis(Dicyanomethyl)-12,13-dibromo-5,10,15,20-tetraphenylchlorin chloroform methanol solvate	2H	NOCGER	0.3656	0.032	0.0796	-0.2512	-0.0081	0.0213	-0.2456	0.0584	0.4137	0.0259	0.016	0.2553	0.0001	0.0007	0.325	0.012
4n	trans-2,3-Di-n-butyl-5,10,15,20-tetraphenylchlorin dichloromethane solvate	2H	QAKLUJ	0.4811	0.0415	0.2207	0.2682	-0.1649	-0.0506	0.2465	-0.1425	0.3085	0.0319	0.0008	0.1191	-0.0468	-0.0124	0.2803	-0.0096
4o	12-Nitro-5,10,15,20-tetraphenyl-2,3-dihydroporphyrin-2,3-diol ethanol solvate hydrate	2H	TIPBIF	1.9416	0.0261	1.9229	0.1931	-0.0395	0.0707	0.1678	-0.0149	0.199	0.0459	-0.0004	0.1817	-0.0648	-0.0087	0.0479	-0.0025
<i>Metallochlorens</i>																			
Zn4a	(2,2-Dimethyl-2,3-chlorinato-N,N',N'',N''',N''''-zinc(ii) cyclohexane solvate	Zn(II)	NIDFEM	0.2957	0.0265	0.0816	-0.0455	-0.2136	0.0588	-0.1591	-0.0656	0.263	0.0292	-0.0293	-0.1655	-0.0485	0.0731	0.1822	-0.0015
Zn4p	(7-Bromo-18,18-dimethyl-10-polychlorinato)-zinc(ii) chloroform solvate	Zn(II)	XIPLEO	0.6479	0.0511	0.5297	0.1002	0.3152	0.0791	0.0752	0.1337	0.213	0.0279	0.0562	-0.0891	0.0055	0.0456	0.179	-0.0103
Zn4q	catena-(μ2-3,3-Dimethylchlorin-2(3H)-onato-N,N',N'',N''')-zinc(ii) cyclohexane solvate	Zn(II)	NIDFAI	0.3438	0.0206	-0.226	-0.2061	0.0351	0.115	-0.0688	0.0739	0.2344	0.0233	0.0094	0.065	-0.0632	-0.0244	0.2114	0.0366
Fe4h	Nitrosyl-(3,3,7,8,12,13,17,18-octaethyl-3H-chlorinato)-iron(ii) chloroform solvate	Fe(II)	QUJZUQ	0.3041	0.0079	0.2311	-0.1924	0.0227	-0.0105	-0.0168	-0.0338	0.0814	0.018	0.0158	0.023	-0.0593	-0.003	0.0439	0.0202
Ni4h^l	(3,3,7,8,12,13,17,18-Octaethyl-3H-porphin-2-onato)-nickel(ii) (mol. 1: N1-N4)	Ni(II)	DOZVIX01	1.023	0.0109	-0.0003	1.0217	-0.0002	0.0002	0.0506	-0.0345	0.2343	0.031	0.0001	0.0267	-0.0211	-0.0002	-0.2318	0.0001
Ni4h^l	" mol. 2: N5-N8	Ni(II)	"	0.4698	0.0091	0.4491	-0.1061	0.0231	-0.0839	0.0104	0.004	0.1336	0.027	0.0056	0.0227	-0.0584	-0.0249	-0.1139	0.0175
Ni4r	(3,3,7,8,12,13,17,18-octaethyl-2-(hydroxyimino)chlorinato)-nickel(ii) n-hexane n-pentane solvate	Ni(II)	WANBIZ	0.2675	0.0135	-0.0247	-0.2184	-0.0222	0.1259	0.082	0.014	0.0708	0.0211	0.0254	0.0146	-0.0565	-0.0095	-0.0289	-0.0053
Fe4g	Chloro-(3,3,7,8,12,13,17,18-octaethyl-2-oxo-2,3-chlorinato)-iron(iii) chloroform solvate	Fe(III)	LAMDUZ	0.5769	0.0087	-0.5632	0.0603	-0.0165	0.1082	0.0068	0	0.1207	0.0253	0.0191	0.0815	-0.0518	0.0054	0.0688	0.0108
Ni4g	(3,3,7,8,12,13,17,18-octaethyl-2-oxochlorinato)-nickel(ii)	Ni(II)	DOZVIX02	0.4396	0.0062	-0.0409	0.1244	-0.0075	0.0983	-0.0275	0.003	0.098	0.0207	-0.0098	0.0347	-0.0664	-0.0351	-0.0449	0.0253
Ni4g^l	(3,3,7,8,12,13,17,18-Octaethyl-2(3H)-chlorinato)-nickel(ii) (mol. 1: N1, N2, N3, N2B)	Ni(II)	DOZVIX	1.0338	0.0147	-0.0001	1.0318	0.0005	-0.0002	0.0411	-0.0508	0.144	0.0471	-0.0001	0.1196	-0.0297	0.0004	-0.0746	-0.0001
Ni4g^{ll}	" mol. 2: N4-N7	Ni(II)	"	0.4709	0.0085	0.4467	-0.1105	0.0374	-0.0779	0.043	-0.0256	0.1171	0.0302	-0.0376	0.0458	-0.0742	-0.0069	-0.0635	0.025
Ni4s	7,13,17-Triethyl-2,8,12,18-tetramethyl-2-methoxycarbonylmethyl-3-methoxycarbonylmethylenechlorin-nickel(ii) methanol solvate	Ni(II)	JUNZUN	0.2799	0.0055	-0.2345	0.1472	0.0331	-0.0055	0.003	-0.0227	0.1375	0.0298	-0.0183	0.0347	-0.0617	0.0693	-0.0934	0.0042
Ni4t^l	RAC-(2,7,12,18-Tetramethyl-2,13,17-tis(2-methoxycarbonyl-ethyl)-3-oxochlorinato)-nickel(ii) (mol. 1: N1-N4)	Ni(II)	PASXEM	0.7608	0.0545	-0.0802	-0.6997	0.1727	-0.1622	0.0829	0.1407	0.1999	0.0334	0.0089	0.0467	0.0619	0.0073	-0.1825	0.0219
Ni4t^{ll}	" mol. N5-N8	Ni(II)	"	0.4171	0.0409	0.0277	0.1784	-0.1903	0.2124	-0.1071	-0.2204	0.1592	0.0428	-0.0398	-0.0115	0.0045	0.0148	-0.1503	0.0286
Cu4u	(20-Ethoxycarbonyl-2,7,8,12,13,17,18-heptamethyl-3-methylidene-2-(p-tolylmethyl)-2-chlorinato)-copper(ii)	Cu(II)	NIJBOX	0.4102	0.0278	-0.2317	0.3028	0.0045	-0.0887	0.0347	-0.1174	0.1849	0.0216	-0.088	0.055	-0.0887	-0.0566	0.1105	0.012
Cu4v	(20-Ethoxycarbonyl-3,7,8,12,13,17,18-heptamethyl-2-methylidene-3-(p-tolylmethyl)-3-hydrochlorinato)-copper(ii)	Cu(II)	NIJBUD	0.757	0.0352	0.6119	0.33	-0.0858	-0.0577	0.2078	-0.189	0.1078	0.0249	-0.0387	0.0057	-0.0422	-0.054	0.0713	-0.0178
Cu4w	(20-Ethoxycarbonyl-2-(2-methoxycarbonylmethyl)-2,3,7,8,12,13,17,18-octamethyl-trans-chlorinato)-copper(ii)	Cu(II)	LICSEV	0.7776	0.0538	-0.0461	-0.7288	0.1	0.0783	-0.149	0.1819	0.1419	0.0212	-0.0675	0.0358	-0.0839	-0.0624	0.0581	-0.0019
Cu4x	(trans-2,3,7,8,12,13,17,18-Octaethyl-5,10-diformyloctachlorinato)-copper(ii)	Cu(II)	LOGYAH	1.5201	0.0406	-0.6415	-1.2606	-0.0017	-0.0051	-0.5174	0.2058	0.0973	0.031	0.0306	0.0586	0.0282	0.0291	-0.0587	0.0018
Ni4y	(2,2'-(5,10,15,20-tetraphenyl-2,3-chlorinato-2,3-diyl)bis(3-oxo-3-phenylpropanenitrile))-nickel(ii)	Ni(II)	XANDOI	1.5781	0.0333	0.1019	1.559	0.0121	-0.0683	0.1249	-0.1702	0.3245	0.029	-0.0106	0.0562	-0.0287	-0.0557	-0.3131	-0.0087
Ni4z	(2,3-Dimethyl-5,10,15,20-tetraphenyl-2,3-dihydroxy-2,3-chlorinato)-nickel(ii)	Ni(II)	ZAZNOF	2.0996	0.0578	-0.1487	-2.0549	0.0414	-0.124	-0.325	0.2026	0.5012	0.0553	0.0318	0.0043	0.0866	0.0631	-0.4884	0.0111
Ni4aa	(2,3-bis(Dicyanomethyl)-7,8,12,13,17,18-hexabromo-	Ni(II)	NOCGAN	3.1927	0.0482	2.3319	-2.1384	-0.0149	0.1744	-0.3609	0.1482	0.8793	0.0997	-0.0236	-0.0335	0.1418	-0.1662	-0.8505	0.0216

5,10,15,20-tetraphenylchlorinato)-nickel(ii) chloroform solvate																			
Fused chlorins																			
4ab	2,3,7,8,12,13,16,16-Octaethylbenzochlorin	2H	JUNZIB	0.2678	0.014	-0.2177	-0.1132	0.0301	-0.0351	-0.0906	-0.0337	0.4907	0.0361	-0.3612	-0.1298	-0.0778	-0.01	0.2903	-0.0556
4ac	Ethyl benzochlorin-27-acetate	2H	QIRHEE	0.2339	0.0073	0.1786	-0.1112	-0.0123	0.099	-0.0165	0.015	0.4171	0.039	-0.2577	0.0808	-0.0301	-0.0898	0.2995	0.0494
Ni4ab	2,2,7,8,12,13,17,18-Octaethylbenzo(3,4,5)porphyrinato-nickel(ii)	Ni(II)	OEBPNI	1.5918	0.0236	1.0997	1.1167	0.1451	-0.0037	-0.2375	0.0025	0.3068	0.0279	-0.0734	0.0185	-0.0019	-0.0187	-0.2929	-0.0474
Ni4ad	(20-(2-Formylvinyl)-2,3,7,8,12,13,17,17-octaethylbenzochlorinato-N,N',N'',N''')-nickel(ii)	Ni(II)	VUFTEV	2.1843	0.0176	0.0483	-2.1514	0.1397	0.3335	-0.0906	0.0349	0.5312	0.0611	0.0409	0.0176	0.0146	-0.025	-0.5263	0.0491
4ae	7-Amido-2,3,7,12,13,17,18,10 ³ -octaethylbenzochlorin	2H	XIXVAB	0.2517	0.0164	-0.1455	0.1417	0.0198	0.0652	0.1247	-0.0438	0.3995	0.0377	-0.3263	-0.1099	-0.0789	-0.0298	0.1747	-0.0588
Ni4af	(7-Cyano-2,3,7,8,12,13,17,18-octaethyl-10 ³ -oxobenzochlorin-N,N',N'',N''')-nickel(ii)	Ni(II)	XIXTUT	1.6953	0.0523	-1.3937	-0.8006	0.1093	0.0563	-0.4152	0.3212	0.3725	0.0312	0.0051	-0.0303	0.034	0.0261	-0.3626	-0.0671
4ag	Anhydrobonellin methyl ester	2H	AHBONM	0.708	0.0404	-0.4204	-0.4339	0.2605	-0.0977	0.2138	0.116	0.3367	0.0364	0.1914	-0.0997	0.0501	-0.0545	0.2458	0.0297
4ah	5-(Benzylimino)-10-mesityl-22,22-dimethyl-4-oxa-8,24,25,26-tetraazahexacyclo[19.2.1.16.9.111.14.116.19.02.7]heptacos-1,6,9(27),10,12,14(26),15,17,19,21(24)-decaen-3-one cyclohexane solvate	2H	OJOXIV	0.5474	0.0217	-0.2392	0.4774	0.0979	-0.0207	0.0118	-0.0656	0.3467	0.0381	0.0562	0.2396	0.0875	-0.009	0.2272	-0.0178
Zn4ah	(10-Mesityl-22,22-dimethyl-5-(phenylimino)-4-oxa-8,24,25,26-tetraazahexacyclo[19.2.1.16.9.111.14.116.19.02.7]heptacos-1,6,9(27),10,12,14(26),15,17,19,21(24)-decaen-3-one)-(tetrahydrofuran)-zinc(ii)	Zn(II)	OJOXUH	0.8982	0.0402	0.7512	0.4524	0.1471	0.0468	-0.0314	0.1144	0.2942	0.0293	-0.0056	-0.2139	0.0158	0.0771	0.1826	-0.0348
4ai	10-Mesityl-22,22-dimethyl-5-(phenylimino)-4-oxa-8,24,25,26-tetraazahexacyclo[19.2.1.16.9.111.14.116.19.02.7]heptacos-1,6,9(27),10,12,14(26),15,17,19,21(24)-decaen-3-one	2H	OJOXOB	0.5192	0.0189	0.1458	-0.4751	-0.0543	0.0062	0.129	-0.0551	0.3135	0.0363	-0.0193	-0.1861	0.0068	0.0925	0.2326	-0.0236
4aj	trans-(13,17-bis(Methoxycarbonyl)ethyl)-2,7,12,18-tetramethyl-8-vinyl-2,3-(4',5'-bis(methoxycarbonyl)benzo)chlorin	2H	PIRCOI	0.4062	0.0192	0.3201	0.1443	-0.1267	-0.118	-0.0399	0.1008	0.2796	0.0279	0.0605	-0.0037	-0.0637	-0.0151	0.265	-0.0029
4ak	cis-(13,17-bis(Methoxycarbonyl)ethyl)-2,7,12,18-tetra-methyl-8-vinyl-2,3-(4',5'-bis(methoxycarbonyl)benzo)-chlorin	2H	PIRCIC	0.7604	0.022	0.1296	-0.73	-0.1009	-0.0122	-0.0958	0.095	0.2487	0.0291	0.0256	0.0618	-0.0516	-0.0116	0.2333	-0.0121
4al	2 ¹ ,2 ² (N,N-Dicarbonyl-N-phenyl)-8,12-bis(2-(methoxycarbonyl)ethyl)-2,7,13,17-tetramethyl-18-vinyl-2,2 ¹ ,2 ² ,2 ³ -tetrahydrobenzo[b]porphyrin (mol. 1: N1-N4)	2H	NEZLOV	0.4621	0.0104	-0.4491	-0.0022	-0.0083	-0.0094	-0.0984	0.044	0.3007	0.0326	-0.0272	-0.0254	-0.0199	-0.0636	0.2909	0.0013
4al^B	" mol. 2: N5-N8	2H	"	0.3404	0.0159	0.2786	-0.1355	0.0542	-0.0284	0.0719	-0.1049	0.3611	0.0349	-0.02	-0.0555	0.004	-0.0524	0.3521	0.0143
Ni4ami	(14,19,24-Triphenyl-9,12,28,29,30-pentaazahaptacyclo[23.2.1.1 ¹⁰ .13.1 ¹⁵ .18.1 ²⁰ .23.0 ²¹ .0 ²² .0 ²³]henciaonta-1(27),2(11),3(8),4,6,9,14,16,18,20(29),21,23,25-tridecaen-31-one 9-oxide)-nickel(ii) dichloromethane n-pentane solvate (mol. 1: N1-N4)	Ni(II)	XUCBEE	1.5765	0.0153	0.1202	-1.5508	-0.1771	-0.0453	-0.1804	0.0112	0.3828	0.0308	-0.0327	0.0026	0.015	-0.0208	-0.379	-0.0341
Ni4ami	" mol. 2: N5-N8	Ni(II)	"	2.0643	0.017	-0.6701	-1.9294	-0.2183	-0.1064	-0.175	-0.0077	0.5383	0.048	-0.0447	0.0089	0.0343	0.0762	-0.5293	-0.0223
4an	3,9,13-tris(2-(Methoxycarbonyl)ethyl)-4,8,14,21-tetramethyl-26,28,29,30-tetra-azahaptacyclo(14.8.3.1 ² .1 ³ .10.1 ¹⁵ .15.0 ²⁰ .2 ²¹ .2 ²²)triacenta-1,3,5,7(29),8,10,12,14,16,18,20(27),25-dodecaen-24-one	2H	YAQXET	0.5937	0.0248	-0.2987	0.3863	0.1885	0.0669	0.2369	-0.1339	0.4592	0.0441	0.104	-0.2585	-0.0711	-0.0173	0.3569	0.0233
4ao¹	4,5,6,7-tetrafluoro-10-(methylsulfonyl)-14,19,24-tris(pentafluorophenyl)-9-oxa-12,28,29,30-	2H	YACGOB	0.6643	0.0359	0.0801	-0.4845	-0.1144	-0.1083	-0.4015	0.1187	0.2133	0.0266	-0.029	-0.0844	0.0061	0.0321	0.1876	-0.0356

4ao^{II}	tetraazaheptacyclo[23.2.1.1 ^{10,13} .1 ¹⁵																			
	^{18,120,22,0³⁻¹¹,0³⁻⁹]hentriaconta-} 1(27),2(11),3,5,7,12,14,16,18,20(29),2 1,23,25-tridecaen-31-one dichloromethane methanethiol solvate (mol. 1: N1-N4) " mol. 2: N5-N8.	2H	"	1.167	0.0322	-0.0962	-1.027	-0.2243	-0.3177	-0.3594	0.1329	0.147	0.0339	-0.0194	-0.0638	0.0425	0.0677	0.1011	-0.0233	